Structure and phase transitions in Langmuir monolayers

Vladimir M. Kaganer

Max Planck Institute of Colloids and Interfaces, D-12489 Berlin, Germany
*and Institute of Crystallography, Russian Academy of Sciences, 117333 Moscow, Russia**

Helmuth Möhwald

Max Planck Institute of Colloids and Interfaces, D-12489 Berlin, Germany

Pulak Dutta

Department of Physics and Astronomy, Northwestern University, Evanston, Illinois 60208

Lipid monolayers on the surface of water have been studied for over a hundred years, but in the last decade there has been a dramatic evolution in our understanding of the structures and phase transitions of these systems, driven by new experimental techniques and theoretical advances. In this review, dense monolayers of simple lipids are described in detail, including structures revealed by x-ray-diffraction experiments, computer simulations, molecular models, and a phenomenological theory of phase transitions. The effects of chirality and the structures of phospholipid monolayers are considered. Open questions and possible approaches to finding answers are discussed.
[S0034-6861(99)00203-2]

CONTENTS

I. INTRODUCTION

Monomolecular insoluble films on the surface of a liquid are called Langmuir monolayers. They are most commonly formed on the surface of water by molecules called lipids or amphiphiles, which consist of two dissimilar parts. One part is hydrophilic (usually polar) and is commonly referred to as the ''head.'' The rest of the molecule is hydrophobic—for example, one or more saturated alkane chains (''tails''). Such asymmetric molecules naturally prefer the surface of water, i.e., they are surfactants. If the tail is hydrophobic enough, the material is insoluble, and then the molecules on the surface of water form an isolated two-dimensional system. Monolayers of amphiphiles consisting of hydrophobic alkane chain(s) and a polar head are the most intensively studied, and we confine the present review to such systems.

Why are Langmuir monolayers interesting? For a physicist, a Langmuir monolayer is an excellent model system for studying ordering in two dimensions. The water surface provides an ideally smooth (uncorrugated) substrate. Two thermodynamical variables, temperature

*Permanent address.

and surface pressure, can be directly controlled; the surface pressure is varied simply by moving a barrier along the surface, keeping the monolayer molecules on one side but letting the water flow freely below it. Such direct mechanical compression, a straightforward analog of hydrostatic compression in three dimensions, is not possible in any other two-dimensional system. Moreover, the intramonolayer and the monolayer-subphase interactions can be widely varied by changing the head or tail parts of the molecule (for example, the length of a hydrocarbon chain can be varied in small steps), or by changing the *p*H or ion content of the subphase. Of course, unlike, say, a rare-gas atom, an organic molecule has orientational and, in principle, numerous internal degrees of freedom. Depending on one's point of view, this is either a manifestation of the diversity of nature or an undesirable complication. Perhaps fortunately, in the condensed phases that are the subject of the present review, the molecules can be treated as rigid rods with noncircular cross sections, without assigning a significant role to internal degrees of freedom. Thus the essential molecular degrees of freedom are the tilt (relative to the water plane) of the long axis of the molecule, the orientation of the molecular backbones, and the orientation of the head group. It turns out that the number of the order parameters is small enough to give a clear picture of the phase changes in the system, and large enough to provide a rich polymorphism.

There are many other reasons to study Langmuir monolayers. They are excellent model systems for membrane biophysics, since a biological membrane can be considered as two weakly coupled monolayers. Langmuir monolayers are used for studies of chemical and biological reactions in two dimensions. They are necessary for the fabrication of Langmuir-Blodgett (LB) films, which are multilayers transferred layer-by-layer from the water surface to a solid support; the process provides, at least in principle, a way to manipulate molecules and construct artificially structured materials for optical, electronic, or sensor applications. LB films can also be used as well-defined coatings in studies of friction, lubrication, wetting, and adsorption. This review will not explore these topics in any detail, but we note that a basic physical understanding of Langmuir monolayers is important for many applications using these systems.

Although Langmuir monolayers have been studied for more than a century, it can safely be said that the field has undergone a revolution within the last decade. In large part this is due to the development of novel experimental techniques or enhancements of traditional techniques. Synchrotron x-ray-diffraction experiments (starting with Kjaer *et al.*, 1987; Dutta *et al.*, 1987) observed structure at the intermolecular level and debunked some traditional views of Langmuir monolayer phases and phase transitions. Subsequent experiments provided evidence for a large number of distinct phases differing by translational order (from liquidlike to crystalline), presence or absence of tilt, and the tilt azimuth. Even minor singularities of the surface pressure—area isotherms were found to be due to structural phase transitions, and all regions of previously known phase diagrams were shown to have different structures. This sounds obvious today, but the physical significance of isotherm features and the differences between regions delineated by these features had at one time been topics of much debate.

Invention of the monolayer-sensitive microscopy techniques, such as fluorescence microscopy (Lösche and Möhwald, 1984), polarized fluorescence microscopy (Moy *et al.*, 1986) and Brewster-angle microscopy (Hénon and Meunier, 1991; Hönig and Möbius, 1991) showed us the mesoscopic structures in Langmuir monolayers. These techniques are often more sensitive to phase transitions in monolayers than classical isotherm measurements. Subsequently, a theoretical treatment accounting for most of the observed phases and transitions was given using a Landau theory of phase transitions (Kaganer and Loginov, 1993, 1995), in terms of a coupling of a limited number of order parameters. The common origins of apparently distinct phase transitions were revealed and interrelationships between the structures of different phases were explained.

The Langmuir monolayer literature is extensive and we have made no attempt to survey all of it. We refer the reader to recent reviews of grazing-incidence x-ray scattering techniques and their applications to monolayer studies, by Als-Nielsen and Möhwald (1991) and Als-Nielsen *et al.* (1994); of experimental studies of surfactant monolayers by other methods, especially optical microscopy, by McConnell (1991) and Möhwald (1993a, 1993b); of structures of monolayer phases and models by Knobler and Desai (1992); of theoretical and experimental studies of spatially modulated and domain structures by Andelman *et al.* (1994) and Seul and Andelman (1995); and of the theory of the kinetics of phase separation and phase ordering by Desai (1997).

II. PHASE DIAGRAMS OF SIMPLE AMPHIPHILES

A. Molecules

Figure 1 shows typical, frequently studied amphiphiles. Each molecule consists of a hydrophobic tail (usually a hydrocarbon chain) and a hydrophilic head group immersed in water. The head groups may be neutral [e.g., fatty ester, Fig. 1(b)] or it may be ionized in certain *p*H and ionic conditions [e.g., fatty acid, Fig. 1(a)]. The amphiphiles most frequently encountered in nature, the phospholipids [Figs. 1(c)–(e)], consist in essence of chemically coupled fatty acids. They are discussed in Sec. VIII.

B. Isotherms

For almost a century, the main source of thermodynamical data about monolayers was surface pressure—area isotherm measurements. A simple experimental setup is sketched on Fig. 2 (top). The area of the monolayer is varied by moving a barrier across the water sur-

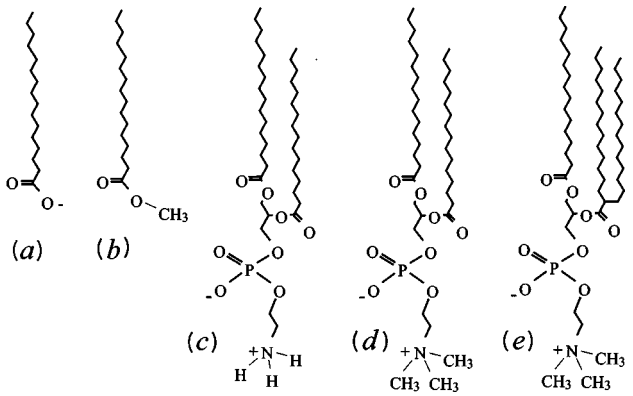

FIG. 1. Some common lipid molecules forming Langmuir monolayers on the surface of water: (a) fatty acid, (b) fatty methyl ester, (c)–(e) phospholipids: (c) diacylphosphatidylethanolamine, (d) diacylphosphatidylcholine, (e) diacylphosphatidylcholine with an aliphatic branch.

face. The surface tension is determined by suspending a plate of a material that is completely wetted by water, and measuring the downward force on it. The surface pressure Π, the two-dimensional analog of the hydrostatic pressure, is the difference between the surface tension of pure water and the surface tension of monolayer-covered water.

The first isotherm measurements were performed by Agnes Pockels (1891) in her kitchen, using a bowl as the water container and a button to measure surface pressure. Her isotherm of stearic acid is now recognized as essentially correct. Lord Rayleigh, who recommended her work for publication, was inspired to make his own experiments, from which he concluded that these layers were a single-molecule thick (Lord Rayleigh, 1899). Langmuir (1917) was the first to give essentially the modern understanding of their structure at the molecular level, in particular the fact that the molecules show a preferential orientation.

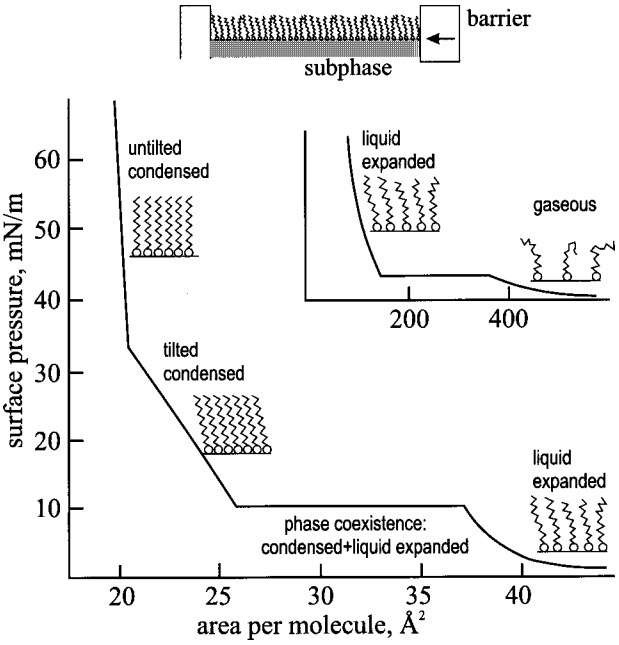

FIG. 2. A schematic diagram of a Langmuir trough (top) and a generalized isotherm of a Langmuir monolayer. Horizontal sections of the isotherm are phase coexistence regions at first-order transitions, and the kink indicates a continuous transition.

Figure 2 shows a generalized isotherm of a Langmuir monolayer of a fatty (n alkanoic) acid, the most extensively studied class of monolayer material. The very dilute monolayer, with an area per molecule in the range of hundreds of square angstroms, is well described as a two-dimensional gas. With decreasing area per molecule (increasing surface pressure), the monolayer proceeds into what has traditionally been called the liquid expanded phase (denoted LE or L_1). In this phase, as in the gas phase, there is no detectable x-ray-diffraction signal; presumably, the heads of the molecules are translationally disordered and the chains are conformationally disordered.

Further compression of the monolayer gives rise to a transition from liquid expanded to a condensed phase, with (usually) a plateau indicating a first-order transition. The plateau is not perfectly horizontal in many systems, and this apparent noncompliance with the Gibbs phase rule was the source of a long-standing controversy about the very existence of a transition and about the order and number of phase transitions. The controversy was resolved by the direct optical observation of the phase coexistence (Lösche, Sackmann, and Möhwald, 1983). Present theoretical treatments of nonhorizontal isotherms are based on formation of small molecular aggregates or surface micelles (Israelachvili, 1994; Fainerman *et al.*, 1996). The gas–liquid-expanded and liquid-expanded–condensed transition lines merge at low temperatures, giving rise to the gas–liquid-expanded–condensed triple point. Below the triple point, a direct first-order transition from a gas to a condensed phase takes place (Moore *et al.*, 1990; Knobler, 1990).

The entropy difference (per molecule) ΔS and the transition enthalpy $\Delta Q = T\Delta S$ between two phases coexisting at a first-order transition can be related to the area change by a two-dimensional Clausius-Clapeyron equation:

$$\Delta S = \frac{d\Pi_c}{dT}\Delta A, \tag{1}$$

where $\Pi_c(T)$ is the transition pressure. Lundquist (1971a, 1971b) and Albrecht, Gruler, and Sackmann (1978) used Eq. (1) to find the entropy difference at the main (liquid expanded—condensed) transition. Extrapolation of the transition enthalpy to $\Delta Q = 0$ gives a critical temperature (Rettig *et al.*, 1984, 1985). Berge *et al.* (1994) employed Eq. (1) to calculate the entropy change upon melting of a monolayer of short-chain alcohols at coexistence with the liquid bulk alcohol phase. Lawrie and Barnes (1994) and Bommarito *et al.* (1996) applied Eq. (1) to study a phase transition between two condensed phases. In the work of Berge *et al.* (1994) and Bommarito *et al.* (1996), the area difference ΔA was accurately measured using x-ray diffraction.

The monolayer is less compressible in the condensed state than in the liquid expanded state. Upon further compression one typically observes a kink on the isotherm, with the compressibility decreasing further after the kink. The kink was first observed and treated as a phase transition by Adam (1922). The two regions of the isotherm possessing different compressibilities are frequently referred to as ''liquid condensed'' and ''solid'' states. This terminology was proposed long before structural data on monolayers became available, and it can be confusing today since it is inconsistent with our present knowledge of the structures. In fact the monolayer possesses the same degree of translational order in both regions of the isotherm, which can be, depending on temperature, either long range in crystalline phases or short range in mesophases. The x-ray-diffraction studies discussed in Sec. III show that the hydrocarbon chains of the molecules are aligned parallel to each other in both sections of the isotherm; the difference is in the orientation of the chains, which are either tilted with respect to the water surface or perpendicular to it. The monolayer is relatively easily compressible in the tilted state, where decrease of the surface area can be achieved by decreasing the tilt angle. In the untitled state, the distance between close-packed vertical molecules determines the areal density, and so such phases are much less compressible.

Therefore the term ''liquid condensed'' will not be used in the rest of this review, and we propose that its use in the monolayer literature be abandoned. We will use the label ''condensed'' to denote all states of the monolayer with the hydrocarbon chains aligned, in contrast with expanded states where the chains are conformationally disordered. Based on information obtained from x-ray-diffraction studies, the two ''condensed'' regions of the isotherms can be distinguished by calling them tilted condensed and untitled condensed.

C. Phase diagrams

The isotherm studies reveal additional weaker singularities, which were considered to be first- or second-order phase transitions based on whether small horizontal sections or kinks were seen in the isotherma. Figure 3(a) represents the surface pressure—temperature phase diagram of behenic acid obtained by Ställberg-Stenhagen and Stenhagen (1945). This study, together with subsequent work by Stenhagen (1955) and by Lundquist (1971a, 1971b) revealed most of the condensed phases known at present; see Table I. This table lists phases observed in different studies, and the nomenclatures used by different authors. It is an extension of the table given by Bibo, Knobler, and Peterson (1991).

More accurate measurements of minor singularities in the isotherms, and hence of the phase-transition lines, became possible with the invention of polarized fluorescence microscopy (PFM) and Brewster-angle microscopy (BAM). In the PFM method, a fluorescent-dye probe is incorporated in the monolayer. One supposes that presence of the dye does not change the state of the monolayer, since concentration of the dye is less than 1%, comparable with the nominal purity of the substances used. In the liquid expanded—condensed phase coexistence region, there is contrast due to the different solubility of the dye in the two phases or due to the different molecular density of the phases. In condensed phases, aligned hydrocarbon chains orient the transition moment of the dye molecule, providing information about the local orientation of the molecules in the monolayer (Moy *et al.*, 1986).

In the BAM method, the incident laser beam illuminates the monolayer at the Brewster angle for water, so that the p-polarized beam is not reflected from the pure water surface and contrast is due to the monolayer only (Hénon and Meunier, 1991; Hönig and Möbius, 1991). Domains with different orientation of tilt give rise to different contrasts. Using the BAM method, Overbeck and Möbius (1993) found a new phase transition between condensed phases of fatty acids, dividing the L_2 phase into two subphases, L_2 and Ov [see Table I and Fig. 3(c)], which was not detected in isotherm studies. Schwartz and Knobler (1993) confirmed the presence of the transition with polarized fluorescence microscopy (PFM), thus proving that the dye does not disturb the order of the monolayer. The structural difference between these phases was revealed soon afterwards (Durbin *et al.*, 1994) and is discussed in Sec. III.C.

Figure 3(c) shows the phase diagram obtained in a more detailed study (Rivière *et al.*, 1994), employing BAM and PFM data. BAM and PFM observations of the transitions between condensed phases can be grouped into three categories with different changes of optical anisotropy: (i) transitions between an isotropic and an anisotropic phase ($L_2'-LS, L_2-LS, Ov-LS, S-LS$) are visible due to the complete loss of contrast; (ii) transitions between a highly anisotropic tilted phase and a weakly anisotropic untitled phase ($L_2''-CS, L_2'-CS, L_2'-S$) also appear as a complete loss of contrast in PFM experiments, but with BAM they are identified by a substantial decrease in the level of contrast between domains; (iii) transitions between two anisotropic phases with approximately the same degree of anisotropy ($L_2-L_2'', L_2'-L_2'', L_2-L_2', L_2-Ov, S-CS$) are visible because the domain structure undergoes a sudden and repeatable rearrangement.

The phase diagrams of Figs. 3(a)–(c) are still not final. In particular, Durbin *et al.* (1997) recently found a narrow region between the L_2 and L_2' phases in eicosanoic (C_{20}) and nonadecanoic (C_{19}) acid monolayers [Fig. 3(d)]. This phase has now been confirmed by the Brewster-angle autocorrelation spectroscopy (Fischer, 1997). There are various other indications for presence of phase transitions, but these are not sufficiently well established and sometimes contradict each other. Some of these are mentioned in Sec. II.H below.

D. Chain-length dependence

The temperature of a phase transition depends on the length of the hydrocarbon chain, with longer molecules

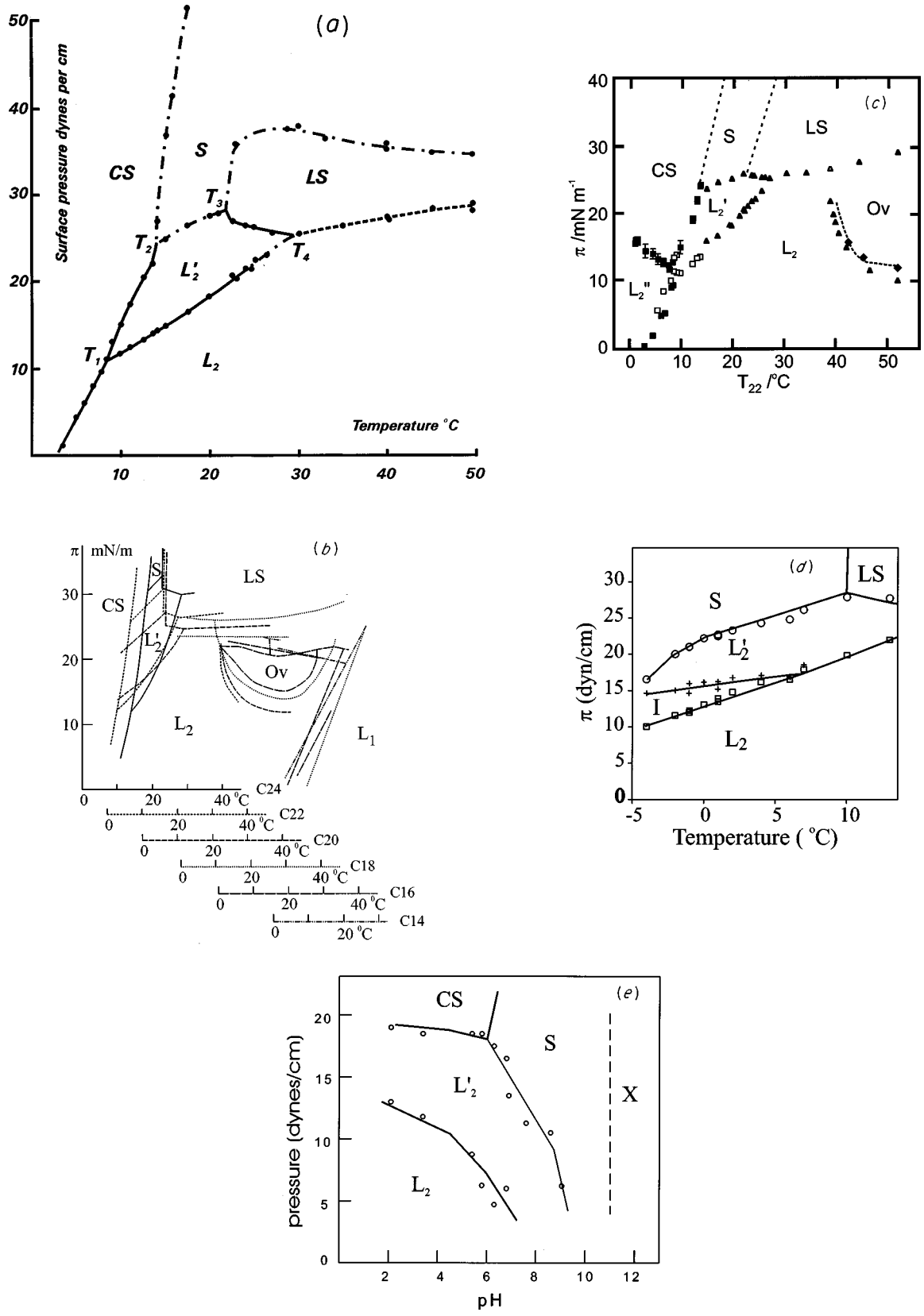

FIG. 3. Phase diagrams of fatty acid monolayers: (a) behenic (C_{22}) acid (Ställberg-Stenhagen and Stenhagen, 1945); (b) C_{14}—C_{24} acids. Adapted from Peterson *et al.* (1992), with data by Overbeck and Möbius (1993) added to locate the relative positions of the C_{16}—C_{20} phase diagrams more precisely; (c) behenic (C_{22}, squares) and arachidic (C_{20}, triangles and diamonds) acids, the temperature for the C_{20} measurements has been shifted by -10 K to overlay the C_{22} data (Rivière *et al.*, 1994); (d) arachidic (C_{20}) acid, showing an intermediate tilted phase (Durbin *et al.*, 1997); (e) heneicosanoic (C_{21}) acid with calcium ions in the subphase (Shih *et al.*, 1992b).

TABLE I. Phases of Langmuir monolayers observed in different studies and nomenclatures used by different authors.

Adam (1922)	liquid expanded	close-packed heads				close-packed chains		
Dervichian (1939)	liquid	mesomorphous				solid		
Harkins, Young, and Boyd (1940),	liquid expanded	liquid condensed				superliquid	solid	
Harkins and Copeland (1942)	L_1	L_2				LS	S	
Stenhagen (1955)	L_1	L_2		L_2'		LS	S	CS
Lundquist (1971a,1971b)	L_1	L_2		L_2'	L_2''	LS/LS'	S/S'	CS/CS'
Lin *et al.* (1990), Shih *et al.* (1992c)		D		C	B	RI-RII	A′	A
Bibo, Knobler, and Peterson (1991):								
monolayer phases		L_2/L_1'		S'/L_2^*	L_2''	LS	S	CS
related smectic categories	SmA	SmI/SmL		SmH/SmF	SmK	SmBH	SmE	
Schwartz *et al.* (1992)		I		F	I'		U	U'
Overbeck and Möbius (1993),								
Durbin *et al.* (1994), Riviére *et al.* (1994)		L_2	Ov	L_2'	L_2''	LS	S	CS
Durbin *et al.* (1997)		L_2		I-L_2'		LS	S	
Theory: Kaganer and Loginov (1995)		L_{2d} L_{2h}	Ov	L_2'	L_2''	LS	S	CS
and present paper								
Azimuth of tilt[1]		NN NN	NNN	NNN	NN	U	U	U
Azimuth of unit-cell distortion		U NNN	U	NN	NN	U	NN	NN
(normal to chains)[1]								

[1]NN=tilt or distortion to the nearest-neighbor molecule, NNN=to the next-nearest neighbor, U=untilted or undistorted hexagonal. Azimuth of distortion is that of stretching of the unit cell.

experiencing the transition at higher temperatures. Bibo and Peterson (1990) matched the phase-transition lines of monolayers of fatty acids on a common phase diagram, by systematically shifting the temperature axis by 5–10 °C per additional methylene group. The phase diagrams for C_{20}–C_{24} fatty acids were matched unambiguously based on positions of the $LS-L_2'-L_2$ triple points, while matching of the shorter-chain phase diagrams remained somewhat ambiguous. Discovery of the $LS-Ov-L_2$ triple point (Overbeck and Möbius, 1993) allows us to place these phase diagrams more precisely. In Fig. 3(b), the phase diagrams are matched by bringing both triple points in coincidence. Then, a fixed shift of the temperature axis by 5 °C per each methylene group is required for chain lengths from C_{16} to C_{22}. Thus, monolayers formed by molecules differing only in the length of the chain experience the same sequence of phase transitions, but at different temperatures. Using this fact, the phase diagram can be determined over a temperature range unavailable with a single substance.

A quantitative comparison of the phase transitions in monolayers differing only in the chain length was performed by Peterson *et al.* (1992) by relating the monolayers in "equivalent states," i.e., the states which possess the same head groups, are kept at the same temperature and with the same subphase content, and have the same tilt of the chains and their packing. The chain-length dependence of the free energy per molecule f for monolayers in equivalent states can be represented in the limit of large chain length l as $f=f_0+lB$, with the length independent quantities f_0 and B. Here f_0 describes the free-energy contribution due to two interfaces, water—monolayer and monolayer—air, and depends on the head groups and the subphase content. The bulk parameter B depends on the state inside the monolayer, characterized by packing of the chains. Differentiating the free energy with respect to molecular area and using the equality $\Pi=\partial f/\partial A$, one obtains

$$\Pi=\Pi_0+lP, \tag{2}$$

where Π_0 describes the contribution of the interfaces to surface pressure, while P is the internal pressure inside the monolayer. Monolayers differing in the chain length are in equivalent states when they experience the same second-order transition between untilted and tilted states. Comparing the experimental data on the $LS-L_2$ transitions of fatty acids, acetate esters, and ethyl esters, Peterson *et al.* (1992) found different values and temperature dependencies of Π_0 for different substances, but the same internal pressure $P=0.24t$ MPa, where t is temperature in °C. Hence, the tilting transitions occur at small internal pressures, in agreement with molecular models (Sec. V).

E. Head-group dependence

The above discussion focussed on fatty acids because these monolayers have been studied in the greatest detail. Many substances slightly different from fatty acids in the chemical structure of the head groups, such as alcohols, esters, acetates, also form stable Langmuir monolayers. Less is known about these systems. The generalized phase diagram of n-alkyl acetates is similar to that for acids (Lundquist, 1971a). However, studies of alcohols of different chain lengths, performed by means of x-ray diffraction (Shih *et al.*, 1992b), Brewster-angle

microscopy (Overbeck, Hönig, and Möbius, 1993), and isotherm measurements (Lawrie and Barnes, 1994) show an important difference: the L_2-L_2' and L_2-Ov phase boundaries are absent. Methyl and ethyl esters show phase diagrams similar to those of the alcohols (Lundquist, 1971b; Foster *et al.*, 1996).

It follows from x-ray-diffraction studies (Shih *et al.*, 1992b; Foster *et al.*, 1996) and from studies of mixtures (see below) that the single phase observed in monolayers of alcohols and esters can be treated as merged L_2' and Ov phases. The phase L_2 is absent from their phase diagrams. Teer *et al.* (1997) attribute the difference between the two types of phase diagrams to the size of the head groups. Presence of the L_2 phase in the phase diagrams of acids and acetates is due to relatively large head groups, which give rise to large tilt angles.

The phase diagrams of alcohols and acids are otherwise quite similar. In particular, a short first-order segment (the transition $LS-L_2'$ in fatty acids) between two second-order segments (corresponding to $S-L_2'$ and $LS-L_2$ transitions in the acids) is also observed for alcohols (Shih *et al.*, 1992b; Lautz, Fischer, and Kildea, 1997; Lautz and Fischer, 1997). The low-temperature boundary of this segment is the $LS-S$ transition. Lautz, Fischer, and Kildea (1997) found, by use of Brewster-angle autocorrelation spectroscopy, that the high-temperature boundary of the segment is the LS_I-LS_{II} transition within the LS phase. Moreover, this transition is continued in the L_2' phase as a first-order transition with a jump of the tilt angle across it.

The interactions between head groups can also be varied by changing the pH of the subphase. Significant effects have been observed on acid monolayers with different metal ions in the subphase (Lin *et al.*, 1989; Shih *et al.*, 1992a). At low pH, the phase diagram is the one shown in Figs. 3(a)–(c), as expected; as the pH is increased, the phase boundaries move down to lower pressures and ultimately the high-pressure phase(s) are present at all pressures [Fig. 3(e)].

It should be noted that the "cleanest" subphase used to study fatty acids, ultrapure water without additional ions in the subphase, is not well defined as regards charge density. A $p\mathrm{H}\approx 5.5$ is established after some time due to dissolution of CO_2 from the air, and the head groups are partially dissociated. The degree of dissociation is sensitive to slight variations of ionic milieu. Theoretically, dissociation should also depend on molecular area as this affects the surface potential, but we are not aware of direct measurements. Judged from experiments and calculations for phospholipids, one should expect a nonmonotonic influence of monovalent ions on Coulomb interactions, since upon increasing the ion concentration one should first observe an increase of the head dissociation and thus Coulomb repulsion, and at higher concentrations the screening of these interactions would dominate. For multivalent ions, the latter effect is expected to dominate at any reasonable concentration.

F. Mixtures

Many amphiphiles are miscible, giving rise to monolayers of uniform mixtures in the whole concentration range. By gradually varying the concentrations of the components and studying the phase diagrams of the mixtures, one can continuously proceed from the phase diagram of one substance to that of the other and thus characterize the phases. Such miscibility studies were proven to be very helpful in the characterization of smectic liquid crystals (Sackmann and Demus, 1966, 1973). The miscibility approach was applied by Bibo, Knobler, and Peterson (1991) to study monolayers of mixtures of fatty acids and their ethyl esters. The observed phases were related to smectic categories (see Table I). The correspondence following from recent observations and the Landau theory of phase transitions does not coincide with that proposed by Bibo, Knobler, and Peterson (1991), and their phase attributions were corrected in a subsequent paper (Teer *et al.*, 1997).

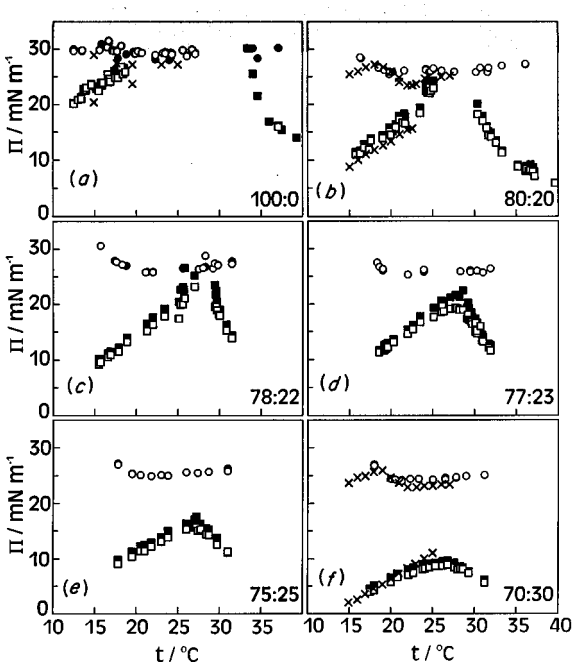

FIG. 4. Phase diagrams for the acid:alcohol mixtures determined by Brewster-angle microscopy at different concentrations of alcohol (Fisher *et al.*, 1995). The open symbols represent observations made with increasing pressure and the closed symbols are observations made with decreasing pressure. Squares indicate transitions between tilted phases and circles indicate transitions between a tilted and an untilted phase. The crosses are experimental points taken from Shih *et al.* (1994).

Shih *et al.* (1994) studied the phase diagrams of fatty acid—alcohol mixtures by means of isotherm and x-ray-diffraction measurements. They established that the components were completely miscible on the microscopic scale and traced changes of the structures. Their results were complemented by Fischer, Teer, and Knobler (1995) and by Teer *et al.* (1997), who followed the changes of the phase diagrams in detail with the aid of BAM. Figure 4 presents a selection of mixture phase diagrams. As the alcohol concentration increases, the lines of the transitions $L_2'-L_2$ and L_2-Ov move close to each other and then merge, giving rise to a single line separating a higher-pressure tilted phase (inheritor of

the L_2' and Ov phases) from the low-pressure L_2 phase. The transition line goes down with increasing concentration of the alcohol and then vanishes below the zero-pressure line, resulting in the single tilted phase seen in pure alcohol. An interpretation of the changes of the phase diagram is given in Sec. VI.E.

Durbin *et al.* (1995) studied mixtures of fatty acids with different chain-lengths. As discussed above, the chain-length dependence is monotonic (and close to linear), so one can expect that the mixtures interpolate the chain-length difference. Curiously, the phase boundaries of the mixtures move down in pressure to below the boundaries of either component. When the difference in chain lengths is sufficiently large, the lower-pressure phases vanish and the CS, S, and LS phases are seen at all pressures. The x-ray data confirm that even at zero pressures, the molecules are vertical rather than tilted. A similar effect is observed in the bulk rotator phases of mixtures of *n* alkanes (Sirota *et al.*, 1995): when the difference between the chain lengths of the two components is increased, the range of stability of the tilted phases decreases in favor of the crystal and untitled rotator phases.

G. Collapse

The range of surface pressures experimentally available is restricted by collapse of the monolayer. The term "collapse" can describe two different effects (Smith and Berg, 1980). When the surface pressure—area isotherms (Fig. 2) are recorded during a constant-rate compression of the monolayer, as in most of the isotherm studies, the compression ends with a "fracture collapse," i.e., abrupt fracture of the monolayer and appearance of three-dimensional structures. The fracture pressures are highly dependent on the rate of compression and often are not reproducible. If the monolayer is allowed to relax (with a typical time of hours) at sufficiently high surface pressure, a bulk solid phase nucleates and grows, reducing the pressure. At some surface pressure, called the *equilibrium spreading pressure*, the monolayer is in thermodynamical equilibrium with the bulk phase. At pressures above the equilibrium spreading pressure but too low for fracture collapse to occur, the state of the monolayer is metastable with respect to formation of the bulk (three-dimensional) phase.

Bommarito *et al.* (1996) performed isotherm and x-ray-diffraction studies of behenic acid, allowing the monolayer to relax for a sufficient time after each step of compression. Not surprisingly, their phase diagram reproduces the low-pressure part of the constant-compression-rate phase diagram (below the equilibrium spreading pressure), Fig. 3, with some transition lines shifted to lower pressures. The high-pressure phases are absent in their phase diagrams.

Thus, the monolayer relaxes much faster in two dimensions than into the third dimension, which allows us to apply two-dimensional equilibrium thermodynamics above the equilibrium spreading pressure.

H. Unresolved issues

Although general features of the phase diagrams have been observed with various techniques in diverse monolayers and are commonly accepted, some details are subject to debate. In particular, the orders of the transitions are still under discussion. The transitions among tilted phases L_2'', L_2', L_2, Ov are first order; this is sometimes but not always evident from isotherm or BAM data, but it follows from the x-ray data showing that they have different symmetries (see Sec. III). The transitions between untilted and tilted phases can be, but do not have to be, continuous. The $LS-L_2'$ transition is known to be first order; the others appear continuous in most studies. However, Rivière *et al.* (1994) reported the tilting transitions $CS-L_2'', S-L_2', LS-Ov$ in fatty acids (observed with BAM and PFM techniques) to be weakly first order, so that the $LS-L_2$ transition is the only second-order transition in their observations. Rivière-Cantin *et al.* (1996) found that the tilting transition $CS-L_2''$ is second order at temperatures below the $L_2-L_2'-L_2''$ triple point and first order above it.

Some studies have reported additional phases at very high surface pressures. Ställberg-Stenhagen and Stenhagen (1945) found a transition from the LS phase to a higher-pressure phase [Fig. 3(a)]. Lundquist (1971a, 1971b) reported the transitions from the phases LS, S, CS to higher-pressure phases which she denoted LS', S', CS', in alkyl acetates and ethyl esters (see Table I). Lawrie and Barnes (1994) reported transitions from S and LS phases to higher-pressure phases S' and LS' in an alcohol monolayer (octadecanol) found in an isotherm study. However, x-ray-diffraction experiments did not reveal any structural difference between LS and LS' phases (Steitz *et al.*, 1995).

Bibo, Knobler, and Peterson (1991) subdivided, based on isotherm data, the phase L_2' to two subphases, which they called S' and L_2^* (see Table I). Similar phases were found also in the isotherm study of octadecanol monolayers (Lawrie and Barnes, 1994). However, these phases have not been seen in x-ray structural studies, and therefore their existence remains an open question. Peterson *et al.* (1996) reported a new intermediate-tilted structure within the L_2 region, but this has not been confirmed. Schlossman *et al.* (1991) and Schwartz *et al.* (1992) reported reentrant phase behavior in a tetracosanoic acid monolayer using x-ray diffraction, along a room-temperature isotherm. This observation is made in a complicated region of the phase diagram with several known triple points within a small temperature range. Foster *et al.* (1996) have observed x-ray-diffraction evidence of a phase, in monolayers of methyl eicosanoate, which possesses a hexagonal unit cell in the horizontal (water surface) plane even though the molecules are tilted. Shih *et al.* (1992c) interpreted x-ray-diffraction data on the LS phase as its subdivision to two subphases, which they called "Rotator I" and "Rotator II." However, the analogy with the rotator phases of bulk alkane crystals with the same name (Sirota *et al.*, 1993) is doubtful (Sirota, 1997) and such notation is misleading.

These regions can be denoted as LS_I and LS_{II} (Kaganer *et al.*, 1995). Kaganer and Loginov (1993, 1995) argued, based on symmetry considerations, that the phase L_2 consists of two subphases, L_{2d} and L_{2h} (cf. Table I). The last two instances are discussed in more detail in Sec. III.C and Sec. VI, respectively.

III. STRUCTURE OF PHASES

A. Structure-sensitive techniques

X-ray diffraction is the primary technique used to study the structures (molecular arrangements) of monolayers directly on the water surface. A wider choice of techniques is available for monolayers on solid supports, but unfortunately the structure of the monolayer usually changes during the transfer (Engel *et al.*, 1991; Shih *et al.*, 1993; Brzezinski and Peterson, 1995). Although structural studies of transferred monolayers cannot be directly employed in the analysis of thermodynamics and structural phase transitions of monolayers on water, they are an excellent source of additional information regarding possible packings of molecules and structures of monolayers.

The very first electron-diffraction study of the multilayer (Langmuir-Blodgett) films (Germer and Storks, 1938) gave evidence of a close-packed structure, where each molecule has six neighbors. The patterns were found to have a constant orientation over distances of the order of millimeters. Peterson *et al.* (1990) interpreted such patterns as due to hexatic order in the films. Atomic-force microscopy provided direct images of the lattice, individual lattice defects, and one-dimensional undulations due to a melting transition in the transferred (Langmuir-Blodgett) films (Bourdieu *et al.*, 1991; Schwartz *et al.*, 1993; Viswanathan *et al.*, 1994; Sikes and Schwartz, 1997).

Several x-ray scattering techniques have been applied to study Langmuir monolayers on the water surface. Specular reflectivity is sensitive to interference between x rays reflected at various depths in the monolayer; by fitting the data to model density distributions, the mean density distribution in the direction of the normal to the monolayer plane can be obtained. This gives, in particular, the thickness of the layer, from which the mean tilt angle of the molecules can be calculated (Helm *et al.*, 1987b; Kjaer *et al.*, 1989; Tippmann-Krayer and Möhwald, 1991). Study of the off-specular (diffuse) x-ray diffraction provides information about the height-height fluctuation spectrum and may be used, for example, to determine the bending elasticity of the monolayer (Gourier *et al.*, 1997). Neutron scattering also has been applied to study monolayers on water (see review by Thomas and Penfold, 1996, and references therein), but it has been limited by available intensities to specular reflectivity studies over a relatively narrow momentum range.

The scattering technique that is sensitive to the in-plane structure of monolayers is grazing incidence x-ray diffraction. A schematic diagram is shown in Fig. 5(a).

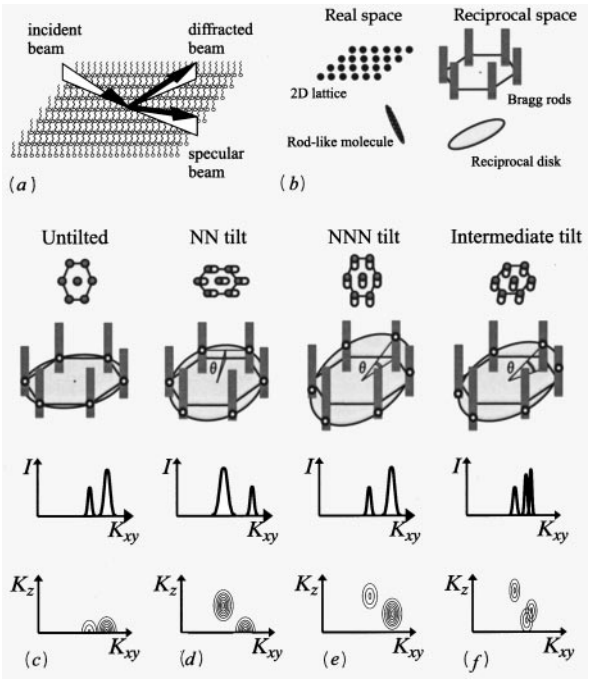

FIG. 5. X-ray-diffraction experiment: (a) schematic diagram of a grazing incidence x-ray-diffraction experiment; (b) formation of the diffraction pattern of a monolayer of rodlike molecules; (c) real-space and reciprocal-space views and characteristic diffraction patterns of the monolayer in untilted phase, (d) NN-tilted phase, (e) NNN-tilted phase, and (f) intermediate tilted phase (Kaganer *et al.*, 1995).

In order to reduce the background scattering from water, the beam is incident on the surface at very shallow angles ($\sim 0.1°$). Since the refractive index for x rays is slightly less than 1, the beam undergoes total reflection and only an evanescent wave penetrates into the subphase. The scattered photons are detected above the surface in various directions (in reciprocal space terms, at various values of the in-plane and normal-to-plane components of the momentum transfer). Any periodicity in positions of the molecules gives rise to a peak of the scattered intensity. The reviews by Als-Nielsen and Möhwald (1991) and Als-Nielsen *et al.* (1994) discuss this technique in detail.

B. Interpretation of the diffraction data

In this section, we summarize the general approach to analyzing the grazing incidence x-ray-diffraction (GID) data from Langmuir monolayers, following Kaganer *et al.* (1995). In GID experiments, the scattered intensity is monitored as a function of two angles, the angle between incident and scattered beams in the water plane and the angle between scattered beam and the water surface. A periodicity of the molecular arrangement in the monolayer manifests itself in a peak in the distribution of the scattered intensity. There is as yet no way of controlling the mosaicity of Langmuir monolayers; in other words, the monolayers are powders within the plane. The diffraction pattern is always averaged over all

domain orientations in the monolayer plane (''powder averaging''). As a result, of the three components K_x, K_y, and K_z of the momentum transfer vector $\mathbf{K}$, only the vertical component K_z can be separately measured. It is not possible to determine the in-plane components K_x and K_y individually, but only the combination $K_{xy}=(K_x^2+K_y^2)^{1/2}$.

Because lattice fluctuations cause the peak intensities to decay rapidly with increasing momentum transfer, the first-order peaks, which correspond to the distances between neighboring molecules, are the most intense and frequently the only observed ones. First-order peaks with a common K_{xy} are an indication of hexagonal packing, with equal distances between the molecules; two distinct values of K_{xy} point to a rectangular unit cell; and three peaks are due to an oblique unit cell. The available diffraction data is obviously not sufficient to perform structural analysis in a classical crystallographic sense. Knowledge of the possible packings of aliphatic chains in bulk organic crystals and lattice-energy calculations is additionally employed to characterize crystalline packings of the molecules more completely (Leveiller *et al.*, 1994; Wang *et al.*, 1994; Als-Nielsen *et al.*, 1994; see Sec. III.D). Fortunately, the structures formed by Langmuir monolayers are rather simple.

An additional and powerful tool to study the local arrangements of the molecules is Fourier transform infrared spectroscopy which has become applicable to monolayers at the air-water interface (Mendelsohn *et al.*, 1995). This technique allows measurement of the number of translationally inequivalent molecules in the unit cell, predominantly via the splitting of the CH_2 scissoring band near 1470 cm^{-1} (Simon-Kutscher *et al.*, 1995; Li and Rice, 1996).

In the simplest model, a domain of the monolayer is treated as a two-dimensional crystal consisting of uniformly oriented rigid molecules. The scattering pattern in reciprocal space is then given by the product of two factors, the structure factor reflecting translational order of the molecular centers in the plane of the monolayer, and the form factor of the individual molecule [Fig. 5(b)]. The structure factor of a two-dimensional (2D) lattice consists of a set of delta-function discontinuities along lines (''Bragg rods'') normal to the monolayer plane. The form factor of a long rodlike molecule is large only on a plane normal to its long axis, which will be called the reciprocal disk of the molecule. The intersections of the first-order Bragg rods with the reciprocal disk give rise to six diffraction maxima [Figs. 5(c)–(f)]. If the molecules do not tilt, the reciprocal disk and hence all the peaks lie in the plane of the monolayer [Fig. 5(c)]. In a phase possessing sixfold symmetry, all six first-order wave vectors $\mathbf{K}$ have equal length and overlap completely in the powder pattern. Because of this degeneracy, the sixfold symmetry cannot be said to have been directly observed on the water surface, but merely inferred from the failure to see any other peaks.

The degeneracy is lifted in cases where the lattice is distorted from hexagonal, for example, as a result of ordering of the backbone planes of the molecules, and distinct peaks at different values of $\mathbf{K}$ are observed. For a distortion where the unit cell stretches or shrinks in the direction of the nearest-neighbor molecule, a symmetry plane normal to the plane of the monolayer is preserved, and the unit cell is centered rectangular. There are then two distinct first-order wave vectors on the powder averaging: one pair with $\pm\mathbf{K}_n$ and the other two with $\pm\mathbf{K}_d$ (the subscripts n and d denote nondegenerate and degenerate peaks). If the unit cell stretches in the direction of the nearest-neighbor molecule, then $|\mathbf{K}_n|>|\mathbf{K}_d|$; the opposite inequality indicates that the unit cell shrinks in that direction.

The degeneracy may also be lifted by molecular tilt. In this case, the peaks move out of the monolayer plane by a distance K_z which depends on both the tilt magnitude and its azimuth, or direction. Since the only points of the reciprocal disk to remain in the monolayer plane are those on the line perpendicular to the tilt direction, diffraction peaks from a tilted phase can remain in the plane only if they lie in this direction. This occurs for one pair of peaks when the molecules tilt towards one of their nearest neighbors (NN). The other four peaks move out of the plane: two upwards and two downwards (naturally, peaks below the water plane cannot be observed); see Fig. 5(d). The wave vectors of the two visible out-of-plane peaks have equal K_z components and are thus degenerate in the powder pattern. The tilt angle θ is given by $\tan\theta=K_{dz}/[K_{dxy}^2-(K_{nxy}/2)^2]^{1/2}$. When the molecules tilt towards a next-nearest-neighbor (NNN) molecule, all the wave vectors move out of the plane. The two distinct values of K_z are in the ratio $K_{nz}:K_{dz}=2:1$, and the tilt angle is given by $\tan\theta=K_{nz}/K_{nxy}$ [Fig. 5(e)].

In these symmetrically tilted phases, the distinction between degenerate and nondegenerate peaks is unequivocal. The ratio $K_{nz}:K_{dz}$ can only be 0:1 or 2:1. In an untilted phase [Fig. 5(c)], the distinction is not as easy. In the idealized model representing the molecules by cylinders, the integrated intensity of the degenerate peak should be twice as large as that of the nondegenerate one, but experimentally there are often significant departures from the ''ideal'' 2:1 intensity ratio. Leveiller *et al.* (1992) calculated the molecular structure factors and intensity ratios from atomic scattering factors, assuming an all trans conformation of the molecules and ideal (zero-temperature) packing and found that the intensity ratio depends on the orientations of the backbone planes of the molecules and symmetry constraints.

If the tilt azimuth is intermediate between NN and NNN [Fig. 5(f)], or if the distortion of the unit cell is asymmetrical, there are three distinct first-order peaks and no indexing problem. Each peak is described by two components of the momentum transfer, giving six measured values in all. Since the monolayer model is completely described by five parameters, three for the in-plane lattice and two for the tilt (magnitude and direction), the measured values cannot be completely independent. The relationship between them is readily shown to be $K_{1z}+K_{2z}=K_{3z}$, where peak 3 is the one with largest K_z. The two K_z ratios 0:1 and 2:1 for the

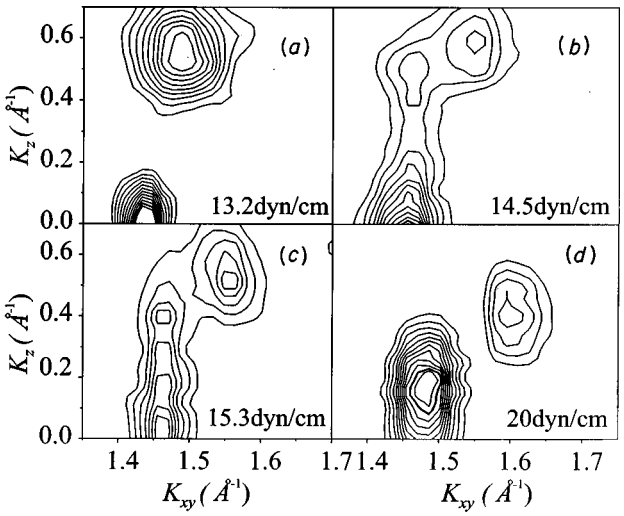

FIG. 6. Contours of equal intensity vs the in-plane and out-of-plane scattering vector components K_{xy} and K_z, for arachidic (C_{20}) acid monolayers at 0 °C and different surface pressures (Durbin *et al.*, 1997). Two peaks at 13.2 and 20 dyn/cm are indications of the centered rectangular unit cell (NN and NNN tilt, respectively) and three peaks at 14.5 and 15.3 dyn/cm are due to an oblique unit cell with an intermediate tilt azimuth.

symmetric tilts follow from this more general relationship, as particular cases in which one of the K_z values is repeated, and correspond to $0+1=1$ and $1+1=2$, respectively. Once the three first-order peaks have been assigned, the shape of the unit cell in reciprocal space is completely determined, as all three sides of a triangle are known. The real-space lattice is now easily determined.

The peaks can be assigned in crystallographic notation in terms of either a hexagonal or a centered rectangular unit cell (Als-Nielsen *et al.*, 1994). The latter notation is more common. Denoting the basic translations of the centered rectangular unit cell containing two molecules by [10] and [01] (when the lattice is hexagonal, the length of the vector [01] is $\sqrt{3}$ times larger than [10]), one finds that, if the two molecules in the rectangular unit cell are equivalent, the reflections (01) and (10) are forbidden, as are all (hk) reflections where $h+k$ is odd. The lowest-order reflections are (02), which is nondegenerate, and two reflections $(11)+(1\bar{1})$, which have equal length and so degenerate in the powder average. In case of the hexagonal unit cell, all three reflections possess equal wave-vector magnitudes. When the two molecules in the unit cell are not equivalent due to packing of the molecular backbones, the structure factors of the odd $h+k$ reflections may become nonzero. The (10) and (01) intensities were considered too weak to be measured (Weissbuch *et al.*, 1993). However, the (12) peak has recently been observed by Durbin *et al.* (1998) in the CS and L_2'' phases (see Sec. III.D).

Figure 6 illustrates the schematic pictures of Fig. 5 with an experimental example of intensity distributions measured along the 0 °C isotherm of the phase diagram of Fig. 3(d). At surface pressures of 13.2 mN/m and lower, the degenerate, more intense, peak is in the water plane and the nondegenerate peak is above the water surface, indicating NN tilt, cf. Fig. 5(d). At a surface pressure of 20 mN/m, there are again two peaks but both are out of the water plane, with the less intense nondegenerate peak possessing twice the K_z of the other peak, characteristic of NNN tilt, cf. Fig. 5(e). At intermediate surface pressures, there are three peaks, showing that the structure is chiral (the tilt direction is intermediate between NN and NNN and the lattice is oblique). This transition is discussed further in Sec. VII.

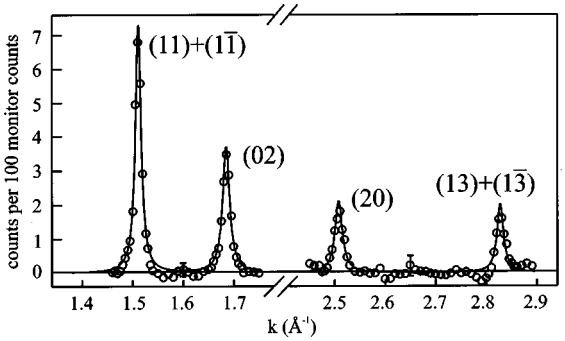

FIG. 7. X-ray-diffraction data in the horizontal plane, from a monolayer of heneicosanoic (C_{21}) acid at 5 °C and 35 mN/m (the phase CS). Two first-order and two second-order peaks are observed; all peaks are resolution limited (Bohanon *et al.*, 1990).

C. Structures of the phases

All phases presented in the phase diagrams (Fig. 3) have been characterized using x-ray diffraction and found to have different structures.

The high-pressure low-temperature phase CS was examined by Bohanon *et al.* (1990); Fig. 7 shows the diffraction peaks observed. The peaks are resolution limited, and the second-order peaks are also seen. The ratios of the intensities of two peaks, which are expected to be 2:1 for the first-order peaks and 1:2 for the second-order peaks, are in fact temperature-dependent. Positions of the peaks give the dimensions of the centered rectangular unit cell: 5.0×7.5 Å^2.

As the temperature is increased at high surface pressures, the monolayer experiences two first-order transitions $CS-S-LS$ (see Fig. 3). Transformation of the diffraction pattern is shown in Fig. 8. The phase S possesses two in-plane diffraction peaks in positions close to that of the CS phase, indicating centered rectangular packing of untitled molecules. Although the peak widths are resolution limited close to the $CS-S$ boundary, they broaden as the temperature is increased, i.e., the correlation length of the translational order decreases. The phase LS has one diffraction peak, but in the temperature range 18.5–20 °C, close to the S phase, the peak is noticeably asymmetric and can be treated as two overlapping peaks. Shih *et al.* (1992c) interpreted the peak transformations as due to an additional phase transition, dividing the phase LS into two subphases, LS_I and LS_{II}. These subphases were initially called Rotator I

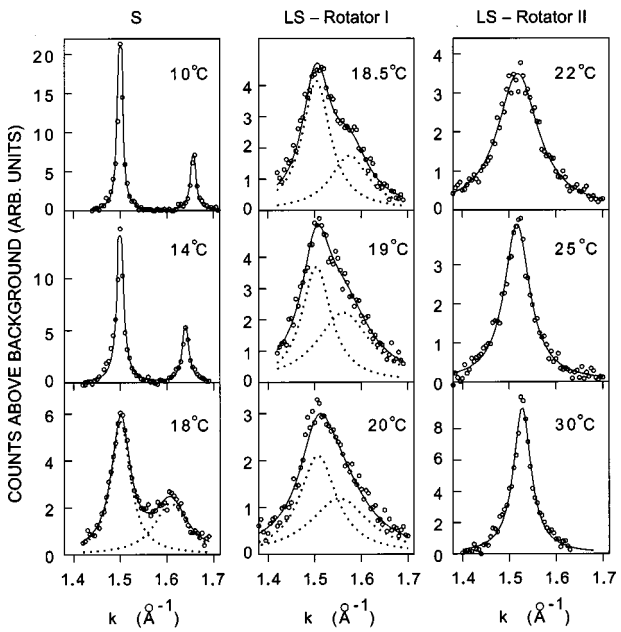

FIG. 8. Diffraction data in the horizontal plane, from heneicosanoic (C_{21}) acid monolayers along a 31 mN/m isobar. The solid lines are fits using one or two Lorentzian functions, as appropriate; the dotted lines are the individual Lorentzians. Notice that the peaks are distinctly asymmetric in the intermediate LS_I region (Shih *et al.*, 1992a).

and Rotator II (cf. Table I), but an analogy with the bulk alkane rotator phases of the same name is doubtful (Sirota, 1997).

The single diffraction peak of the LS phase is commonly treated as due to hexatic order, i.e., long-range orientational order of the intermolecular bonds connecting neighbor molecules, with a short-range positional order. Although there is no direct evidence of hexatic order, there are several indirect arguments in favor of such attribution. The LS phase is optically isotropic (Rivière *et al.*, 1994) and possesses only one first-order diffraction peak in the powder pattern. Hence the mean distances between all neighbors are equal and this phase can be either 2D liquid, or hexatic, or hexagonal crystal. The width of the diffraction peak exceeds the resolution limit but the correlation length is large in comparison to that expected for a liquid. Therefore hexatic order is the most plausible in the LS phase. Sirota (1997) noted that all diffraction experiments on Langmuir monolayers were performed at rather low resolution, and a hexagonal crystalline phase with strong diffuse scattering can be mistakenly treated as hexatic. Despite this ambiguity, the sixfold symmetry of the LS phase is sufficiently proven by the experimental data. It is also confirmed by the existence, at the same temperatures but at lower pressures, of two tilted phases differing by tilt azimuths (described below), as well as by the sixfold symmetry of long-range tilt order in domains of the L_2 phase coexisting with the liquid expanded phase (Qiu *et al.*, 1991).

The diffraction peak of the LS_{II} phase becomes narrower upon increasing the temperature, Fig. 8 (right column). Effectively higher temperatures can be reached with shorter chains of the molecules. Renault *et al.* (1993), Berge *et al.* (1994), and Zakri *et al.* (1997) performed a grazing incidence x-ray-diffraction study of the short-chain (10 to 16 carbon atoms) alcohols. To compensate for solubility, the monolayer was kept in contact with the drop of the same substance, i.e., at the equilibrium spreading pressure. The experiment revealed a hexagonal crystal phase with extremely large (exceeding 10 μm) correlation lengths and its direct melting to a phase which gives no diffraction signal, presumably a liquid expanded phase. One can therefore speculate that the increase of temperature in the LS phase gives rise to a transition from a hexatic to a hexagonal crystal, probably due to a decoupling of the rotations of the molecules about their axes. Such an unusual crystallization upon increasing temperature has not been observed directly, however. A similar narrowing of the diffraction peaks upon increasing the temperature was observed in bulk rotator phases of mixtures of n alkanes (Sirota *et al.*, 1995; Sirota, 1997). Mixing of the alkanes with different chain lengths reduces the interaction between layers and makes the system similar to a Langmuir monolayer.

The low-temperature low-pressure phase L_2'' is entered from the phase CS by decreasing the surface pressure. Lin *et al.* (1990) found that in the L_2'' phase the molecules are tilted towards a nearest neighbor (NN), and that the dimensions of the unit cell in the plane perpendicular to the long axes of the molecules remain unchanged from that of the CS phase. The diffraction peaks were resolution limited in the monolayer plane. However, the room-temperature data by Leveiller *et al.* (1992) for triacontanoic (C_{30}) acid, which can also be attributed to the phase L_2'' because of the large chain length, show a resolution-limited nondegenerate peak and a broad degenerate peak.

Figure 9 shows variations of the diffraction pattern along an isotherm crossing the $L_2-L_2'-S$ phase sequence (Kenn *et al.*, 1991). To speed up the time-consuming data collection, the in-plane peak positions were determined using a large K_z window, and then the K_z dependence of the intensity was found by "Bragg-rod" (K_z varying) scans at the K_{xy} peak positions. Each of the three phases shows two diffraction peaks. Differences in tilt azimuths are unambiguously indicated by the Bragg-rod scans. In the phase L_2 (NN tilt), the nondegenerate peak has a maximum in the horizontal plane, and the degenerate peak has a maximum out of the horizontal plane. In the phase L_2' both peaks are out of plane, with their K_z positions in a 1:2 ratio, thus proving that the tilt is NNN. The phase S is untitled, as shown by the two in-plane maxima.

Figure 10 presents structural information derived from the diffraction data of Fig. 9. Transformations of the unit cell shape, which follow from Fig. 10(a), are illustrated in Fig. 11. The unit cell of the S phase is stretched in the NN direction due to ordering of the backbone planes of the molecules. In the L_2' phase, the molecules tilt in the NNN direction normal to the initial

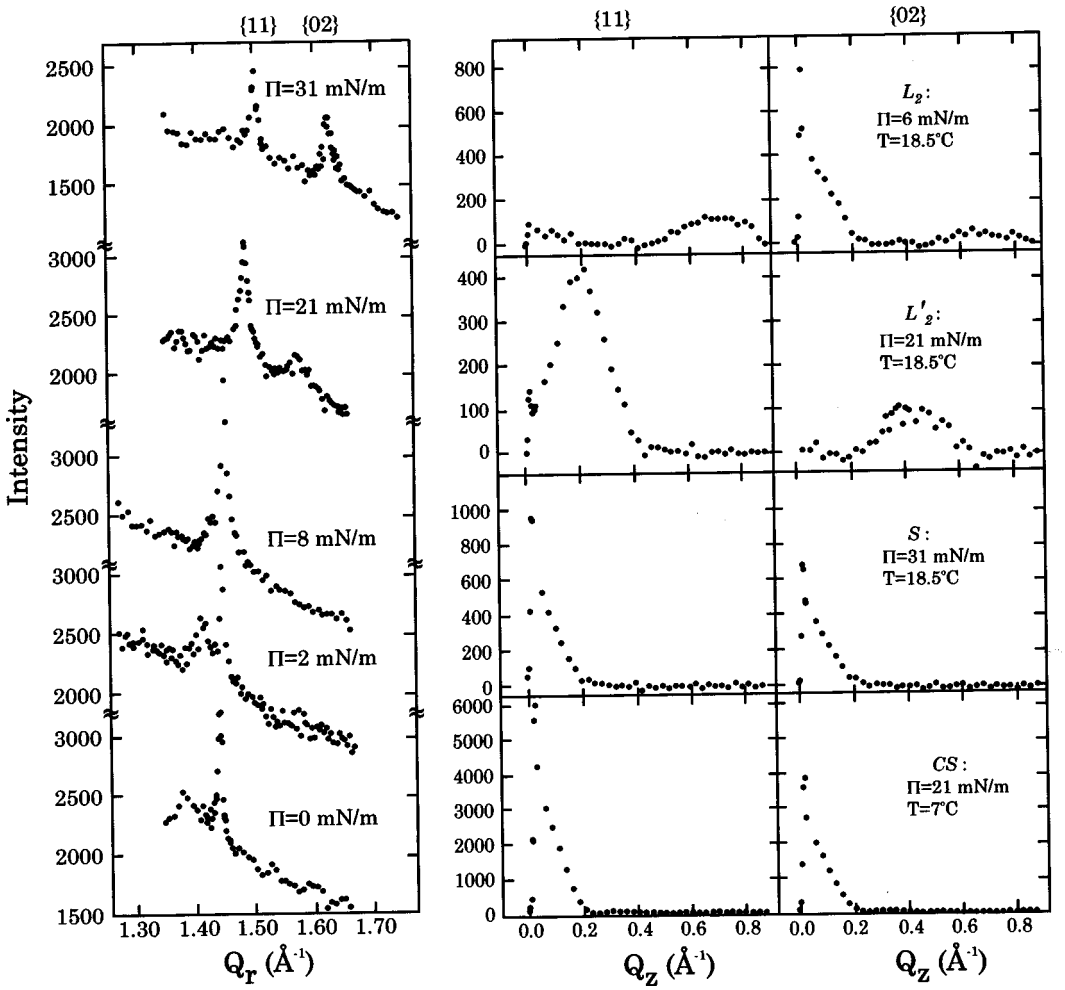

FIG. 9. X-ray scattering intensity as a function of the in-plane (left) and out-of-plane (right) components of scattering vector for the behenic (C_{22}) acid monolayers at 18.5 °C (Kenn *et al.*, 1991).

stretching, so that the tilt acts to decrease the distortion. When the tilt direction is changed to NN at the $L_2'-L_2$ transition, one might expect a further increase of the stretching under the action of tilt. However, in fact the unit cell discontinuously shrinks in the NN direction and its distortion azimuth jumps to NNN. The subsequent continuous decrease of the distortion in the L_2 phase is due to the action of increasing tilt angle. Beyond the intercept where the unit cell is hexagonal in the water plane, the stretching direction is NN. This behavior indicates that not only the tilt direction but also the packing of the backbone planes of the molecules changes discontinuously at the $L_2'-L_2$ transition. The effect of tilt can be excluded by plotting the unit cell parameters in the plane normal to the long axes of the molecules [Fig. 10(b)]. These spacings remain constant within each tilted phase, without any change at the continuous transition $S-L_2'$ and with a jump at the $L_2'-L_2$ transition. The unit-cell parameters in the cross section normal to the chains are explored further in our analysis of packings (Sec. III.D). The tilt magnitude θ, Fig. 10(c), continuously decreases with increasing surface pressure and reaches zero in the S phase.

The high-temperature tilted phases were studied by Durbin *et al.* (1994). The diffraction patterns unambiguously show that the tilt is NNN in the Ov phase and NN in the L_2 phase. The tilt angle is continuous over the transition. The modification of the unit-cell shape, which follows from the peak positions, is illustrated in Fig. 11. The phase LS is the hexatic phase and gives a triply degenerate diffraction peak. At the transition to the Ov phase where the molecules start to tilt in the NNN direction, the peak splits, indicating a symmetrical distortion of the unit cell with stretching in the tilt direction, i.e., the distortion azimuth is NNN. At the $Ov-L_2$ transition the tilt direction changes to NN and the peaks interchange, showing that the unit cell is stretched in the new tilt direction. One can conclude that the distortion here is induced only by tilt and not by ordering of the molecular backbone planes; this conclusion is confirmed below by further analysis of the data. The x-ray data of Durbin *et al.* (1994) show that the $Ov-L_2$ transition occurs without a measurable change in the area per molecule, thus explaining why the transition is never seen in isotherms. However, there is an unambiguous change in symmetry, so that this is a first-order transition.

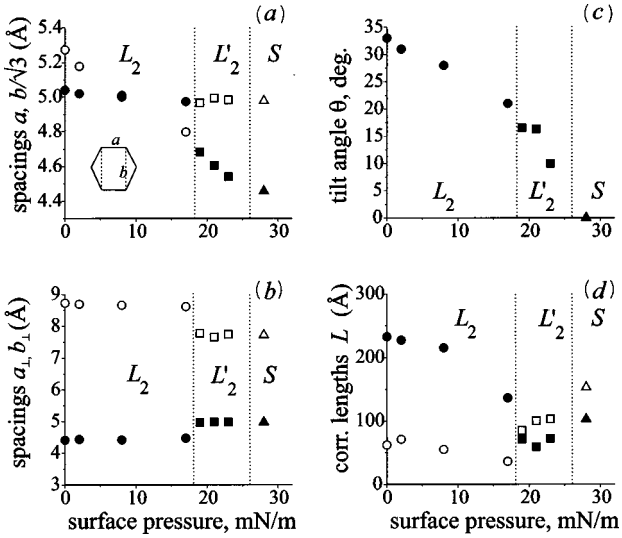

FIG. 10. Lattice spacings of the centered rectangular unit cell (a) in the monolayer plane and (b) in the cross section normal to chains, (c) tilt angle, and (d) the correlation lengths derived from the data of Fig. 9.

To quantify the distortion, one can consider the ellipse passing through six neighbors of a given molecule. Then the distortion can be expressed via the ratio of the main axes of the ellipse, and the distortion azimuth is that of the major axis. In particular, for the rectangular unit cells, the distortion can be represented as $d=\frac{8}{3}(K_{dxy}-K_{nxy})/(K_{dxy}+K_{nxy})$ for NN-tilted phases and $d=\frac{8}{3}(K_{nxy}-K_{dxy})/(K_{dxy}+K_{nxy})$ for NNN-tilted phases (Kaganer *et al.*, 1995). Both the analysis of chain packings in the monolayer phases (Sec. III.D), and the Landau theory of phase transitions (Sec. VI), reveal two sources of unit-cell distortion with respect to the hexagonal: ordering of the backbone planes of the molecules, and tilt. Landau theory predicts that the tilt contribution to the distortion is proportional to $\sin^2\theta$, where θ is the tilt angle. Then, by plotting distortions measured along an isotherm as a function of $\sin^2\theta$ and extrapolating to $\theta=0$, one can separate the contribution due to the

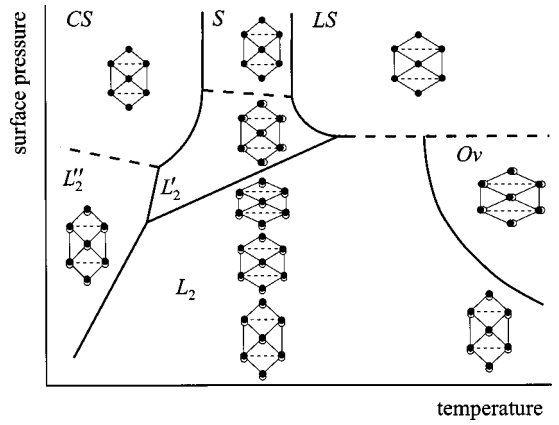

FIG. 11. A phase diagram showing transformations of the unit-cell shape in all phases according to the x-ray-diffraction data.

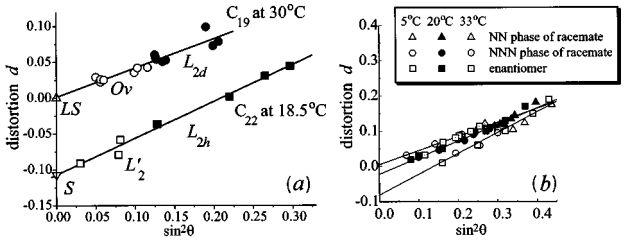

FIG. 12. The unit-cell distortion versus $\sin^2\theta$: (a) fatty acids (data from Kenn *et al.*, 1991 and Durbin *et al.*, 1994); (b) a chiral substance 1-hexadecyl-glycerol (Scalas *et al.*, 1996, 1998). At a given temperature, different phases contribute to a common regression line, confirming the commonality of the structures.

backbone ordering. In Fig. 12(a), the data are plotted in this way. The data points from both tilted phases at a given temperature lie on the same line, suggestive of commonality of structures and confirming the Landau-theory prediction that the distortion induced by tilt is proportional to $\sin^2\theta$. The slope of the lines does not depend on the temperature or the chain length of the acid (Kaganer *et al.*, 1995); this is not true for other substances, however. At high temperatures, the data points for the Ov and L_2 phases lie on the same straight line passing through the origin. Hence the distortion is induced by tilt only. In contrast, the zero-tilt-angle intercept of the lower-temperature line passing the $S-L_2'-L_2$ phase sequence is nonzero. Hence there exists another contribution to the distortion, the ordering of the backbone planes of the molecules.

The effects of backbone ordering can be suppressed by replacing the hydrogens in the alkane chain with fluorines. The fluorocarbon chain makes a helicoid, which is more rigid in comparison with the hydrocarbon chain and carries a much lower density of conformational defects. Barton *et al.* (1992) and Acero *et al.* (1993) studied almost completely fluorinated molecules with carboxylic acid head groups. These monolayers have two phases, a disordered (liquid expanded) phase at large areas per molecule and a hexagonally ordered phase at small areas per molecule. The ordered phase is essentially incompressible and has a small, constant tilt angle. Goldmann *et al.* (1994) and Huang *et al.* (1996) studied semifluorinated molecules, with part of the hydrocarbon groups replaced by the fluorocarbons. The fluorinated blocks always form hexagonal structures, while diffraction peaks attributed to ordering of the hydrocarbons were seen in some cases.

In a tilted state of the monolayer, the uniform two-dimensional compression mainly influences the lattice spacing in the tilt direction [Fig. 10(a)]. Qualitatively, compression of the monolayer in tilt direction occurs by decreasing of the tilt angle, without change of the distances between the hydrocarbon chains, and costs little energy. In contrast, compression in the perpendicular direction requires decrease of the distance between chains and is energetically unfavorable. Fradin *et al.* (1998) performed quantitative measurements of the lin-

ear compressibilities in different phases of fatty acid monolayers. They found that in the tilted phases L_2 and L_2' the compressibility in the tilt direction is about 5 m/N while in the perpendicular direction it is about 0.5 m/N, i.e., an order of magnitude lower. In the phase S, the compressibility remains anisotropic (0.1 and 0.5 m/N in two perpendicular directions), and only the phase CS shows a uniform low compressibility of 0.1 m/N.

D. Local packing and crystalline structures

The positions of the diffraction peaks contain information about the dimensions of the unit cell and about the arrangement of molecules in the unit cell. The problem of determination of Langmuir monolayer structures differs from the classical crystallographical problem in two essential ways. First, the available diffraction data are extremely limited and in some cases consist of first-order diffraction peaks only. Lack of data can be partially compensated for by a knowledge of the packings of the long-chain molecules in bulk crystals. Second, the local packing determined for a mesophase cannot be extended to the long-range length scale, as is routinely done in crystallography, since the range of positional correlations is finite. The symmetry of the local packing, describing relative positions of the molecules within some tens of intermolecular distances, need not coincide with the long-range symmetry governing the thermodynamics of the monolayer. In the present section, we concentrate on the local packing only. The relation between short-range and long-range symmetries of the monolayer phases is discussed in Sec. VI.F.

The parameters of the unit cell in the water plane vary when the surface pressure and hence tilt angle are changed, cf. Fig. 10(a). The parameters of the unit cell in the cross section perpendicular to the long axes of the molecules are much less influenced by tilt, cf. Fig. 10(b), since they are governed by an equilibrium between van der Waals attraction and short-range repulsion of the chains (as well as their rotational and conformational freedom at a given temperature). The packing of the chains can be characterized by the dimensions $a_\perp \times b_\perp$ of a rectangular cell projected onto a plane perpendicular to the chain axes. A distribution of the cell dimensions, extracted from available grazing incidence x-ray-diffraction data on monolayers of nonchiral substances and racemic mixtures, is shown in Fig. 13. An analogous plot was originally proposed by Steitz *et al.* (1991), who compared lattice spacings of monolayers deposited on solid substrates with those of monolayers on the water surface.

All data points of Fig. 13 lie, with some scatter, on a large arc. The middle part of the arc corresponds to nearly hexagonal packing of orientationally disordered molecules at high temperatures. Orientational disorder requires a relatively large area per molecule (20–21 Å^2). Lowering the temperature is accompanied by a reduction in the area per molecule and a concomitant rectangular distortion of the initially hexagonal unit cell. There is no discontinuity in the packing between mesophases and crystalline phases. The two ends of the arc correspond to relatively dense packings of the chains, with projected areas per chain of 18.6 and 19.0 Å^2. The average dimensions of the projected rectangular unit cell $a_\perp \times b_\perp$, containing two molecules, are 5.0×7.5 and 4.4 ×8.8 Å^2, respectively.

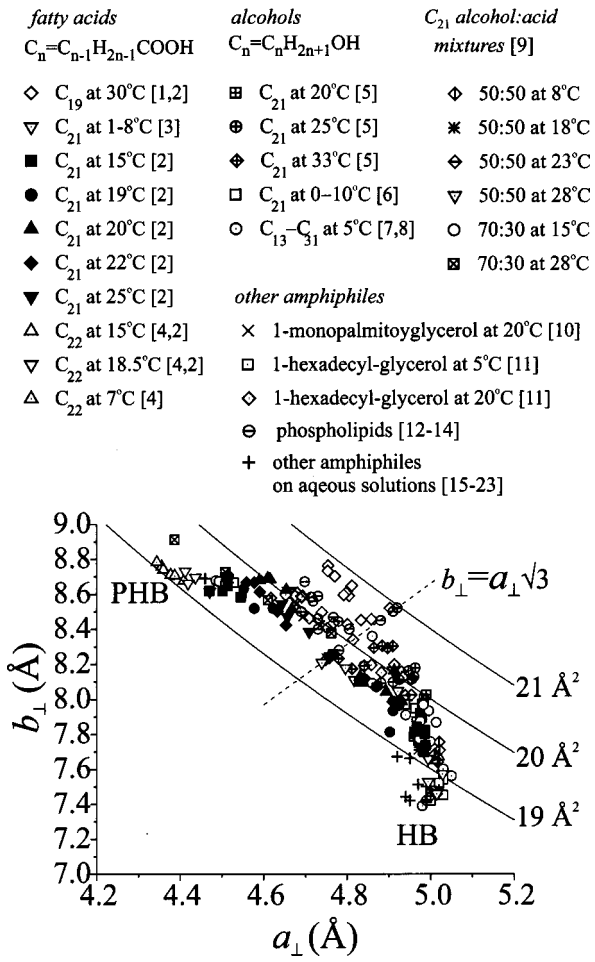

FIG. 13. Distribution of unit-cell parameters $(a_\perp, b_\perp)$ in the cross section normal to chains extracted from the x-ray-diffraction data of various nonchiral and racemic Langmuir monolayers: [1] Durbin *et al.* (1994); [2] Kaganer *et al.* (1995); [3] Lin *et al.* (1990); [4] Kenn *et al.* (1991); [5] Shih *et al.* (1992b); [6] Bohanon *et al.* (1990); [7] Wang *et al.* (1994); [8] Majewski *et al.* (1995); [9] Shih *et al.* (1994); [10] Brezesinski, Scalas *et al.* (1995); [11] Scalas *et al.* (1996); [12] Böhm *et al.* (1993); [13] Brezesinski, Dietrich, Dobner *et al.* (1995); [14] Bringezu *et al.* (1996); [15] Jacquemain *et al.* (1991); [16] Leveiller *et al.* (1992); [17] Weinbach, Jacquemain *et al.* (1993); [18] Weinbach, Kjaer *et al.* (1993); [19] Weissbuch *et al.* (1993); [20] Weissbuch *et al.* (1997); [21] Leveiller *et al.* (1994); [22] Böhm *et al.* (1994); [23] Weissbuch *et al.* (1995). Solid lines correspond to specified values of constant cross-sectional area $A = a_\perp b_\perp/2$ occupied by a single hydrocarbon chain. The dashed line corresponds to the hexagonal projected unit cell with $b_\perp = a_\perp\sqrt{3}$. Labels HB and PHB denote the regions characteristic for herringbone and pseudo-herringbone packing modes, respectively (Kuzmenko, Kaganer, and Leiserowitz, 1998).

The dense molecular packing characterized by the unit cell of dimensions 5.0×7.5 Å^2 is a fingerprint of the

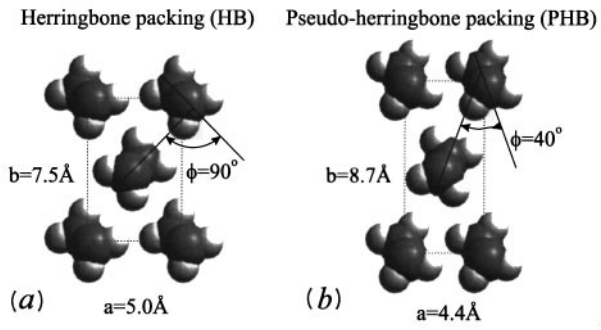

FIG. 14. Packing modes of hydrocarbon chains. (a) herringbone, (b) pseudoherringbone (Kuzmenko, Kaganer, and Leiserowitz, 1998).

herringbone (HB) arrangement, the common packing mode of the hydrocarbon chains in bulk organic crystals (Kitaigorodskii, 1961). Direct confirmation of HB packing has recently been obtained by Durbin *et al.* (1998) in the CS and L_2'' phases of heneicosanoic acid. They see the (12) peak, but they find that the (10) peak is absent. Both peaks are allowed in general if the two sites in a centered rectangular unit cell are not equivalent. However, for HB structure, the (10) peak has zero intensity because the two backbone orientations are symmetrical about the (10) direction. Thus, the failure to see a (10) peak means that the doubling of the unit cell indicated by the (12) peak is due to an HB arrangement. It should be noted that they found no diffraction evidence of herringbone order in the S, L_2, and L_2' phases.

The noticeable difference between the 4.4×8.8 Å^2 unit-cell parameters and those of the standard HB implies a different packing arrangement of the hydrocarbon chains. A search for a possible packing mode that satisfies the 4.4×8.8 Å^2 cell leads to a mode described as implausible by Kitaigorodskii [1961, Fig. 13(b)] because of a lower packing density than that of the HB structure, and which we label as the pseudoherringbone packing mode (PHB). The HB and PHB packing modes are shown in Fig. 14. The PHB motif, as characterized by Kitaigorodskii based on the van der Waals radii of the carbon and the hydrogen atoms, should have an angle of 40° between the backbone planes of the chains. The projected cell parameters of the PHB arrangement as estimated by Kitaigorodskii are $a_\perp=4.2$ Å, $b_\perp=9.0$ Å. The slightly different values shown on Fig. 14 follow from lattice-energy calculations (Kuzmenko, Kaganer, and Leiserowitz, 1998). The majority of densely packed NN-tilted monolayer phases have cell dimensions $a_\perp$ and $b_\perp$ very close to those of the pseudoherringbone motif, which means that this packing is common in 2D amphiphilic systems.

The mechanism of molecular rearrangement during the transition $L_2'-L_2$, where there is a simultaneous change in the packing and in the tilt azimuth, is not clear. A possible mechanism, proposed by Benattar *et al.* (1983) for the smectic-I—smectic-F transition, consists of movement of the grain boundaries containing 5–7 coordinated disclination pairs.

E. Peak widths and anisotropic correlations

Langmuir monolayers are in a crystalline state, characterized by resolution-limited diffraction peaks (Fig. 7), only at low temperatures. The peaks measured at higher temperatures are generally broader than the experimental resolution in the K_{xy} plane. It is worthwhile to note that all existing diffraction measurements on Langmuir monolayers were performed at rather low resolution, and narrow peaks accompanied with diffuse scattering cannot be resolved (Sirota, 1997). New generation synchrotron radiation sources will allow a substantial increase in resolution (at least 50 times, Zakri *et al.*, 1997) and thus make studies of Langmuir monolayers on larger-length scales possible.

As of now, an adequate model to describe the peak shapes is absent. The full width at half maximum (FWHM) of the peak is the only parameter derived from the peak shapes; its interpretation in terms of a characteristic length is ambiguous. Helm *et al.* (1987a) assumed an exponential correlation function $\exp(-r/l)$. Its Fourier transform in two dimensions gives the line shape for a single domain $(l^{-2}+q^2)^{-3/2}$, where $\mathbf{q}$ is the wave-vector deviation from the peak position. After "powder averaging" over random orientations of the domains the line shape becomes Lorentzian, $(l^{-2}+q^2)^{-1}$. A Lorentzian line shape gives better fits to the experimental data than a Gaussian. The correlation length l is related to the FWHM of the peak by

$$l=2/\mathrm{FWHM}, \tag{3}$$

where the FWHM is determined from the measured value $\mathrm{FWHM_{mes}}$ by deconvolution with the resolution $\mathrm{FWHM_{res}}$.

It is customary to perform the deconvolution with the formula $\mathrm{FWHM}^2=\mathrm{FWHM}_{\mathrm{mes}}^2-\mathrm{FWHM}_{\mathrm{res}}^2$. Strictly speaking, this formula is valid only for the convolution of two Gaussian-shaped peaks. Two Lorentzians are deconvolved by $\mathrm{FWHM}=\mathrm{FWHM}_{\mathrm{mes}}-\mathrm{FWHM}_{\mathrm{res}}$. The resolution function is usually close to a Gaussian but the measured peaks are not Gaussians or Lorentzians, so that the use of any deconvolution formula is only approximate. Nevertheless, the FWHM is a quantity characterizing positional order in the monolayer and we shall discuss it in detail.

Leveiller *et al.* (1992) treated the widths of the diffraction peaks as due to finite sizes of the crystalline domains, and determined the average domain size (the "coherence length") L in the direction of the diffraction vector through the Scherrer formula (Guinier, 1968):

$$L\approx0.9\times2\pi/\mathrm{FWHM}. \tag{4}$$

As a result of the discrepancy between Eqs. (3) and (4), the characteristic lengths reported for very similar systems by different research groups may differ by a factor of 3.

A prominent feature of some diffraction patterns from Langmuir monolayers of different substances is a noticeable difference between the widths of the two low-order diffraction peaks, indicating difference in the cor-

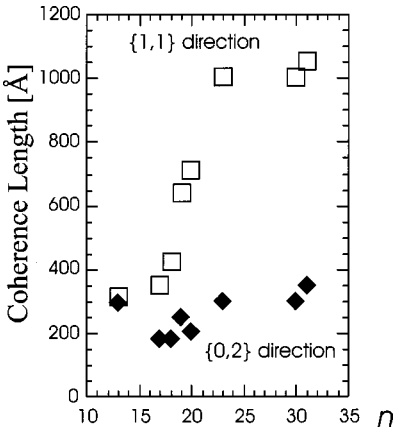

FIG. 15. Correlation lengths L deduced from the FWHMs of the diffraction peaks with the Scherrer formula [Eq. (4)] for alcohols with n (=13 to 31) carbon atoms, at zero surface pressure and 5 °C. The {2,0} reflection (observed for $n=23$, 30, and 31) was resolution limited and thus $L_{20}>1000$ Å (Majewski *et al.*, 1995).

relation lengths in different directions, which is related to the tilt azimuth. A typical example is presented in Fig. 10(d). In the phase L_2, possessing NN tilt, i.e., the tilt along the [10] lattice vector, the narrow (02) peak evidences longer correlations in direction normal to tilt direction. The ratio of the correlation lengths for two reflections measured, l_{02}/l_{11}, typically varies from 3 to 5, with the longer correlation length close to the resolution limit. After transition to the NNN-tilted phase L_2' on increasing surface pressure, the degenerate peak $(11)+(1\bar{1})$ becomes narrower than the nondegenerate peak (02), and one can expect that the higher-order peak (20), if observed, will be even narrower. The correlation length normal to the tilt direction is, again, larger. The phase S shows the same orientational dependence of the positional correlations as the phase L_2', since these phases are related by a continuous tilting transition.

Determination of the longest correlation length in the NNN-tilted phase requires measurement of width of the higher-order peak (20). In the L_2' phase of fatty acid monolayers, this peak has recently been observed for the first time (Durbin *et al.*, 1998), but it is very small and the width cannot be reliably measured. It has also been found in monolayers of alcohols at zero surface pressure; for alcohols, the NNN tilt is realized in the whole range of surface pressures (cf. Fig. 4). Majewski *et al.* (1995) determined the correlation lengths for the long-chain alcohols containing from 13 to 31 carbon atoms at zero surface pressure and the same temperature (Fig. 15). As each additional methylene group shifts the phase-transition temperatures by approximately 5 °C (see Sec. II.D), this study is equivalent to an examination of a single substance in a temperature range of about a hundred degrees. The monolayers of longer chains (or equivalently the low-temperature state of monolayers) reveal significant differences between the coherence lengths of the lowest-order peaks, with the ratio $L_{11}/L_{02}\approx 3$ (higher than that for the corresponding NNN-tilted phase L_2' of fatty acids). More noticeably, the peak (20) was seen for the chain lengths 23 and larger (see also Jacquemain *et al.*, 1991) and found to be resolution limited. Note that again the direction of longest correlations is perpendicular to the tilt direction.

Similar anisotropy of the correlations has been observed in other layered systems of long-chain molecules, such as Langmuir-Blodgett films on solid substrates (Tippmann-Krayer *et al.*, 1992; Sikes and Schwartz, 1997), lamellar Lβ' phases of the oriented multilamellar films (Smith *et al.*, 1990), and tilted hexatic phases of smectic liquid crystals (Brock *et al.*, 1986; Sirota *et al.*, 1987). Neundorf *et al.* (1993) found two distinct smectic phases of a chiral compound with diffraction patterns characteristic for NN-tilted hexatic phase and differing in the x-ray-diffraction peak widths. Most of the diffraction studies of smectics pay little attention to the widths of the peaks. We speculate that the customary treatment of a smectic phase possessing long-range orientational order and NN tilt as smectic I fails to distinguish between two phases, one with isotropic and the other with highly anisotropic positional correlations.

The Landau theory of phase transitions (Sec. VI) provides two possible mesophases with different symmetries, both with hexatic order and the same tilt azimuth, the more ordered phase also possessing one-dimensional periodicity in the layer plane. The anisotropic correlations may be an experimental manifestation of this periodicity (which is not truly long range in the low-dimensional systems). Langmuir monolayers offer better possibilities to study the in-layer phase transitions than smectics, due to direct experimental control of the surface pressure and the richer phase diagram. Some of the monolayer phases, which do not have direct analogues among known smectic categories (cf. Table I), may exist in smectics but have not been discerned as separate phases yet.

Some insight into the structure of the monolayer on an intermediate length scale can be obtained by comparing optical microscopy and the x-ray-diffraction data. According to Brewster-angle microscopy and polarized fluorescence microscopy, monolayers have an uniform tilt azimuth over tens of microns. On the other hand, the x-ray data show that the orientation of the unit cell is fixed with respect to the tilt azimuth. Therefore, on a length scale intermediate between the correlation length of positional order (hundreds of angstroms) and the optical domain size (tens of microns) the monolayer can be treated as a well-oriented texture. It seems most probable that the positional correlations are destroyed by lattice defects which are at thermal equilibrium in a given phase rather than rheology dependent. Indeed, the same anisotropy of positional correlations, with larger correlation length normal to the tilt direction, is observed in monolayers of different substances. As the tilt azimuth changes, the anisotropy of correlations readily and reversibly follows the tilt. Thus we speculate that the anisotropic correlations are due to thermally excited defects, whose nature, concentration, and orientation may depend on the short-range molecular structure of a

given phase. Note that the phases under consideration possess a rectangular, rather than hexagonal, unit cell. Dislocation-mediated melting in such a system should be anisotropic, giving rise to a phase with one-dimensional periodicity on the intermediate length scale, due to creation of dislocations with only one orientation of the Burgers vector (Ostlund and Halperin, 1981).

Thus finite widths of the diffraction peaks in the mesophases of Langmuir monolayers and their strong anisotropy may be due to the presence of one or the other type of dislocations, depending on the direction of the unit-cell distortion, with positional correlations of the dislocations due to elastic interactions between them and possible organization of the dislocations in small-angle domain boundaries. Detailed calculations of the peak profiles in different models and analysis of the experimental peaks are needed to ascertain the structure of Langmuir monolayers on the intermediate length range.

IV. COMPUTER SIMULATIONS

A. Simulations with atomic models of molecules

1. Model systems

The structures and phase transitions in Langmuir monolayers can be modeled by means of computer simulation in two different ways. The models which include all atoms of the molecule (or CH_2 and CH_3 groups treated as ''united atoms'') attempt to simulate the corresponding experimental system as closely as possible. The simplified models, which include only some selected degrees of freedom of the molecules, aim to mimic the essential features related to these degrees of freedom. In this section, we discuss the atomic models. The simplified models are considered in the next section. We focus on general features of the models employed in the simulations and analyze the results of the simulations with reference to our knowledge of the symmetry, structure and behavior of real Langmuir monolayers described in the previous sections.

The molecular models include the Lennard-Jones interaction between pairs of the atoms, a bending potential for each C–C–C segment, and a torsion potential for each C–C–C–C segment. The CH_2 and CH_3 groups are treated, in most of the studies (see, for example, Bareman, Cardini, and Klein, 1988; Harris and Rice, 1988; Karaborni and Toxvaerd, 1992a, 1992b), as single interaction sites (''pseudoatoms'') which can be thought of as the result of averaging over the motion of the hydrogens. Results of simulations with united-atom and all-atom models have some quantitative differences, in particular the values of tilt angles derived from these models (Bareman and Klein, 1990; Moller *et al.*, 1991). Karaborni and Toxvaerd (1992a, 1992b), Karaborni, Toxvaerd, and Olsen (1992), Karaborni (1993a, 1993b), and Schmidt, Shin, and Rice (1996a, 1996b) used the anisotropic united-atom model proposed by Toxvaerd (1990). In this model, the interaction center of a pseudoatom is located at the geometrical center of the group it represents, while the mass of the pseudoatom is located at the carbon nucleus site.

The substrate is not modeled explicitly, but is replaced by a smooth potential. Cardini, Bareman, and Klein (1988) represented the substrate by a flat surface interacting with pseudoatoms via the one-dimensional 3-9 Lennard-Jones potential (the result of integration of the standard 6-12 potential over the half space). This potential was widely employed in subsequent studies (see, for example, Harris and Rice, 1988; Bareman and Klein, 1990; Hautman and Klein, 1990; Collazo, Shin, and Rice, 1992). It is assumed that the head groups are anchored at the interface and the surfactant methylenes are completely insoluble in water. Karaborni and Toxvaerd (1992a, 1992b) proposed, using solubility data, a potential which imposes finite energy walls for methylenes and head groups upon penetrating in and out the water half space. The head-head interactions were treated as purely repulsive, consisting of a strong dipolar repulsion and an excluded volume term. This potential was applied further by Karaborni, Toxvaerd, and Olsen (1992), Karaborni (1993a, 1993b), and Karaborni and Verbist (1994).

The simulation box usually contains up to 100 molecules [at maximum, 256 molecules were included in simulations by Karaborni and Siepmann (1994)]. Periodic boundary conditions are used in most of the studies. We note that not only the area of the simulation box but also its shape are fixed during the simulation. This restriction can significantly influence the behavior of the simulated system, since the translational diffusion of the molecules is negligibly small in the state of aligned chains (Karaborni and Toxvaerd, 1992a; Karaborni, Toxvaerd, and Olsen, 1992). The periodic boundary conditions restrain the unit-cell dimensions to be commensurate with the size of the simulation box. In particular, the ratio $\sqrt{3}/2$ of the box dimensions, frequently applied in the simulations, gives rise to a hexagonal arrangement of molecular heads in the monolayer plane. In contrast, the dense packings of the hydrocarbon chains are characterized by a $\sim 10\%$ distortion with respect to the hexagonal unit cell, with direction of the distortion depending on the type of packing (see Sec. III.D). Therefore the fixed shape of the simulation cell may cause a nonhydrostatic pressure in the simulated system; this has been confirmed by the constant-pressure Monte Carlo simulations on simplified models of the molecules (Haas and Hilfer, 1996), as discussed in the next section. Harris and Rice (1988), and Shin, Collazo, and Rice (1992) also simulated finite clusters of molecules with free boundaries. Despite the limited size of the clusters (100 molecules), the interior of the cluster shows well-ordered periodic arrangements of molecules.

2. Some results

Computer simulations tell us the position of each atom of the simulated system and its time evolution. This is illustrated in Fig. 16, which shows the distribution of methylene-group positions. As the area per molecule

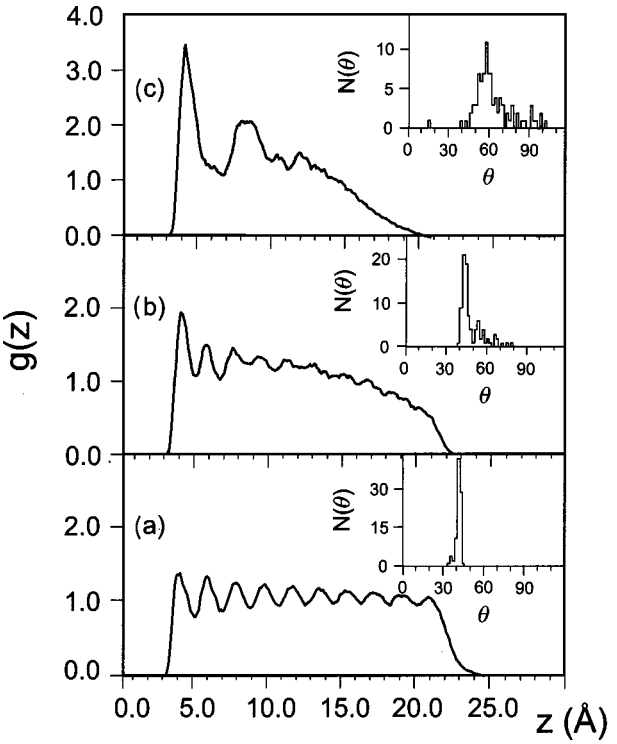

FIG. 16. Density distributions for methylene groups (normal to the substrate) received in the molecular dynamics simulations of an alkyl chains monolayer at surface densities: (a) 21 Å^2/chain, (b) 26 Å^2/chain, (c) 35 Å^2/chain. Insets are the distributions of chain mean tilt angle with respect to the surface normal (Bareman, Cardini, and Klein, 1988).

is increased, the chain disorder and the tilt angles also increase. A large number of average parameters characterizing the static and dynamic properties of the system can be derived from the simulation data. We do not intend to review all results of the simulations. We restrict ourselves to several representative examples giving additional insight into the structures and phase transitions in Langmuir monolayers. Further results of the simulations can be found in the cited papers.

The orientation of an individual molecule is characterized by three angles, describing the tilt angles with respect to the monolayer normal, azimuth of the tilt, and orientation of the backbone plane. The angle $\langle\theta\rangle$ plotted in many simulations is defined as the average angle which the molecular axes form with the surface normal. The tilt angle calculated in this way represents the mean tilt of the individual molecules, but does not distinguish between collective tilt of the molecules in a common azimuthal direction and independent tilt of the molecules in random directions. The order parameter of the collective tilt was introduced by Somoza and Desai (1992) in their molecular model of the tilt phase transition, and employed in the molecular dynamics simulations of Shin, Collazo, and Rice (1993). The results of the simulations show that the azimuth of the collective tilt precesses, while the mean tilt angle remains almost constant.

Precession of the tilt azimuth is observed in many simulations. Figure 17 presents two snapshots made with

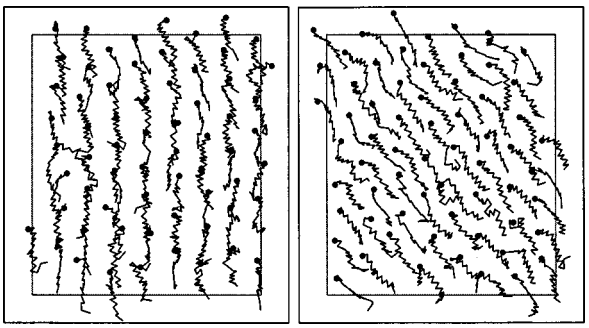

FIG. 17. Two snapshots of the simulated monolayer demonstrating (a) the NN tilt after 20 000 time steps and (b) the NNN tilt after 40 000 time steps (Karaborni and Toxvaerd, 1992b).

some time interval during the same simulation run. The first snapshot clearly shows an NN tilt, while the second one shows an NNN tilt. For simulations performed at larger areas per molecule, the tilt azimuth is well defined. Siepmann and McDonald (1993) found, in a Monte Carlo simulation of a large system (224 molecules), a coexistence of domains with different tilt azimuths separated by walls where the molecules contained more conformational defects than elsewhere. These indicate a small difference between the energies of NN- and NNN-tilted states. One can speculate that the hexagonal arrangement of the molecules due to the fixed simulation cell shape decreases the barrier between the two states and simplifies reorientational jumps between them.

The orientation of the backbone plane of the molecule can be characterized by the orientation of the vector $\mathbf{R}$ defined as $\mathbf{R}=\Sigma_i(-1)^i\mathbf{r}_i$, where $\mathbf{r}_i$ is the vector from the ith to the $(i+1)$th carbon of the molecule; the multiplier $(-1)^i$ is introduced to take into account the zigzag arrangement of the hydrocarbon chain (Hautman and Klein, 1989). We have omitted here, for simplicity, some multipliers of the original formula. The probability distribution of the angle between the vector $\mathbf{R}$ and the surface has sharp peaks at low temperatures and a weak angular dependence at high temperatures, indicating a transition to the free-rotator phase. The relaxation time of the correlation function $\langle\mathbf{R}(t)\cdot\mathbf{R}(0)\rangle$ also quickly decreases upon a transition to the rotator phase (Hautman and Klein, 1990).

Translational order in the monolayers was characterized in the simulations by the structure factor $S(\mathbf{k})=|\Sigma_j\exp(i\mathbf{k}\cdot\mathbf{r}_j)|^2$, where $\mathbf{r}_j$ is the position of jth atom and the summation runs over all atoms of the system. Figure 18 shows a drastic change of the calculated structure factor due to melting of the chains. The structure factor at an area per molecule of 24 Å^2 is indicative of a crystal structure. Upon expansion of the monolayer to 25 Å^2/molecule, the peak heights decrease drastically, the peak positions are no longer well defined and form a ring, implying disappearance of the periodicity. The number of gauche defects and the number of disclinations, determined by the Voronoi polygon construction, grows rapidly at the transition (Karaborni, 1993a, 1993b). The widths of the peaks in the ordered phases

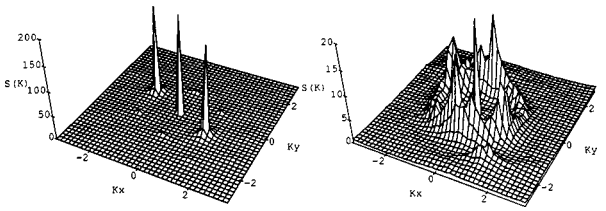

FIG. 18. Structure factors $S(k_x,k_y)$ of (a) the simulated monolayer at 24 Å^2/chain and (b) the simulated monolayer at 25 Å^2/chain (Karaborni, 1993a).

are limited by the size of the simulation cell. Therefore all phases of Langmuir monolayers with correlation lengths of translational order exceeding a half dozen spacings are treated as crystalline in the simulations. Simulation of hexatic order needs much larger simulation cells (see Strandburg, 1988, for a review) and cannot be performed with flexible molecules consisting of 15–20 atoms. This can be done with simplified models of the molecules (see next section).

All these simulation studies restrict the structure factor calculation to wave vectors $\mathbf{k}=(k_x,k_y)$ lying in the monolayer plane. For example, Fig. 18(a) presents the structure factor for the NN-tilted phase. The two strong peaks of $S(\mathbf{k})$ at $\mathbf{k}\neq 0$ are the in-plane peaks, while the four weak peaks are in fact traces of the out-of-plane peaks, cf. Fig. 5(d). Two of them are located above the substrate, $k_z>0$, and two below it, $k_z<0$. These peaks are expected to be as strong as the in-plane peaks.

Collazo, Shin, and Rice (1992) and Shin, Collazo, and Rice (1992) simulated completely and partially fluorinated monolayers with a united-atom model using potential parameters different from those used for hydrocarbon groups. The fluorinated amphiphiles are more rigid and have a much lower concentration of gauche defects, Fig. 19. Even and odd members of the series, at the same temperature and surface pressure, tilt in different directions, NNN and NN, respectively. Simulations give a hexagonal packing of the molecules, even at an area per molecule as large as 70 Å^2. In the latter case, the molecules arrange in a cluster inside the simulation cell. Shin, Collazo, and Rice (1993) improved the model by changing the dihedral potential to mimic the helical structure of the fluorinated chain. Schmidt, Shin, and Rice (1996a, 1996b) determined the probability distributions of the relative orientations of the short axes of neighboring molecules (determined as principal axes of the inertia tensors of the molecules). The distributions are peaked at $\pm 90°$, as expected for herringbone packing, despite the helical shape of fluorinated chains.

Siepmann, Karaborni, and Klein (1994) performed simulations of the phase equilibrium between liquid and gaseous phases. The Monte Carlo simulations were carried out in two coupled simulation boxes in parallel. Monte Carlo rules which allow for changes in the number of particles and the volume ensure that the two boxes are in thermodynamic equilibrium with each other. Because the two boxes are not in direct contact, there is no interface, and the bulk properties can be determined with a surprisingly small number of particles.

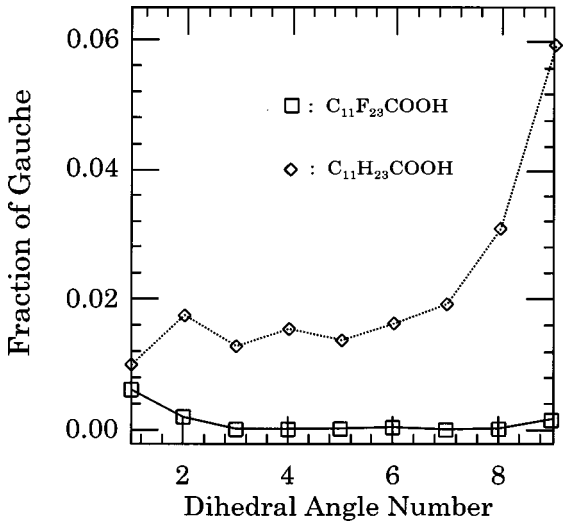

FIG. 19. Distribution of the gauche bonds in a fluorinated monolayer and its hydrocarbon analog simulated at the same temperatures and surface pressures (Collazo, Shin, and Rice, 1992).

Peters *et al.* (1994, 1995, 1998) simulated monolayers of a more complicated substance, a diglyceride, whose molecules contain two hydrocarbon chains. They found two pressure-induced phase transitions. One is the tilting transition, confirmed by both isotherm and x-ray-diffraction data. The other transition, which was found in the isotherms but not in x-ray diffraction, was found to be due to changes in the packing of the ester groups of untilted molecules. At high surface pressure, when alkyl chains are close packed, both ester groups cannot simultaneously be in contact with the water phase. Upon expansion, sufficient space is created that both ester groups can be exposed to water simultaneously.

B. Simulations with simplified models of molecules

1. Energy minimization

Some particular features of structure and behavior of Langmuir monolayers can be understood with simplified models, which neglect some of the degrees of freedom of the molecules. The models considered in this section employ computer simulations as a primary tool. Analytical models are discussed in the next section.

The low-temperature structures of Langmuir monolayers are governed by dense packing of the chains. They can be found by neglecting thermal effects, as well as interactions of the polar heads of the molecules between each other and with water. Jacquemain *et al.* (1992), Leveiller *et al.* (1992), Wang *et al.* (1994), Swanson, Luty, and Eckhardt (1997), and Kuzmenko, Kaganer, and Leiserowitz (1998) calculated the energies of two-dimensional crystals of hydrocarbon and fluorocarbon chains for different symmetries of crystals. In this way, the energy can be found as a function of one of the parameters characterizing the packing, while other pa-

rameters are either fixed at the values determined from the experiment, or allowed to relax to minimize the energy with the given symmetry constraints.

The lattice-energy calculations alone are not sufficient to predict even the low-temperature structure, since they neglect the head-head and head-water polar interactions. Generally, the calculations provide several minima, and one of them (not necessarily the deepest one), possessing unit-cell parameters close to the experimental data, can be attributed to packing of the chains in the modeled monolayer. In this way, the two chain packings commonly realized in monolayers of various aliphatic chain derivatives, herringbone (HB) and pseudoherringbone (PHB), Figs. 14(a) and (b), were found in Sec. III.D.

Packings of the backbones have not been adequately taken into account in molecular dynamics simulations of atomic models. Hautman and Klein (1990) chose starting configurations in the molecular dynamics simulations by calculating the energies of the states with parallel and antiparallel backbones on a hexagonal lattice. Moller *et al.* (1991) minimized the energy of the chains fixed on a hexagonal lattice with one molecule per unit cell. Neither the dense packings of the chains (Fig. 14), nor the accompanying distortion of the lattice, which is as large as 10%, were taken into account.

2. Models for the tilting transitions and backbone ordering

At high temperatures, the molecules independently rotate about their long axes and can be treated as axially symmetrical. Kreer, Kremer, and Binder (1990), Scheringer, Hilfer, and Binder (1992), and Haas, Hilfer, and Binder (1995, 1996) performed constant-area Monte Carlo simulations on the model molecules consisting of a small number (5 to 7) of effective spherical monomers, grafted on the plane by the end. The first papers assumed that the molecules are rigid and grafted onto a lattice, and the later ones considered semiflexible molecules whose heads are allowed to move along the plane. The zigzag arrangement of the carbons and the torsion energy were excluded from the model. Simplifications of the molecular model allows an increase (by an order of magnitude) in the number of the simulated molecules, and thus an investigation of the dependence of the simulated system on temperature and mean density in more detail. The simulations give a phase transition from an untitled to a tilted phase. The surface pressure was found to be anisotropic in the tilted phase, the pressure component in the tilt direction being consistently higher than the component in the direction perpendicular to the tilt. The constant-pressure Monte Carlo simulations (Haas and Hilfer, 1996) give a large (15–20 %) distortion of the simulation box. They reveal the same sequence of phases as constant-area simulations, but the phases appear in a much narrower temperature range. Further constant-pressure simulations of the flexible chains by Schmid, Stadler, and Lange (1997) showed that the phase diagrams, in particular the tilt azimuth in the condensed phase, depend on the size of the head group.

Even simplified models of the chains do not allow researchers to find a transition between hexatic and crystalline phases. The latter problem requires an enormous simulated system, and is not resolved ultimately even for the simplest purely two-dimensional systems of isotropic particles (see Strandburg, 1988, for a review). Purely two-dimensional models of noncircular particles, representing projections of the molecules along their long axes onto the monolayer plane, can be used to study the ordering of the backbone planes of the molecules. Swanson, Hardy, and Eckhardt (1993) and Gibson *et al.* (1997) used a model potential possessing fourfold symmetry and found a first-order transition between phases of rotationally ordered and disordered particles. The disordered phase is characterized by short-range positional and quasi-long-range bond orientational (hexatic) order. The fourfold symmetry of the employed potential does not reproduce the herringbone ordering, which needs a twofold symmetry.

V. MOLECULAR MODELS

A. Tilting transitions

The complicated phase diagrams of Langmuir monolayers are the result of interplay between the different degrees of freedom of amphiphilic molecules. The simplified molecular models take into account only some of them, with the aim of giving some qualitative insight into particular aspects of the behavior of the system.

The features of tilting phase transitions can be understood with models treating the molecules as cylindrical rods grafted on a two-dimensional lattice. Cylindrical rods represent rotationally disordered chains in the high-temperature condensed phases. The rods are put on a lattice, hexagonal or distorted hexagonal, reflecting the presence of (albeit short-range) translational order in the hexatic phases. Models of cylindrical rods were considered by Safran, Robbins, and Garoff (1986), Cai and Rice (1990, 1992), Kaganer, Osipov, and Peterson (1993), Balashov and Krylov (1994), Shin and Rice (1994), Schmid, Johannsmann, and Halperin (1996), Wang and Gong (1996), and Schmid and Lange (1997). Swanson, Hardy, and Eckhardt (1996) studied a closely related model of ''beaded strings.'' We will discuss first the common qualitative picture of the tilting phase transition, which follows from these papers, and then mention the differences between particular models.

Consider cylindrical rods which experience a long-range attraction and a short-range repulsion. There is an equilibrium mean distance between the rods. Standing upright on a plane and preserving this distance, the rods arrange in a densely packed hexagonal 2D crystal [Fig. 20(a)]. The compressibility of this system is very low, due to short-range repulsion of the rods. The expansion of the hexagonal lattice is an external action in the framework of the model, which is treated as a result of the repulsion of the polar heads (not included explicitly in the models). When the lattice spacing increases, the energy of the system of untitled rod increases, due to the

FIG. 20. (a) Untilted monolayer; (b) uniformly tilted monolayer; (c) a micellar cluster (after Safran, Robbins, and Garoff, 1986).

long-range attraction between them. The energy can be reduced, if the molecules tilt and thus decrease the distance between them to the equilibrium distance [Fig. 20(b)]. If the lattice is constrained to be hexagonal and the rods tilt in direction to the nearest neighbor (NN), the distance to two of the six neighbors can be optimized, while the distance to the four "side" (with respect to tilt azimuth) neighbors is not optimal. In contrast, the NNN tilt (in direction between the nearest neighbors, to the next-nearest neighbor) optimizes the distance to four neighbors. As a result, the transition from untilted to tilted rods on the hexagonal lattice occurs in the NNN direction. In the tilted state, Fig. 20(b), the end parts of the rods are exposed to "air" and "water," instead of the contact to another rod in the untilted state. Depending on the details of the interaction potential, a small tilt angle might be unfavorable. As a result, the order of the transition depends on the model potential.

If the lattice is allowed to distort, the distances to all six neighbors can be optimized. In the limit of very long rods, when the effects of the rod–"air" and rod–"water" interfaces are neglected, the tilted state preserves hexagonal packing of the rods with equilibrium distances between them in the cross section perpendicular to the long axes of the rods. In this limit, variation of the area per molecule in the monolayer plane changes the tilt angle, but does not influence the state inside the bulk of the monolayer. The models support the small internal pressure derived from the experimental data [Eq. (2)]. The tilt azimuth and the transition order are governed by the interfacial energies and depend on the model potential.

Temperature effects, treated in different ways in the papers cited above, do not qualitatively change the general picture. Cai and Rice (1992) and Wang and Gong (1996) calculated the entropy in terms of phonons in the 2D crystal of rods. The entropy considered by Kaganer, Osipov, and Peterson (1993) is due to motion of a rod in the hard-core repulsive potential of the six neighbors fixed in the mean positions. Balashov and Krylov (1994) considered a similar problem with the Lennard-Jones potential. The polar interactions between the heads of the molecules, although discussed in the literature (Andelman, Brochard, and Joanny, 1987; Urbakh and Klafter, 1993), were not included in models of the tilting transition. The size of the headgroups, which can exceed the diameter of the rods, imposes an additional restriction to the packing of rods. Safran, Robbins, and Garoff (1986) discussed a nonuniform tilt, Fig. 20(c), which can be realized in surface micelles. Schmid and Lange (1997) noted that the increasing size of the head group can result in a change of the tilt azimuth.

B. Backbone ordering

A model for ordering of the molecular backbones can be constructed by projecting the molecule on the plane along its long axis. Such a model was developed the first time by Meyer (1975, 1976) to describe the transition between smectic B and E phases in liquid crystals. He showed that the interactions between the molecules can be modeled by a potential of the quadrupole-quadrupole type:

$$u\cos(2\phi_1+2\phi_2-4\theta_{12})+v\cos(2\phi_1-2\phi_2), \tag{5}$$

where ϕ_1 and ϕ_2 are the orientations of the backbones of the two molecules and θ_{12} is the orientation of the radius vector connecting their centers. For the pure electric quadrupole-quadrupole interaction, the ratio of the coefficients is $u/v=35/3$, and the first term completely dominates. For molecules arranged on a hexagonal lattice, the herringbone structure minimizes the energy Eq. (5). Felsteiner, Cabib, and Friedman (1978) described all other structures resulting from arbitrary ratios u/v.

Berlinsky and Harris (1978) and Harris and Berlinsky (1979) included the coupling to the crystal field of the substrate to describe the ordering of diatomic molecules adsorbed on a surface. In the mean-field approximation, the herringbone ordering transition is continuous. Chacón and Tarazona (1989) took correlations into account by applying the cluster variational method. They showed that the transition remains continuous, but the transition temperature is significantly reduced and agrees much better with the results of computer simulations. Tarazona and Chacón (1989) argued that long-range fluctuations induce a first-order phase transition instead of the continuous one predicted by mean-field theory. A later computer simulation (Cai, 1991) gives a continuous transition, however. Schofield and Rice (1995) compared different approximations of the density functional theory to describe the herringbone ordering transition.

Luty and Eckhardt (1995, 1996) treated the phase transitions in Langmuir monolayers in terms of multipolar interactions of the molecules placed on a hexagonal lattice. The free energy found in this microscopic model can be related to the one derived by Kaganer and Indenbom (1993) from a symmetry point of view. Swanson, Luty, and Eckhardt (1997) used the atomic model of the molecules to calculate the energy of the uniformly strained lattice; possible packings of the backbones were taken into account in this way. Then the partition function was calculated by integrating over the strains, thus neglecting fluctuations.

We note that all papers cited above are severely restricted by the use of lattice models, i.e., the mass centers of the molecules are assumed to be fixed on a hexagonal lattice and the transition occurs between orientationally disordered and ordered states in the translationally ordered system. This model is adequate for monolayers of diatomic molecules which are adsorbed in structures commensurate with the crystalline substrates. The experimental data on Langmuir mono-

layers (Sec. III) and the Landau theory (Sec. VI) show that in the latter system translational and orientational ordering occur simultaneously, which demands off-lattice models for herringbone ordering.

C. Fluid-fluid transitions

Although this is outside the main line of present review, we discuss briefly here some models for the gas–liquid-expanded–condensed phase transitions. The challenging problem is to explain two successive fluid-fluid transitions in Langmuir monolayers. Halperin *et al.* (1987) and Chen *et al.* (1988) showed that a system of rigid rods grafted on a plane does not experience an orientational (''standing-up'') transition if the rods interact via hard-core repulsions only. A second-order transition is not possible due to presence of the plane, which breaks 3D-rotational symmetry: the orientations of the grafted rods are limited by the upper half-sphere, and thus the monolayer system cannot be completely orientationally disordered. Absence of a first-order transition is a consequence of the solely hard-core repulsive interaction. Costas *et al.* (1992), Kramer *et al.* (1992), Somoza and Desai (1992) proposed models which include attractive interactions between the rigid rods and give two phase transitions. One of the transitions can be treated as a gas-liquid transition and the other one as a tilting transition.

Molecular theories of the gas–liquid-expanded–condensed phase sequence for the monolayers of flexible chain molecules were developed by Popielawski and Rice (1988), Cantor and McIlroy (1989a, 1989b), Shin, Wang, and Rice (1990), Szleifer, Ben-Shaul, and Gelbart (1990), Schmid and Schick (1995), and Schmid (1997). A common qualitative picture, which follows from different models, is the following. In the gaseous phase, the chains are conformationally disordered, and the molecules move freely. At the gas–liquid-expanded transition, the loss of translational entropy is compensated by the gain in attraction energy. The gas condenses, while the conformational disorder of individual molecules is preserved. At the second transition, the liquid-expanded–condensed, the chains stretch, and the loss of configurational entropy is compensated by the gain in attraction energy due to the closer contact between the chains. Schmid and Schick (1995) and Schmid (1997) showed that the two phase transitions occur only for sufficiently flexible chains: the increase of rigidity gives rise to a single transition from the gaseous to the condensed phase.

VI. LANDAU THEORY OF PHASE TRANSITIONS IN MONOLAYERS

A. Types of ordering

1. Orientational ordering

We will first consider the possible types of ordering in monolayers of long-chain molecules from the standpoint of symmetry. The degrees of freedom of an individual molecule are sketched in Figs. 21(a)–(c). The molecules are assumed to be conformationally ordered in all condensed phases. When molecules freely and independently rotate about their long axes, they can be treated as cylindrical rods. In the highest symmetry condensed phase, the heads of the molecules form a 2D liquid. Note that even in this state there is an alignment of the long axes of the molecules in the direction normal to the monolayer plane. This nematic order is present in all phases under consideration and will not be mentioned again. The 2D liquid phase of conformationally ordered molecules is not realized in Langmuir monolayers of aliphatic compounds and the most symmetrical observed phase is the hexatic phase [Fig. 21(d)]. Such a phase possesses sixfold orientational order of the intermolecular bonds connecting the neighbor molecules, while the translational order is short range.

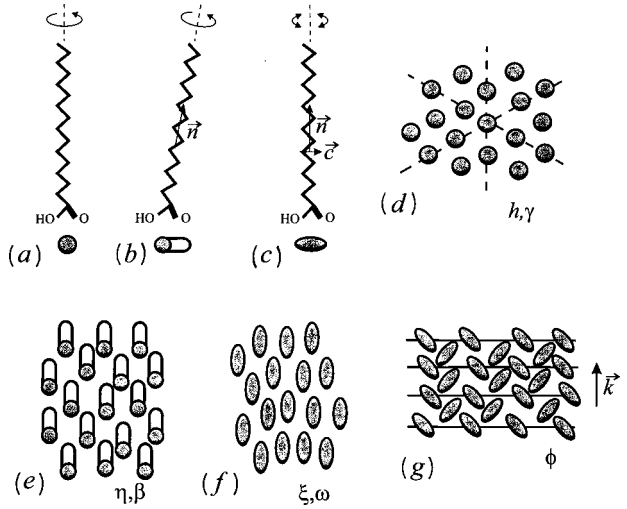

FIG. 21. Molecular degrees of freedom and ordering: (a)–(c) degrees of freedom of the individual molecules; (d) hexatic order; (e) collective tilt; (f) parallel ordering of the backbones in a 2D nematic; (e) crystallization in one direction in a herringbone structure. The letters in (d)–(g) denote corresponding order parameters.

Tilt of the effective cylindrical rods is sketched in Figs. 21(b) and (e). When tilt occurs in the hexatic phase, the tilt azimuth is not arbitrary but related to azimuth of the hexatic. Two symmetry-related tilt directions are along hexatic bonds (to the nearest neighbor, NN) or between them (to the next-nearest neighbor, NNN). An intermediate tilt azimuth is also possible.

Hindered rotation of the molecule (upon decreasing the temperature) gives rise to a definite orientation of its backbone plane (plane of the carbon skeleton, the short axis of the molecule) [Fig. 21(c)]. We do not distinguish here between the two states of the molecule differing by a 180° rotation about its long axis. The order of the backbones parallel to each other, Fig. 21(f), is a 2D nematic order in the monolayer plane. The azimuth of the 2D nematic is not arbitrary with respect to the hexatic azimuth: the two symmetry-favored directions are NN and NNN, and an intermediate azimuth is also possible. When the molecules order in the way shown in Fig.

21(f), the lowest-order peak in the scattering pattern of the liquid or the hexatic phase splits into two peaks, reflecting ''long'' and ''short'' distances between neighboring molecules. In describing x-ray-diffraction experiments, the splitting is usually referred to as a distortion of the unit cell. Although the term ''unit cell'' cannot be rigorously applied to noncrystalline phases, it provides an easily understood description of the diffraction data. There is no potential for misunderstanding from the use of this terminology, and we shall use it below. In fact, the nematic order parameter in these mesophases corresponds to the distortion in crystalline phases.

Considering the tilted free-rotator state of Fig. 21(b) more precisely, one finds that the orientations of the backbone plane in the tilt direction and perpendicular to it are not equivalent, and hence tilt induces some parallel alignment of the backbones. This effect is experimentally observed as a splitting of the diffraction peaks in the tilted hexatic phases, which increases with increasing tilt angle (Durbin *et al.*, 1994). Two orientations of the head of the molecule differing by a 180° rotation about the long axis of the molecule also become nonequivalent in the tilted state. Thus tilt induces orientational order of the molecular heads. The tilt and ordering of the heads are not distinguishable from the standpoint of symmetry: Fig. 21(e) can equally represent tilt or orientations of the heads. Therefore we do not consider the ordering of the heads separately.

The hexatic, tilt, and 2D nematic are orders of the monolayer system with respect to orientation (either individual molecules or intermolecular bonds) which preserve translational disorder on the long-range length scale. The azimuths of all these types of order are not independent but coupled to each other. The actual relative orientations depend on molecular interactions and cannot be derived from symmetry arguments only.

2. Translational ordering

Translational ordering, i.e., the appearance of periodicity in the monolayer, can be considered in the framework of Landau theory as a ''weak crystallization.'' Initially Landau (1937) considered the amplitudes of density waves as components of the order parameter and showed that the transition from liquid to crystal is first order. In the 2D case, the resulting structure is a 2D hexagonal crystal, due to an equilateral triangle formed by three wave vectors of equal length. A first-order transition from 2D liquid or hexatic to a hexagonal crystal is not observed in Langmuir monolayers of aliphatic molecules. However, the amplitude of the density wave is not the only possible crystallization order parameter in the Landau theory (Marchenko, 1991).

Figure 21(g) illustrates the alternative type of order parameter. Here the molecules are arranged in equidistantly spaced rows (with liquidlike order in the rows) and have preferred orientation of the backbones in each row. The system can be transferred to itself by a translation by one row (i.e., by half of the period) with subsequent reflection about the wave-vector direction. In other words, the system possesses glide symmetry in the direction of the wave vector. This type of order can be called herringbone, by analogy with the crystalline structure. The same symmetry corresponds to the antiferroelectric order of transverse dipoles. The free-energy expansion over powers of this order parameter does not contain a third-order term, since this term changes sign on reflection. Hence the transition can be continuous. The number of waves involved in the crystallization is not related to construction of an equilateral triangle, and the transition can result in only one wave of the herringbone order (Kaganer and Loginov, 1993, 1995).

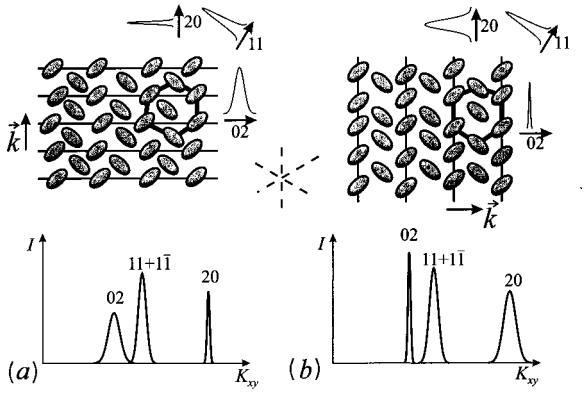

FIG. 22. Crystallization waves (a) along and (b) normal to orientation of the hexatic bonds and corresponding diffraction patterns. The solid lines denote equidistantly spaced rows of the molecules, with liquidlike order within each row. Narrow diffraction peaks correspond to the directions of the normals to the rows. A star of broken lines in the center of the figure shows orientation of the hexatic order, which is the same in both cases.

When the transition occurs from the hexatic phase, the direction of the wave vector is not arbitrary but related to the azimuth of the hexatic. Two symmetry-related directions are along and normal to the bonds (NN and NNN, respectively). Figure 22 sketches the structures of the phases with periodicity along and normal to the hexatic azimuth. There is no periodicity of the molecular positions within the periodically spaced rows. However, the short-range order is preserved: the molecules are mostly surrounded by six neighbors. Dislocations and disclinations which, in fact, destroy periodicity inside the rows, are not shown on the figure since the number of molecules is not large enough.

The wave vector of the herringbone wave is in the NN direction in Fig. 22(a) and in the NNN direction in Fig. 22(b). The short-range order in the positions of the molecules gives rise to broad diffuse peaks in the x-ray scattering pattern. One-dimensional periodicity narrows some peaks. When the monolayer enters the two-dimensional crystal phase at lower temperatures, all other peaks narrow, while their positions change only slightly since the local arrangement of the molecules does not change. Then the diffuse peaks of the mesophases can be labeled in terms of the diffraction peaks of the crystal, as discussed in Sec. III.B.

In the phase sketched in Fig. 22(b), the periodic rows of molecules contain intermolecular bonds connecting the neighbor molecules. Diffraction from the rows gives rise to the narrow nondegenerate peak (02). Periodicity in other directions is destroyed by the translational disorder within the rows, giving rise to the broad scattering peaks. The peak in the direction along the rows is expected to be the broadest one. In contrast, Fig. 22(a) represents the phase where all lowest-order peaks are broad due to translational disorder in the rows. The periodicity gives rise to the narrow higher-order peak (20). Comparing the expected scattering patterns of the one-dimensional crystals of Figs. 22(a) and (b) with the observed patterns discussed in Sec. III, one can attribute the wave in the NN direction [Fig. 22(a)] to the phases S and L_2', while the NNN-directed wave of Fig. 22(b) corresponds to the phase L_2.

All types of order parameters discussed above are characterized by their strengths and azimuths. The azimuths of each pair of order parameters are coupled. For example, tilt and appearance of periodicity along hexatic bonds or normal to them cost different energies. Tilts in the herringbone-ordered structures of Fig. 22 along the rows and normal to them also differ energetically. Both tilt and herringbone order cause distortions in the directions related to their orientations. The interplay between different types of order results in the complicated phase diagrams of Langmuir monolayers. The Landau theory of phase transitions in Langmuir monolayers proposed by Kaganer and Loginov (1993, 1995) treated the transitions between condensed phases as a result of successive ordering of the hexatic phase. The phase diagrams were explained by using three coupled order parameters, with one of the parameters governing the collective tilt of the molecules and the other two describing appearance of periodicity in NN or NNN directions, respectively. The phases L_2' and L_{2h} were treated as two independent ways of ordering. Recent experimental data, in particular on the fatty acid—alcohol mixtures (Fig. 4) and chiral monolayers (Sec. VII) indicate a more close relationship between these phases. Below we present a generalized variant of the theory, which considers the ordering starting from the symmetry of an isotropic two-dimensional liquid. This approach allows us to relate phases initially treated as independent.

B. Symmetry of phases

In this section, we give a qualitative description of the phases and phase transitions in terms of symmetry changes. Quantitative arguments, based on the free-energy expansions, are presented in the next sections. The theoretical phase diagram, Fig. 23, is constructed to simultaneously satisfy the symmetry requirements of the Landau theory and the thermodynamical and structural data on fatty acid monolayers (cf. the experimental phase diagrams, Fig. 3). The most symmetrical condensed phase present in the phase diagram, the high-temperature high-pressure phase LS, is treated as the untilted hexatic phase. As we have already discussed in

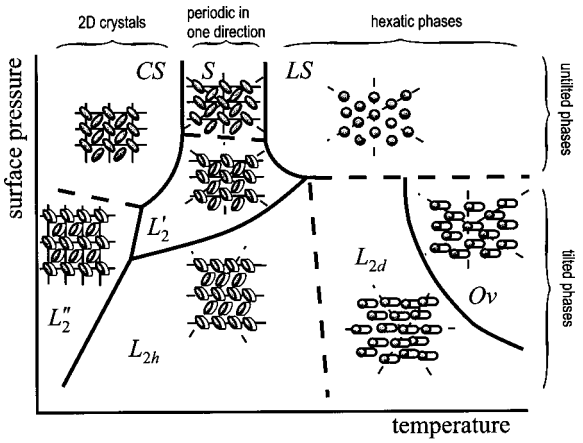

FIG. 23. Theoretical phase diagram of Langmuir monolayers. Solid lines represent first-order transitions and broken ones second-order transitions.

Sec. III.C, there is no direct unambiguous experimental proof for the hexatic structure of the phase LS. This phase is optically isotropic and possesses equal mean distances between all neighbor molecules. Rather narrow diffraction peaks rule out a 2D liquid, but the choice between the hexatic and the 2D hexagonal crystal cannot be made unambiguously with the existing low-resolution diffraction data. The Landau theory presented here treats the phase LS as hexatic, which seems a more suitable choice from the standpoint of both experiment and theory. In fact, the essence of the theory is not sensitive to the difference between a hexatic and a 2D hexagonal crystal. The theory was formulated initially in terms of phase transitions between crystalline phases (Kaganer and Indenbom, 1993) and then reformulated in terms of hexatic phases (Kaganer and Loginov, 1993, 1995) using essentially the same free-energy expansions.

The two main modes of ordering of the phase LS are tilt (upon decreasing surface pressure) and ordering of the backbone planes (upon decreasing temperature). For symmetry reasons, we subdivide the phase L_2, which is observed as a single phase in experiments, into two phases L_{2d} and L_{2h}, possessing disordered and herringbone-ordered backbone planes, respectively. Two tilted hexatic phases L_{2d} and Ov differ in their tilt azimuth (NN and NNN, respectively). Both tilted hexatic phases possess a distortion (or, more appropriate for noncrystalline phases, a 2D nematic order) in the tilt direction.

The transition $LS-S$ upon decreasing temperature is due to ordering of the backbone planes (short axes) of the molecules, revealed experimentally by splitting of the triply-degenerate diffraction peak of the phase LS. Experimentally, the phase S is a mesophase with finite correlation lengths of translational order. The potentially simplest explanation of the transition as due to 2D nematic ordering of the backbones (or equivalently, distortion of the unit cell) fails to explain the tilt azimuths (Kaganer and Indenbom, 1993). In short, the distortion observed in the phase S is in the NN direction (note that

the distortion direction is that of stretching of the unit cell). The NN tilt in the phase L_{2d} is known to cause an NN distortion. One expects, therefore, that the tilt at the transition $S-L_2'$ from the NN-distorted phase will be in the NN direction, provided the distortion is the order parameter of the transition $LS-S$. However, the tilt azimuth is NNN.

The alternative explanation of the transition $LS-S$, supported by observation of anisotropic positional correlations in the phases S, L_2', and L_{2h}, is translational ordering in one direction. The transition can be continuous in the framework of mean-field theory. However, the crystallization transitions are significantly influenced by fluctuations. Brazovskii (1975) pointed out that at the crystallization of an isotropic system, the energy of the fluctuation does not depend on the orientation of the wave vector, and the phase space occupied by fluctuations is large. As a result, fluctuations give rise to first-order transitions even in the absence of a cubic term in the free-energy expansion. This can explain the first-order transition $LS-S$ between untilted phases of Langmuir monolayers. Tilt of the molecules violates the isotropy, and the fluctuation corrections are expected to be a minor effect on the translational ordering of the tilted phases.

The transition $S-L_2'$ is treated as a transition between untilted and tilted phases possessing periodicity in one direction. The azimuth of tilt in the phase L_2' and that of distortion in the phase S are not directly coupled to each other, giving rise to the NNN tilt in the NN-distorted phase. The low-pressure phase L_{2h} reveals anisotropic positional correlations in the diffraction experiments and is also treated as periodic in one direction. In both phases L_2' and L_{2h}, the longest correlations are observed in the direction perpendicular to the tilt direction. This can be treated as a result of a coupling between the tilt and the herringbone order parameters, which causes the tilt direction to be orthogonal to the wave vector.

The azimuth of the hexatic order serves as a reference in diffraction studies, giving rise to the NN and NNN symmetry-related azimuths of tilt and distortion. However, it is advantageous to choose the azimuths of the tilt and the crystallization wave vector (which are mutually orthogonal in the phases where both kinds of order are present) as a reference. In the phase diagram of Fig. 23, the azimuth of the tilt and that of the wave vector do not change from one phase to another. All orientational changes between the mesophases consist in change of orientation of the hexatic order with respect to that of the tilt and the crystallization and occur along a single line, whose segments are the phase transition lines $Ov-L_{2d}$, $LS-L_{2d}$, and $L_{2h}-L_2'$. In the fatty acid–alcohol mixtures, Fig. 4, the two outer segments of the line merge, giving rise to a continuous line separating the higher-pressure NNN tilted state from the NN tilted low-pressure state. The transition between them consists of a 30°-rotation of the hexatic azimuth. Landau theory predicts that each tilted state, NN and NNN, consists of two phases, the lower-temperature phase possessing one-dimensional periodicity and the higher-temperature tilted hexatic phase with orientationally disordered backbones. The treatment of the orientational phase transition in terms of rotation of the hexatic azimuth is further confirmed by the observation of its continuous rotation in chiral monolayers (Sec. VII). The 30° rotation of orientation of the hexatic implies a complete rearrangement of the neighbors. The "swiveling" transitions $Ov-L_{2d}$ and $L_2'-L_{2h}$ in the real monolayer systems are seen in Brewster-angle microscopy as a sudden and massive restructuring of the tilt-domain mosaic accompanied by a streaming motion in the film (Rivière *et al.*, 1994).

The low-temperature high-pressure phase CS in the phase diagram of Fig. 23 is a 2D crystal phase, characterized by resolution-limited peaks in the x-ray-diffraction experiments. The experimental data for the low-temperature tilted phase L_2'' (Sec. III.C) are not sufficient to distinguish between a 2D crystal and a mesophase. Its interpretation as a 2D crystal in Fig. 23 seems more logical, but is not unambiguous. The 2D crystal phases are treated as due to a second crystallization transition from the phases with one-dimensional periodicity.

In the next sections, the symmetry considerations are supported by Landau free-energy expansions. The phase diagrams are treated as a result of the interplay between hexatic ordering, tilt, and crystallization of the monolayer. The phase changes are considered with the unified free-energy expansion due to couplings between order parameters. In this way, the topology of the phase diagram and the relations between different phases are explained. These general qualitative conclusions of the Landau theory persist when fluctuation effects are taken into account. The most pronounced effects of the fluctuations are changes of the critical exponents and the transition orders. However, at present, experimental studies of Langmuir monolayers are not accurate enough to measure the critical exponents. The distinction between mean-field and fluctuation effects on the orders of the transitions is not straightforward. Two fluctuation effects especially relevant to Langmuir monolayers are discussed below, namely, fluctuations at the crystallization of the isotropic system (Brazovskii, 1975) and fluctuations at the transitions between tilted hexatic phases (Selinger and Nelson, 1988, 1989).

C. Orientational ordering

1. Tilt

The initial phase of the monolayer of long-chain molecules is assumed to be an isotropic two-dimensional liquid, i.e., its state does not change under arbitrary rotations about the normal to the monolayer plane, reflections in the planes containing it, and translations in the monolayer plane. This phase is not related to any experimentally observed condensed phase of Langmuir monolayers and serves only as a reference. Although the

liquid expanded phase possesses the symmetry of a two-dimensional liquid, the transition liquid expanded–condensed is strongly first order and cannot be treated with Landau theory. The normal to the monolayer plane is a polar axis, since the air-monolayer and monolayer-water interfaces are not equivalent. We consider here the orientational order parameters, Fig. 21(d)–(f): collective tilt of the long axes of the molecules, ordering of their short axes (backbone planes) parallel to each other, and hexatic ordering of the intermolecular bonds. The coupling between them describes the high-temperature condensed phases of Langmuir monolayers LS, L_{2d}, and Ov.

Collective tilt of the molecules [Fig. 21(e)] is described by two components n_x, n_y in the plane of the monolayer of the unit vector **n** along the mean direction of the long axes of the molecules. It is convenient to convert the two-component order parameter (n_x, n_y) to polar coordinates:

$$n_x = \eta \cos\beta, \quad n_y = \eta \sin\beta. \tag{6}$$

Here β is the azimuthal angle of the collective tilt and $\eta = \sin\theta$, where θ is the tilt angle. One has $\eta = 0$ in the phase of untilted molecules and $\eta \neq 0$ for collective tilt. The free-energy expansion contains the components of the order parameter only as powers of the combination $\eta^2 = n_x^2 + n_y^2$, due to rotational invariance of the initial 2D isotropic liquid in the monolayer plane. Hence the free-energy expansion begins with the terms

$$\Phi_\eta = A\,\eta^2 + B\,\eta^4. \tag{7}$$

The coefficients A and B depend on the temperature and the surface pressure. Equation (7) describes the second-order phase transition at $A(T,\Pi) = 0$, provided $B > 0$ (Landau and Lifshitz, 1980): for $A > 0$, the minimum of the free energy is achieved at $\eta = 0$; as A changes sign, the minimum continuously shifts to $\eta^2 = -A/2B$. If $B < 0$, the transition is first order and a term of the order η^6 is needed to ensure stability of the ordered phase.

2. Ordering of backbones

The in-plane nematic order of the backbone planes of Fig. 21(f) is described by the director **c**—the vector in the plane of the monolayer parallel to the backbone plane orientation, **c** and $-\mathbf{c}$ being equivalent. The last statement distinguishes the director from the tilt vector **n** considered above. Following the standard description of the nematic phases (de Gennes and Prost, 1993), one can introduce the nematic order parameter $\hat{Q}$—a symmetrical 2D traceless tensor with components $Q_{ij} = c_i c_j - \frac{1}{2}\delta_{ij}$ $(i,j = 1,2)$. This tensor plays the same role here as the strain tensor in crystalline phases, thus justifying the terminology discussed above. The two independent components of the traceless 2D tensor $\hat{Q}$ can be represented in polar coordinates: $Q_{xx} = -Q_{yy} = \xi \cos 2\omega$, $Q_{xy} = Q_{yx} = \xi \sin 2\omega$. The argument 2ω reflects symmetry with respect to the 180° rotation about the long axes of the molecules: the transformation $\omega \to \omega + \pi$ does not change the state of the system. Note that the orientation of the long chains is described by the vector **n**, rather than a director. The free-energy expansion over the powers of ξ begins with the lowest-order invariant $Q_{ij}Q_{ji} = 2\xi^2$:

$$\Phi_\xi = C\xi^2, \tag{8}$$

which is independent of the azimuth ω, due to the rotational invariance of the 2D liquid. Equation (8) with $C > 0$ is the elastic energy of distortions. The third-order term is absent in the expansion, since $Q_{ij}Q_{jk}Q_{ki} = 0$. If the coefficient $C(T,\Pi)$ changes sign, one has to include the next term $Q_{ij}Q_{jk}Q_{kl}Q_{li} = 2\xi^4$, to describe the transition isotropic liquid–2D nematic. We show below that such a transition does not appear on the phase diagram of Langmuir monolayers of aliphatic molecules and thus restrict ourselves to positive C.

The coupling between the tilt and the distortion (or, equivalently, 2D nematic) order parameters is due to the lowest-order invariant $n_i n_j Q_{ij} = (n_x^2 - n_y^2)Q_{xx} + 2n_x n_y Q_{xy}$, or proceeding to polar coordinates,

$$\Phi_{\xi\eta} = -V\xi\eta^2 \cos 2(\beta - \omega). \tag{9}$$

The polar-coordinate notation makes the rotational symmetry evident. A positive coefficient V provides a minimum of the free energy (9) with respect to azimuth at $\beta = \omega$ and thus describes a distortion in the tilt direction, as is observed in the high-temperature condensed phases L_{2d} and Ov and qualitatively explained as preservation of the packing in the cross section normal to chains. In the tilted phases $(\eta \neq 0)$ the distortion is nonzero: taking into account Eq. (8), one finds the minimum of the free energy $C\xi^2 - V\xi\eta^2$ at $\xi = (V/2C)\eta^2$, i.e., the distortion induced by tilt is proportional to the square of the tilt angle. This linear dependence is observed experimentally, Fig. 12, and discussed in Sec. VI.E in more detail.

Two-dimensional nematic order, i.e., the spontaneous ordering of backbone planes parallel to each other at $C < 0$, as shown on Fig. 21(f), would be the simplest explanation for the $LS - S$ transition, since the experimental manifestation of the transition is splitting of the diffraction peaks. This type of order could be imagined as a result of the average of the local herringbone packing of the chains. However, this explanation must be rejected on the basis of the experimental data (Kaganer and Indenbom, 1993). The observed continuous tilting transition $S - L_2'$ gives rise to tilt in a direction perpendicular to that of the distortion in the S phase, i.e., $\beta - \omega = \pi/2$. On the other hand, observation of the induced distortion along the tilt azimuth in the higher-temperature tilted phases fixes V to be positive, which provides a minimum at $\beta = \omega$ in Eq. (9). In other words, based on the NN distortion in the phase S, one expects NN tilt at the transition $S - L_2'$, since the NN tilt is known to cause NN distortion in the phase L_{2d}. However, the observed tilt azimuth in the phase L_2' is NNN. An appropriate order parameter for the transition $LS - S$ is described in the next section. We do not consider

the possibility of a transition over ξ further and take $C>0$ in Eq. (8); terms of the order of ξ^4 and higher can be neglected.

3. Hexatic order

Hexatic order is described by a sixth-rank tensor with only two independent components. It is convenient to proceed to polar coordinates, $h_x=h\cos 6\gamma$, $h_y=h\sin 6\gamma$, thus taking the strength h and azimuth γ of the hexatic order as two components of the order parameter. The argument 6γ reflects the symmetry of the hexatic with respect to a 60° rotation: the transformation $\gamma\rightarrow\gamma+\pi/3$ does not change the state of the system. The free-energy expansion over the powers of the hexatic order parameter does not depend on the azimuth γ and consists of the powers of h^2. Description of a first- or second-order transition from the isotropic liquid to the hexatic is straightforward. Hexatic order is present in all phases of Langmuir monolayers. Therefore we do not consider this transition, but take $h\neq 0$ in all free-energy expansions below.

Consider now the coupling between the hexatic and the tilt order parameters:

$$\Phi_{h\eta}=-Dh\eta^6\cos 6(\beta-\gamma)+Eh^2\eta^{12}\cos 12(\beta-\gamma). \tag{10}$$

The terms of Eq. (10), higher order in comparison with the ones of Eq. (7), are the lowest-order terms depending on the tilt azimuth β, and are included in the free-energy expansion owing to the degeneracy of the fourth-order term with respect to β. The polar coordinates provide a compact notation for the anisotropic terms. They can be expanded if necessary in powers of the components n_x, n_y and h_x, h_y of the order parameters by expressing the cosine terms as mixed homogeneous polynomials in $\sin\beta, \cos\beta$ and $\sin 6\gamma, \cos 6\gamma$. For example, the term $h\eta^6\cos 6(\beta-\gamma)$ is equal to

$$h_x(n_x^2-n_y^2)[(n_x^2-n_y^2)^2-12n_x^2n_y^2]+2h_yn_xn_y[3(n_x^2-n_y^2)^2-4n_x^2n_y^2].$$

The polar-coordinate notation makes the sixfold symmetry of the expression evident. Similar sine terms are absent in the free-energy expansion due to the reflection symmetry of the system: the free-energy does not change under transformation $\beta\rightarrow-\beta, \gamma\rightarrow-\gamma$. Violation of reflection symmetry in chiral monolayers is considered in Sec. VII.

For $D>0$, minimization of $\Phi_{h\eta}$ over azimuths gives the NN tilt, $\beta=\gamma$. If $D<0$, the minimum is achieved at $\beta-\gamma=\pi/6$, i.e., the azimuth of tilt is turned by 30° with respect to the azimuth of the hexatic. Thus the tilt is halfway between the nearest neighbors (NNN tilt). As D varies from positive to negative values, the second term in Eq. (10) becomes comparable with the lower-order one. If $E<0$, the first-order transition NN—NNN occurs at $D=0$. If $E>0$, the tilt azimuth takes on intermediate values $0<\beta<\pi/6$ (I phase) over the range $|D|<4Eh\eta^6$ with second-order phase transitions NN-I-NNN at each end. The range of the intermediate phase increases with increasing tilt angle. The transitions between tilted hexatic phases were analyzed in detail by Selinger and Nelson (1988, 1989) taking fluctuations into account. It was shown that, over a certain range of the coefficients, both D and E tend to zero upon renormalization to macroscopic scale. This introduces an "unlocked tilted phase" to their phase diagram.

The two tilted hexatic phases observed in fatty acid monolayers, L_2 and Ov, possess NN and NNN tilt, respectively, and the free-energy expansion Eq. (10) with $E<0$ describes both of them, yielding the L_2 phase for $D<0$ and the Ov phase for $D>0$. Possible hexatic phases with intermediate tilt azimuth are not considered here in more detail.

D. Weak crystallization

1. Density waves

Crystallization of a liquid or hexatic consists of the appearance of periodic spatial variations in the density function. Consider first the more common example, when the amplitudes of the density waves form the order parameter of the crystallization transition (Landau, 1937). In the case of "weak crystallization," all essential terms $\rho_{\mathbf{k}}\exp(i\mathbf{k}\cdot\mathbf{r})$ in the Fourier expansion of the density function have equal lengths of the wave vectors. The components $\rho_{\mathbf{k}}$ obey the condition $\rho_{-\mathbf{k}}=\rho_{\mathbf{k}}^*$, since the density is a real quantity (the asterisk denotes complex conjugation). The free energy can be expanded over powers of $\rho_{\mathbf{k}}$, each term containing the wave vectors constituting a closed polygon ($\Sigma_j\mathbf{k}_j=0$) to ensure translational invariance. The expansion starts with the term $\Sigma_{\mathbf{k}}P\rho_{\mathbf{k}}\rho_{-\mathbf{k}}$, with the coefficient P depending on the length of the wave vector (and also temperature and surface pressure). The crystallization transition occurs when P approaches zero upon decreasing the temperature, and the actual wave vector of the crystallization is the one which realizes this condition first. The next term is $\Sigma_{\mathbf{k}_1,\mathbf{k}_2,\mathbf{k}_3}Q\rho_{\mathbf{k}_1}\rho_{\mathbf{k}_2}\rho_{\mathbf{k}_3}$, and the condition $\mathbf{k}_1+\mathbf{k}_2+\mathbf{k}_3=0$ selects equilateral triangles of the wave vectors. The transition is first order because of the presence of the cubic term in the free-energy expansion. The free energy is minimized by maximizing the number of equilateral triangles of the wave vectors. In three dimensions, this is achieved by forming a tetrahedron, which gives rise to crystallization to the bcc structure (Alexander and McTague, 1978). Other structures arise, depending on the angular behavior of the fourth-order term (see Kats, Lebedev, and Muratov, 1993, for a review).

In two dimensions, only one equilateral triangle can be formed, giving rise to a transition to the 2D hexagonal crystal. The two-dimensional hexagonal crystal phases were observed in monolayers of short-chain alcohols on water in contact with a drop of the alcohol (Berge *et al.*, 1994; Zakri *et al.*, 1997) and on the surface of liquid alkanes (Wu *et al.*, 1993), but the relation of these phases to the phase diagrams of Langmuir monolayers discussed in the present paper is not ascertained. We do not discuss this type of crystallization in more

detail and proceed to the alternative way of crystallization via herringbone ordering [Fig. 21(g)].

2. Herringbone ordering

The amplitude $\phi_{\mathbf{k}}$ of the wave of herringbone order changes sign upon reflection in the plane containing the wave vector and the normal to the monolayer plane, in contrast to the density which is a scalar quantity. These two order parameters exhaust the list of symmetry-distinct crystallization order parameters in 2D systems, since any function can be split into odd and even parts. In particular, the antiferroelectric order of transverse polarization possesses the same symmetry as the herringbone. The waves of the herringbone order and polarization accompany each other, being shifted by a quarter of the period (Kaganer and Loginov, 1995).

The free-energy expansion over powers of $\phi_{\mathbf{k}}$, in contrast with the expansion over powers of density wave discussed above, does not contain the cubic term which changes sign on reflection. Then the free-energy expansion begins with the terms

$$\Phi_{\varphi}=\sum_{\mathbf{k}} F\phi_{\mathbf{k}}\phi_{-\mathbf{k}}+\sum_{\mathbf{k}_1,\mathbf{k}_2} G\phi_{\mathbf{k}_1}\phi_{-\mathbf{k}_1}\phi_{\mathbf{k}_2}\phi_{-\mathbf{k}_2}, \tag{11}$$

with the coefficients F and G depending on the length of the wave vector k (and also temperature and surface pressure). The coefficient $G(k,\mathbf{k}_1\cdot\mathbf{k}_2)$ depends also on the angle between the wave vectors $\mathbf{k}_1$ and $\mathbf{k}_2$. A variety of ordered phases can result, depending on its functional dependence (Marchenko, 1991). Two waves with nonparallel wave vectors $\mathbf{k}_1$ and $\mathbf{k}_2$ give rise to 2D crystalline structures. However, if $G(k,\mathbf{k}_1\cdot\mathbf{k}_2)$ has sharp minima at $\mathbf{k}_1\cdot\mathbf{k}_2/k^2=\pm 1$, only one wave $\phi_{\mathbf{k}}\exp(i\mathbf{k}\cdot\mathbf{r})$, together with the oppositely directed one $\phi_{-\mathbf{k}}=\phi_{\mathbf{k}}^*$, is created at the transition. Our aim is to describe the phases of Langmuir monolayers with order intermediate between that of a hexatic and a 2D crystal; these phases demonstrate significantly larger correlation lengths in one direction than in the perpendicular one. Then it is reasonable to consider the transition with appearance of periodicity in only one direction in more detail.

For translational ordering in one direction, the free-energy expansion reduces to

$$\Phi_{\varphi}=F\varphi^2+G\varphi^4, \tag{12}$$

where $\varphi=|\phi_{\mathbf{k}}|$ is the amplitude of the crystallization wave. In the liquid phase, $F>0$ and the minimum of the free energy is at $\varphi=0$. The crystallization transition occurs when $F(T,\Pi)$ approaches zero upon reducing the temperature, and the wave vector k is the one which realizes this condition first. If $G>0$, the mean-field theory predicts a continuous transition. However, this transition is strongly influenced by fluctuations, since the energy of a fluctuation does not depend on orientation of $\mathbf{k}$ and the phase space occupied by fluctuations is large. As a result, fluctuations give rise to a first-order transition even in the absence of a cubic term in the free-energy expansion (Brazovskii, 1975).

The wave of herringbone order causes a periodic variation in the density of the molecules, as is clearly seen in Fig. 21(g), with the period of the density being half the period of the structure. Thus the wave of the herringbone order with the wave vector $\mathbf{k}$ induces a density wave with the wave vector $2\mathbf{k}$. The coupling between the herringbone and the density waves is due to the invariant $\Sigma_{\mathbf{k}}\rho_{2\mathbf{k}}\phi_{-\mathbf{k}}^2$. Minimizing it together with the term $\Sigma_{\mathbf{k}}\rho_{2\mathbf{k}}^2$, one obtains $\rho_{2\mathbf{k}}\propto\varphi^2$.

3. Coupling of the order parameters

The crystallization order parameter is coupled with the orientational order parameters, as was qualitatively discussed above: tilt or distortion along and normal to the crystallization direction cost different energies. The crystallization order parameter $\phi_{\mathbf{k}}$ can enter into the lowest-order coupling invariants only in the combination $\phi_{\mathbf{k}}\phi_{-\mathbf{k}}$, to ensure translational invariance. Rotation by an arbitrary angle α transforms the tilt azimuth β to $\beta+\alpha$, whereas the wave $\phi_{\mathbf{k}}$ is transformed to $\phi_{\mathbf{k}'}$, the wave vector $\mathbf{k}'$ making the angle α with $\mathbf{k}$. Then the lowest-order coupling invariant term is $\Sigma_{\mathbf{k}}J\phi_{\mathbf{k}}\phi_{-\mathbf{k}}\eta^2\cos 2(\beta-\delta_{\mathbf{k}})$, where $\delta_{\mathbf{k}}$ is the azimuth of the wave vector $\mathbf{k}$. In terms of the gradients of the wave $\tilde{\phi}_{\mathbf{k}}(\mathbf{r})=\phi_{\mathbf{k}}\exp(i\mathbf{k}\cdot\mathbf{r})$ the coupling is proportional to $|\mathbf{n}\cdot\nabla\tilde{\phi}_{\mathbf{k}}|^2$. When only one wave of the amplitude φ and the wave-vector azimuth δ is created at the transition, the coupling reduces to

$$\Phi_{\varphi\eta}=J\varphi^2\eta^2\cos 2(\beta-\delta). \tag{13}$$

When $J>0$, this term possesses a minimum at $\beta-\delta=\pi/2$. Then the tilt azimuth is orthogonal to that of the wave vector, in agreement with observations of the tilt in direction perpendicular to the longer correlations in both phases L_2' and L_2 of fatty acids (Sec. III.C).

Analogously, the coupling between crystallization order parameter $\varphi_{\mathbf{k}}$ and the distortion ξ is given by the invariant term $\Sigma_{\mathbf{k}}U\varphi_{\mathbf{k}}\varphi_{-\mathbf{k}}\xi\cos 2(\omega-\delta_{\mathbf{k}})$, which reduces, for the case of one crystallization wave, to

$$\Phi_{\varphi\xi}=-U\varphi^2\xi\cos 2(\omega-\delta). \tag{14}$$

Taking into account Eq. (8) with positive C, one concludes that the herringbone ordering induces distortions $\xi=(U/2C)\varphi^2$. In particular, the distortion is zero at the point of the continuous phase transition ($\varphi=0$). Qualitatively, at the transition point the backbones in the adjacent rows form angles $\pm 45^\circ$ with respect to the wave vector, see Fig. 21(g), and the mean orientational order is zero. At reduced temperatures, the angles deviate from $\pm 45^\circ$, resulting in a net orientation of the backbones. The observation of stretching in the NN direction in the phases S and L_2' is described by Eq. (14) with $U>0$, which gives the minimum at $\omega=\delta$.

The coupling of the crystallization wave φ with the hexatic order parameter can be derived analogously and is equal to

$$\Phi_{h\varphi}=-H\varphi^2 h\cos 6(\gamma-\delta). \tag{15}$$

It results in a crystallization wave in the NN direction (along the intermolecular bonds) for $H>0$ and in the NNN direction (perpendicular to the bonds) for $H<0$. The one-dimensional translational ordering of the hexatic phase occurs when, upon decreasing the temperature, the difference $F-|H|h$ approaches zero, and the wave vector k is the one which meets this condition first (note that the coefficients F and H depend on k). In the next section it will be shown that, for crystallization of the tilted hexatic phase at sufficiently strong coupling (13), the azimuth $\gamma-\delta$ may not follow the minimum of Eq. (15). Then the crystallization transition occurs when the difference $F-Hh\cos 6(\gamma-\delta)$ approaches zero, and the length of the wave vector k depends on the azimuths. In particular, for translational ordering along and perpendicular to the hexatic azimuth (NN and NNN directions) the lengths of the wave vectors are given by the minima of $F\mp Hh$ with respect to k and thus can differ from each other.

E. Interpretation of the phase transitions

We can now describe the phase diagram of Fig. 23 in terms of the free energy introduced above. It is worthwhile to collect here all essential terms from the free-energy expansions introduced above:

$$\begin{aligned}\Phi = {} & A\eta^2 + B\eta^4 - Dh\eta^6\cos 6(\beta-\gamma) \\ & + Eh^2\eta^{12}\cos 12(\beta-\gamma) + F\varphi^2 + G\varphi^4 \\ & + J\varphi^2\eta^2\cos 2(\beta-\delta) - H\varphi^2 h\cos 6(\gamma-\delta). \end{aligned} \quad (16)$$

Equation (16) involves the hexatic order parameter (with the strength h and the azimuth γ), the tilt order parameter (with the polar tilt angle η and the tilt azimuth β), the herringbone order parameter (with the amplitude of the wave φ and the azimuth δ of the wave vector), and the couplings between them. The distortion ξ and its azimuth ω can be found as a minimum of the free energy

$$\Phi_\xi = C\xi^2 - V\xi\eta^2\cos 2(\beta-\omega) - U\varphi^2\xi\cos 2(\omega-\delta) \quad (17)$$

with the other order parameters already determined from minimization of the free energy Eq. (16).

The most symmetrical phase, the high-temperature high-pressure condensed phase LS, is treated as the untilted hexatic phase, $h\neq 0$. The two main ordering modes are tilt upon decreasing surface pressure and ordering of the backbone planes upon decreasing temperature. The tilting transitions are found to be continuous in experimental studies. The continuous transitions from untilted to tilted hexatic phases $LS-L_{2d}$ and $LS-Ov$ are described as the line $A(T,\Pi)=0$ [see Eq. (7)], provided $B>0$.

The two tilted hexatic ($h\neq 0$, $\eta\neq 0$) phases L_{2d} and Ov differ by tilt azimuth, NN and NNN, respectively. These tilt azimuths are given by the minima of the coupling terms Eq. (10) at positive and negative D respectively. The transition $L_{2d}-Ov$ is described as the line $D(T,\Pi)=0$. The transition is first order, provided $E<0$. Both tilted hexatic phases possess distortion (or, more appropriate for the noncrystalline phases, 2D nematic order) in the tilt direction, which is described by minimizing Eq. (9) with $V>0$ over the angles. The distortion induced by tilt can be found by minimizing $C\xi^2 - V\xi\eta^2\cos 2(\beta-\omega)$ with respect to ξ. To keep the formulas applicable to the lower-temperature phases where the tilt and distortion azimuths may not coincide, we do not minimize over the azimuths here. Then the tilt contribution to the distortion is found to be $\delta\xi = (V/2C)\eta^2\cos 2(\beta-\omega)$. It is convenient to introduce the signed distortion parameter:

$$d = \xi\cos 2(\beta-\omega). \quad (18)$$

When the directions of tilt and distortion are NN or NNN, $\cos^2 2(\beta-\omega)=1$ and $\delta\xi\cos 2(\beta-\omega)$ is simply proportional to η^2. Then the plot of d versus η^2 is a common straight line for phases with different azimuths of tilt and distortion. If the distortion is caused solely by tilt, extrapolation of the line to $\eta=0$ gives $d=0$. The nonzero extrapolated distortion d at zero tilt is a manifestation of another source of distortion, namely, ordering of the backbone planes. This explains the choice of the coordinates in Fig. 12.

The transition $LS-S$ is treated as herringbone ordering with appearance of periodicity in one direction, which is supported by the observation of anisotropic positional correlations in the phases S, L_2', and L_{2h}. The transition is described by the free energy Eq. (12) with herringbone order parameter φ. The transition at $F(T,\Pi)=0$ is continuous in the framework of the mean-field theory, provided $G>0$, but fluctuations drive it to first order.

The transition $S-L_2'$ is between untilted and tilted phases with periodicity in one direction. The azimuth of the tilt in the phase L_2' and that of the distortion in the phase S are due to two different coupling terms, Eq. (13) and Eq. (14), respectively: the stretching of the unit cell along the wave vector is due to $U>0$, and the tilt normal to it is due to $J>0$. Therefore the tilt direction is perpendicular to the wave vector, which agrees with the observation of shorter correlation lengths in the tilt direction. Then one can conclude that $H>0$ in Eq. (15), resulting in the NN azimuth of the wave vector, the NN azimuth of the unit cell stretching, and the NNN azimuth of the tilt, also in agreement with the observations. The signs of all coefficients in the actual free-energy terms are fixed now and further features of the phases and phase transitions can be derived without additional assumptions.

The phase L_{2h}, which is entered from the phase L_2' upon decreasing surface pressure, possesses highly anisotropic correlations and is also considered as periodic in one direction. In this phase, the tilt remains perpendicular to the direction of the longest correlations. Thus the coupling of Eq. (13) between the tilt and the herringbone order parameters with $J>0$ fits the observations in both L_2' and L_{2h} phases, giving $\beta-\delta=\pi/2$. Then, collecting the remaining actual azimuthal terms, the tilt azimuth can be found by minimizing the free energy:

$$\Phi = c_6 \cos 6(\beta - \gamma). \tag{19}$$

The contribution to the coefficient c_6 from Eq. (16) is equal to $(H\varphi^2 - D\eta^6)h$, and the terms of order $\varphi^2\eta^4 h$ and $\varphi^4\eta^2 h$ also contribute to c_6. The coefficient c_6 is positive at small tilt angles where the backbone order (the term $H\varphi^2 h$) dominates in it, and changes sign when the surface pressure is decreased and hence the tilt order parameter η increases. Then the condition $c_6 = 0$ is realized at some tilt angle η_0 and describes the transition from the NNN-tilted phase, $\beta - \gamma = \pi/6$ for $\eta < \eta_0$, to the NN-tilted phase, $\beta = \gamma$ for $\eta > \eta_0$. The transition upon decreasing surface pressure is driven by the increasing tilt angle, while the order of backbone planes depends on temperature rather than surface pressure. That explains the observed weak temperature dependence of the tilt angle at the transition $L_2' - L_{2h}$.

The order of the transition depends on the sign of the coefficient c_{12} at the next higher-order term $c_{12}\cos 12(\beta - \gamma)$: if $c_{12} < 0$, the transition is first order, as is observed experimentally for the $L_2' - L_{2h}$ transition; the opposite inequality $c_{12} > 0$ gives rise to two second-order transitions with an oblique phase in between. When the coefficient c_{12} is small, the next higher-order term $c_{18}\cos 18(\beta - \gamma)$ results in one first- and one second-order transition, which can explain the observation of the $L_2' - I - L_{2h}$ phase transitions by Durbin *et al.* (1997), cf. Fig. 3(d). The original explanation by Durbin *et al.* (1997) is given in terms of the twofold rather than sixfold symmetry, and thus retaining the 2nd-, 4th- and 6th-order terms. One can expect that further variation of the experimental conditions (e.g., the chain length) will give two continuous transitions $L_2' - I - L_{2h}$.

We proceed now to an analysis of the unit-cell distortions along the phase sequence $S - L_2' - L_{2h}$. Keeping in mind that the tilt is perpendicular to the crystallization direction, $\beta - \delta = \pi/2$, one has from Eq. (17) the free-energy expansion

$$\Phi_{\xi\eta\varphi} = C\xi^2 + (U\varphi^2 - V\eta^2)\xi \cos 2(\beta - \omega). \tag{20}$$

The coefficients C, U, and V are positive, as fixed above by comparison with the observations. When the tilt angle η is small and $V\eta^2 < U\varphi^2$, the distortion azimuth is governed by the herringbone order and the unit cell stretches in the crystallization direction perpendicularly to the tilt direction, $\beta - \omega = \pi/2$. Note that, if the tilt azimuth is chosen as a reference, both the magnitude and the azimuth of the distortion are continuous at the transition $L_2' - L_{2h}$, in agreement with the experiments. The distortion decreases with increasing tilt angle and approaches zero at the nonzero tilt angle $\eta^2 = (U/V)\varphi^2$. At this tilt angle, the unit cell becomes hexagonal in the monolayer plane. On further increase of the tilt angle, the unit cell stretches in the tilt direction, $\beta = \omega$. This behavior is experimentally observed in the phase L_{2h} of fatty acids, Fig. 10(a), and has been illustrated in Fig. 11. The change of the distortion azimuth occurs continuously and is not related to a phase transition.

The crystalline phases CS and L_2'' can be treated as a result of further crystallization. Note that, in the phase S, the herringbone wave $\phi_{\mathbf{k}}$ induces the density wave $\rho_{2\mathbf{k}}$ collinear with it. The transition $S - CS$ can be described as a spontaneous appearance of two other density waves, directed approximately 120° with respect to the first one. The amplitude of the density wave coupled with the herringbone wave is not equal to the amplitudes of two other density waves. That results in an additional azimuth-dependent coupling with the tilt order parameter and can change the tilt azimuth of the tilted crystalline phase L_2'' with respect to that in the phase L_2'. The NN tilt azimuth in the phase L_2'' can be explained in this way. The NN tilt ($\beta = \delta$) also minimizes the free energy Eq. (10) with $D > 0$, so that, in contrast to the higher-temperature tilted phases L_2' and L_{2h}, the tilt azimuth does not change on increasing tilt angle, in agreement with the experiments.

F. Symmetry of crystalline phases and mesophases

Continuous variation in cross-sectional cell dimensions from mesophases to crystalline phases in Langmuir monolayers, as given by the distribution in Fig. 13, indicates minor variations in the local packing of the hydrocarbon chains at these phase transitions. However, in mesophases the symmetry of the local packing is not maintained over long distances, in contrast to crystalline phases. We will discuss here the relationships between symmetry of mesophases, as determined in the Landau theory, and symmetry of crystalline phases, which follows from x-ray-diffraction data and packing considerations (Kuzmenko, Kaganer, and Leiserowitz, 1998).

Symmetry of the mesophases with one-dimensional periodicity obeys one of the seven groups of borders, whereas the symmetry of the two-dimensional crystalline phases belongs to one of 17 plane groups (Vainshtein, 1994). Figures 24(a) and (b) reproduce the symmetry of the phases S and L_2' from the theoretical phase diagram (Fig. 23). Figures 24(a) implies twofold rotational disorder of the chains about their long axes. Equidistantly spaced thin solid lines along the molecular rows represent one-dimensional periodicity in the NN direction. Every two neighboring rows of molecules are related by the glide symmetry in the NN direction.

The tilt of the molecules in the NNN direction in the phase L_2', Fig. 24(b), breaks the original NN glide symmetry and the twofold symmetry. Therefore two orientations of the backbones related by the twofold rotation around long molecular axis are no longer equivalent. Tilting of the molecules during the phase transition from the S to the L_2' phase is a dominant effect in response to decrease of the surface pressure, while the twofold ordering of the chains occurs as a consequence of symmetry reduction.

Figure 24(c) presents the symmetry of a 2D crystalline phase CS, which can be derived from the phase S by acquiring additional periodicity in the NNN direction. The phase preserves the twofold orientational disorder

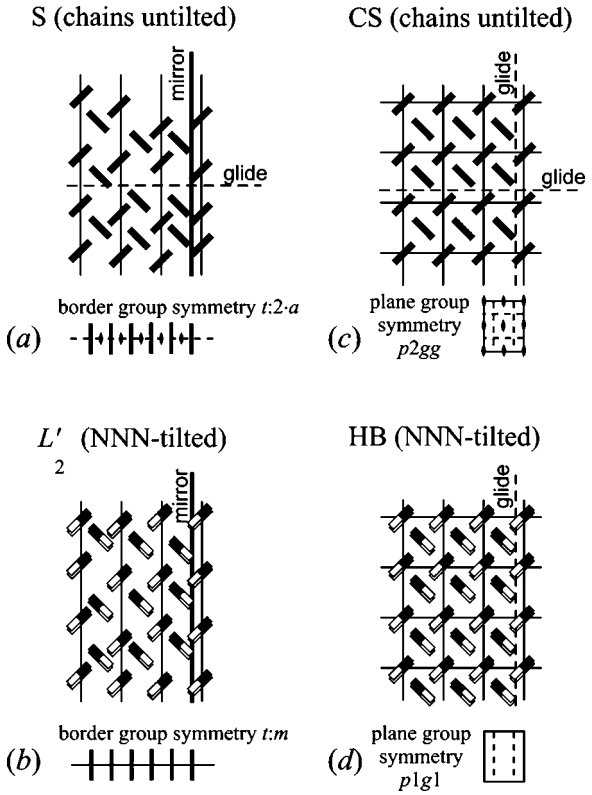

FIG. 24. Symmetry of monolayer phases with one-dimensional and two-dimensional periodicity: (a) the phases with one-dimensional periodicity in positions of vertically aligned hydrocarbon chains possessing twofold molecular disorder and translational disorder in the NNN direction; (b) same hydrocarbon chains, tilted; (c) a two-dimensional crystal with vertically aligned hydrocarbon chains possessing twofold disorder; (d) an ordered crystal with hydrocarbon chains arranged in the herringbone motif and tilted in the NNN direction (Kuzmenko, Kaganer, and Leiserowitz, 1998).

of the hydrocarbon chains, as in the S phase. The plane symmetry of this phase incorporates two glide planes along both NN and NNN directions and generated twofold axes perpendicular to the layer plane.

Figure 24(d) depicts the symmetry of the herringbone (HB) crystalline phase. The HB phase does not possess the NN glide symmetry, unlike the S or CS phases. Therefore molecules can tilt in the NNN direction even in a compressed state, as a result of the twofold ordering of the backbone planes of the chains which decreases the entropy of the system and lowers the symmetry. The small values of molecular tilt (less than 5°) were actually revealed by fitting the experimental Bragg rods for highly crystalline monolayer phases (Böhm *et al.*, 1994).

The transition from the phase S with one-dimensional periodicity to the crystalline HB phase involves two independent steps of ordering. In other words, the representation of the symmetry group which governs the transition $S-\mathrm{HB}$ can be reduced to two irreducible representations. One of them describes translational ordering in the NNN direction, the other represents the twofold ordering of the hydrocarbon chains and their tilt ordering. The phases CS and L_2' [Figs. 24(b) and (c)] are the intermediate phases that correspond to two possible paths of subsequent ordering from S to HB. The symmetry for the experimentally observed phase CS cannot be identified with that of the true crystalline HB phase [Fig. 24(d)], because the transition from the HB phase with NNN-tilted molecules towards the phase L_2'' with NN-tilted molecules has to be accompanied by a change in the glide-plane direction from NNN to NN and must be of the first order. This would contradict the experimental observations of a continuous $CS-L_2''$ phase transition.

The assignment of the LS phase as a hexagonal crystal, rather than a hexatic (which cannot be excluded owing to low resolution of the diffraction data; see Sec. III.C and Sirota, 1997), would entail the attribution of the structure in Fig. 24(c) to the phase S. Then the phase CS has to be attributed to the true crystalline HB phase of Fig. 24(d) and the tilting transition $CS-L_2''$ is first order, as argued in the previous paragraph.

The HB phase shown in Fig. 24(d), with a slight molecular tilt in the NNN direction, cannot be identified with any of the observed phases of long-chain fatty acids or alcohols, but may exist in highly crystalline Langmuir monolayers of other substances. This phase may potentially be obtained from the phase CS by decreasing temperature or increasing the surface pressure.

There exists a straightforward correspondence between the symmetries of some phases in the theoretical phase diagram of Langmuir monolayers, Fig. 23, and that of smectic liquid crystals (see Gray and Goodby, 1984, and Pershan, 1988, for review of smectic structures). The untilted hexatic phase LS corresponds to the hexatic smectic SmBH; the tilted hexatic phases Ov and L_{2d} possess the same symmetry as SmF and SmI, respectively. The crystalline phases CS and L_2'' correspond to SmE and SmK. The present assignment only partially coincides with these by Bibo, Knobler, and Peterson (1991) and Schwartz *et al.* (1992), cf. Table I. We treat the phases S, L_2', and L_{2h}, occupying the intermediate temperature range in Langmuir monolayers, as periodic in one direction. They do not have direct analogues among commonly accepted smectic categories. However, as discussed in Sec. III.E, some of the observed diffraction patterns of smectics attributed as SmF and SmI are very similar to the diffraction patterns of the L_2' and L_{2h} phases.

There is also some analogy between the phases of Langmuir monolayers and the rotator phases of bulk alkanes. However, this analogy is not as straightforward, and there are several distinct interpretations (Peterson and Kenn, 1994; Sirota, 1997).

To conclude, the ordering in condensed phases of Langmuir monolayers occurs due to tilting of the molecules upon decreasing the surface pressure and ordering of their backbones (short axes) upon decreasing the temperature. The intermediate temperature range between the high-temperature hexatic phases (untilted and tilted) and the low-temperature crystalline phases is occupied by mesophases possessing herringbone order of

the backbones. These mesophases possess highly anisotropic positional correlations in the experiments and are treated in the Landau theory as periodic in one direction. Tilt of the molecules always occurs in the direction perpendicular to the crystallization wave vector. The complexity of the phase diagram is due to rotation of the hexatic azimuth with respect to directions of tilt and crystallization. The distortion and corresponding splitting of the diffraction peaks is a secondary effect caused by the primary order parameters. Further ordering upon decreasing the temperature involves translational ordering in the second direction and ordering with respect to a 180° rotation of the backbones about the long axes of the molecules. (See *Note added in proof.*)

VII. CHIRALITY EFFECTS ON STRUCTURE OF MONOLAYERS

Many biological systems consist of chiral molecules and their functions depend strongly on molecular chirality. The question specific to Langmuir monolayers concerns the structure of biological membranes, which are composed of chiral molecules. Chirality gives rise to a loss of symmetry due to only small changes of energy. A local chiral arrangement results in macroscopically chiral systems, which often reflect the beauty of nature in spirals or helices. These macroscopic structures may help to deduce the structure on the molecular length scale.

A structure is chiral if its mirror image cannot be brought in coincidence with it by a rotation. In monolayer systems, only rotations about the monolayer normal and mirror reflections with respect to planes containing the normal are available symmetry operations. Reflection in the monolayer plane is not possible since the monolayer-water and monolayer-air interfaces are different. Consequently, the monolayer system is chiral if its symmetry group does not contain a reflection in the plane containing the monolayer normal. An oblique structure in the monolayer system is chiral and can correspond to either a monoclinic or a triclinic bulk structure.

Chiral structures can be formed by achiral molecules, if tilt or distortion occurs in a direction intermediate between NN and NNN. In particular, a transition involving a change of orientations from NN to NNN can occur as either a discontinuous jump or continuous variation of the azimuths (Sec. VI). In the latter case, the intermediate phase is chiral. Almost all ''swiveling'' transitions NN-NNN in Langmuir monolayers are discontinuous. Several exceptions were reported, however. Peterson *et al.* (1996) reported a chiral phase, denoted as L_1' (cf. Table I), between L_{2d} and Ov phases, but the observations were not unequivocal. Durbin *et al.* (1997) found an intermediate chiral phase between L_2' and L_{2h} phases.

The left- and right-hand molecules (*enantiomers*) of the same chiral substance tend to form a uniform nonchiral mixture, called *racemic mixture* or *racemate*, because the mixing entropy is thus maximal. However, if the interactions between molecules of the same handness (homochiral interactions) dominate, the system can separate into domains with specific chirality. Clockwise and anticlockwise domains are commonly observed in Langmuir monolayers of chiral substances (see McConnell, 1991, for a review). The chiral shape of domains does not necessarily correspond to a chiral packing of the molecules, however. Rietz *et al.* (1993, 1996) observed left- and right-handed domains in the racemic mixture of a chiral diol, but the x-ray-diffraction study gives a centered rectangular (nonchiral) unit cell. For another system, chiral structures have been observed using x-ray diffraction in monolayers of both the enantiomer and the racemate, even though the racemate domains are not chiral (Brezesinski *et al.*, 1994). On the other hand, using a third chiral molecule, the structures of both the racemate and the enantiomer have been observed to be nonchiral within experimental accuracy (Brezesinski, Scalas *et al.*, 1995).

Chiral segregation is rarely observed in structural studies. Eckhardt *et al.* (1993) observed, by means of atomic force microscopy, chiral domains in the monolayer of the racemic mixture of a chiral tetracyclic alcohol transferred to a solid substrate. The relation to structure of the water-supported monolayer remains obscure, however. Nassoy *et al.* (1995) observed, by x-ray diffraction, the same oblique lattice in both the racemic mixture and the enantiomer of myristoyl-alanine, indicating spontaneous chiral segregation in the monolayer of the racemate. Weissbuch *et al.* (1997) observed separation of enantiomers in the monolayers of α amino acid amphiphiles.

To provide theoretical insight into the origin of chiral phase separation in monolayers, Andelman (1989, 1990) and Andelman and Orland (1993) considered a model of a tripodal amphiphile, i.e., a molecule which touches the water surface at three nonequivalent atoms. The theory predicts heterochiral behavior for van der Waals interactions and homochiral behavior for electrostatic interactions. Presence of a specific polar direction in the monolayer system, namely the normal to the monolayer, gives rise to a special coupling between chirality and tilt, which leads to complex macroscopic patterns with modulation in tilt azimuth (Selinger *et al.*, 1993).

Short-range chiral interactions are due to the excluded volume effect: more close contact between chiral molecules is possible if there is an oblique distortion of positions of the neighbor molecules. For example, dense packing of hydrocarbon chains with parallel backbones gives rise to an oblique distortion (Kitaigorodskii, 1961). Such packing was observed by Viswanathan *et al.* (1994) in an atomic force microscopy study of the surface of a calcium arachidate monolayer transferred onto a solid substrate. However, the structures of the monolayers transferred to a solid substrate do not generally coincide with those of monolayers on water.

Long-range chiral interactions result from electrostatic interactions between distributed charges in chiral molecules. These interactions can explain the chiral structure of the monolayer of triple-chain phosphaidyl-

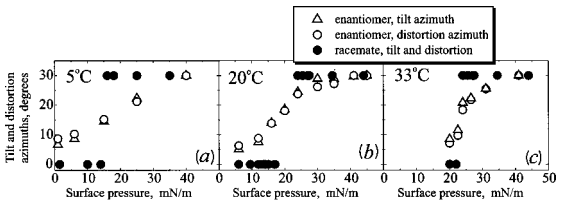

FIG. 25. Azimuth of tilt and that of the unit-cell distortion in a chiral monolayer of 1-hexadecyl-glycerol and in the racemic mixture of its left- and right-hand enantiomers (Scalas *et al.*, 1996, 1998). The nonchiral racemic monolayer experiences a first-order transition from NN to NNN tilt, while the chiral monolayer of the enantiomer undergoes a continuous variation of the tilt azimuth from a state close to the NN tilt to the one close to the NNN tilt. The azimuth variation becomes steeper with increasing temperature.

choline (Bringezu *et al.*, 1996). The molecule consists of three hydrocarbon chains attached to a single head group. The size of the head group is smaller than the cross section of three chains, so that direct contact between the head groups in the monolayer is prohibited. An alternative explanation can be given in terms of the short-range chiral interactions, if one assumes that three chains of each molecule line up, thus allowing contact between the head groups.

Chiral interactions are generally weak in comparison with other interactions, since only a small part of the molecule carries the chiral center. As a result, the angles between lattice vectors in the monolayers of chiral molecules differ from 90° by only several degrees of arc (Böhm *et al.*, 1993). An important exception is the situation when different interactions compensate each other (Scalas *et al.*, 1996, 1998). When the racemic mixture experiences a discontinuous transition between NN and NNN tilted states, which corresponds to the $L_2'-L_{2h}$ transition in fatty acids, the interactions controlling the tilt azimuth are compensated. As a result, the structure of a monolayer of the enantiomer differs from that of the racemate. The enantiomer experiences a continuous variation of the tilt azimuth in the surface-pressure region near the transition point in the racemate, and adopts structures close to those of the racemate far from the transition.

The range of surface pressures where the manifestation of chiral interactions is essential decreases with increasing temperature (Fig. 25). This can be explained by the increasing rotational disorder of the backbones: when neighboring molecules spin freely and independently about their long axes, they become effectively achiral, and the chiral interactions are washed out. Thus chiral interactions exist only if there is a correlation between the directions of short axes of the molecules (Harris *et al.*, 1997).

The Landau theory can be extended to chiral monolayers by supplementing each cosine term in the free energies of Sec. VI by an analogous sine term resulting from lack of reflection symmetry. The effect of chirality is generally small and the chiral terms give a weak (albeit symmetry-breaking) effect. The exception is a situation when the coefficient at the cosine term is close to zero. This happens when the effects of tilt and backbone ordering compensate each other at the swiveling transition [Eq. (19)]. Adding the chiral term, the free-energy expansion can be represented as

$$\Phi = c_6 \cos 6(\beta-\gamma) - c_6' \sin 6(\beta-\gamma). \tag{21}$$

The coefficient c_6' arises from the chiral complements to Eqs. (10) and (15). According to the discussion above, the contribution due to order of the backbones dominates c_6'. The coefficient c_6 is zero at the surface pressure $\Pi_0(T)$ of the transition NN-NNN in the racemate monolayer. Minimizing the free energy Eq. (21), one finds $\cot 6(\beta-\gamma) \propto (\Pi_0-\Pi)$. As the surface pressure is increased, the azimuth of tilt with respect to that of the hexatic $\beta-\gamma$ varies from 0 at surface pressures below the transition to $\pi/6$ above it, in agreement with the experiment [Figs. 25(a)–(c)]. Referring to the theoretical phase diagram for achiral monolayers, Fig. 23, one can state that the chiral monolayer experiences the same rotation of the hexatic azimuth with respect to tilt and one-dimensional periodicity, but this rotation proceeds continuously.

The distortion d is proportional to η^2, Fig. 12(b), as predicted by Landau theory. The data points for the enantiomer, as well as NN and NNN tilted phases of the racemate at the same temperature, lie on the same straight line. This behavior demonstrates the similarity in the packing of the enantiomer and the racemate and supports the interpretation of the NN–NNN swiveling transition in achiral monolayers as a change of orientation of the hexatic axes. In the chiral monolayer, the same change of orientation occurs continuously.

VIII. PHOSPHOLIPID MONOLAYERS

A. General

Having discussed in detail the physics of monolayers of single-chain compounds, we now proceed to molecules with more than one chain per head group, and the most suitable candidates are phospholipids. They are essential building blocks of biological membranes, which consist of two weakly coupled monolayers. Consequently, studies of phospholipid monolayers are of great biophysical interest, although in fact the biological membrane is a complex mixture of various lipids and proteins. Going from single-chain compounds to multiple-chain molecules, one moves a step towards amphiphilic polymers. Many of these polymers consist of hydrophobic side chains linked by a hydrophilic backbone. They can be arranged at interfaces and also be assembled as layered films, one of the most important nanostructures in polymer physics (Embs *et al.*, 1991). Polymer monolayers will not be discussed in the present review.

In a typical phospholipid, two fatty esters are linked via a hydrophilic and a more extended head group than in fatty acids [Figs. 1(c)–(e)]. One may expect to find the structures discussed above for fatty acids, albeit with some restrictions and additions. First, the phases with

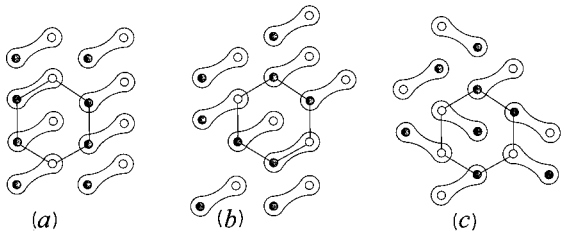

FIG. 26. Possible arrangement of the head groups linking two aliphatic tails with tails forming a hexagonal lattice. Since the two tails are inequivalent, the head sketched as a bojoom may be considered as possessing a center and an orientation. Hence one may expect (a) arrangements with positional and orientational order, (b) with orientational order and with positional disorder of the centers, or (c) with disorder concerning both head-group parameters.

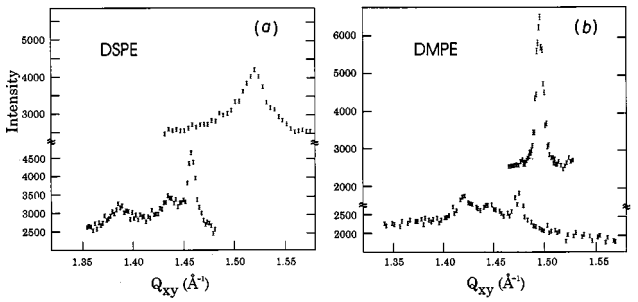

FIG. 27. X-ray scattering intensity as a function of in-plane wave-vector transfer Q_{xy} for a monolayer of DSPE (C_{18} chain) and DMPE (C_{14} chain) at low (bottom) and at high (top) lateral pressures. The intensities are integrated over Q_z. The tails form an oblique lattice of tilted chains at low pressure and a hexagonal lattice without tilt at high pressures (Kenn *et al.*, 1996).

free rotation of the chains about the long molecular axes should not exist, since the coupling of two tails prevents rotation. Second, the lateral motion of a molecule requires movement of two chains and is hindered. This should reduce the role of translational freedom compared to the internal degrees of freedom of a molecule. Third, positions and orientations of the head groups can also be involved in ordering (Fig. 26). The interactions between the head groups can be laterally anisotropic. Linking two inequivalent tails can cause additional types of order, in particular superlattices in the tail arrangement and the orientational order of the vectors linking the two tails.

Until now, x-ray experiments have revealed the order of the aliphatic tails but not of the head groups. However, by varying the chemical composition and interaction of the head groups, one can obtain indirect evidence about their arrangements.

B. Phosphatidylethanolanolamines (PE)

Phospholipids with the ethanolamine head group [Fig. 1(c)] have proven to be best suited for monolayer studies for several reasons. First, the changes of slope in the surface pressure–area isotherms are especially well pronounced and thus the phase boundaries can be clearly localized. This is probably due to the high purity of available material or due to a reduced sensitivity to purity. We presume the first, although impurity levels near 1% are difficult to quantify. Second, for $p\mathrm{H}=7\pm2$ the polar head is uncharged, and therefore the surface pressure—area isotherms are not sensitive to small variations of $p\mathrm{H}$ or ionic milieu (Standish and Pethica, 1968). Third, the molecular area at high pressures, as deduced from the pressure–area isotherms, is given by the area of two aliphatic tails. Hence the area per head group is sufficiently small and does not impede tail ordering. This contrasts with molecules with the choline head group, requiring a minimum molecular area near 45 Å^2 (Albrecht, Gruler, and Sackmann, 1978).

For the PE with a C_{14} chain (DMPE) at room temperature one observes a transition from a liquid expanded phase to ordered phases which yield x-ray-diffraction signals (Fig. 27, right) (Helm *et al.*, 1991). The peaks are broader than the resolution, which means that these are mesophases. At low surface pressures, the lattice is oblique, with the tilt direction close to the nearest neighbor (NN). At high pressures the tilt is absent and the lattice is hexagonal, with the cross section per tail close to 20 Å^2. These structural features are typical for the rotator phases L_{2d}, LS of fatty acids. However, here the tails cannot freely rotate. Thus there must be sufficient static disorder to provide (on average) a rather large and circular cross section of the aliphatic tails.

In analogy with fatty acids, one can enter crystalline phases by increasing the chain length or reducing the temperature. This is shown in the x-ray data presented in Fig. 27 (left). In this case, the film is too rigid to enable any meaningful pressure measurement (Kenn, Kjaer, and Möhwald, 1996). One observes an oblique lattice (close to a rectangular lattice with the NN chain tilt) for expanded films at low surface pressure, and a hexagonal lattice without tilt or with very small tilt upon high compression. The broad peaks clearly show that the monolayer is not in a crystalline phase. This can again be confirmed from an inspection of the tail cross sections. These are well above 19 Å^2, an upper border for crystalline alkanes. They are not dependent on pressure and temperature within an accuracy of ±0.2 Å^2 and decrease with increasing chain length from 20.6 Å^2 (for DMPE, C_{14}) to 19.9 Å^2 (for DPPE, C_{16}) and to 19.5 Å^2 (for DSPE, C_{18}). The decrease of the cross sections can be qualitatively explained by the increasing van der Waals attraction.

Going from DMPE near 20 °C to DSPE near 10 °C, which in analogy with the behavior of single-chain compounds [Fig. 3(b)] corresponds to a temperature decrease of ~40 °C, one might reach the crystalline phase. However, on the contrary, diffraction lines are broadened. A reason for this may be the rigid coupling between chains, imposed by the glycerol backbone, which is incommensurate with the crystalline lattice of chains. The misfit between this coupling and the chain lattice may also be responsible for the unusual peak broaden-

ing observed for DSPE on increasing the pressure. However, there exist bulk crystals and multilayers of PE in a crystalline state (Elder *et al.*, 1977). Hence the confinement of the molecules in two dimensions is responsible for the inhibition of the 2D crystal formation. The most probable explanation is a disordered arrangement of the glycerol backbones. Imagining an ordering process via lateral molecular transport, the attachment of a double-chain molecule to an existing ordered domain may occur randomly as regards position and orientation of the backbone. Generally there would follow an annealing process to improve order, but this may be impossible due to confinement to the water surface. In a 3D layered system, annealing could occur via molecular exchange (flip-flop) with an adjacent monolayer which is not existing here. Hence the glycerol backbones are arranged as in a glass. Direct structural data on these backbones are absent and we cannot tell if they are disordered positionally and/or orientationally. An alternative explanation for the lack of crystalline phases in phospholipid monolayers may be the lack of interlayer coupling via the head groups. These might order the heads in lamellar structures with low water content and hence enforce positional order.

First using x-ray diffraction on DPPE (Böhm *et al.*, 1993), later using Brewster-angle microscopy on other lipids (Weidemann and Vollhardt, 1995) it was also observed that the monolayer at low pressure is in a chiral state, the chirality being due to the chiral carbon atom of the glycerol. This shows that chiral head-group interactions affect the tail arrangement. It is unfortunate that up to now it has not been possible to observe scattering from the head groups, presumably due to low positional order. The PE head groups are generally thought to form a hydrogen bonded network (Seddon *et al.*, 1984), and one may ask if a chiral structure is peculiar to hydrogen bonding. This, however, is not the case, since chiral lattices are observed also for lipids with other head groups (Brezesinski, Dietrich, Struth *et al.*, 1995).

C. Phospholipids with variations in head and tail interactions

1. Varying head-group interactions

The most frequently studied phospholipid, DPPC, is distinguished from the PE's by three methyl groups replacing the protons bound to the nitrogen at the head [Fig. 1(d)]. This effectively increases the size of the head and prevents a vertical tail arrangement of monolayers. In the ordered phase of DPPC the tails tilt to an angle of about 30° which is almost pressure independent. On the other hand, the (nonhydrated) phosphocholine group oriented normally to the surface requires a molecular area less than 40 $Å^2$. This can explain the finding that a protein (phospholipase A2) binding to DPPC monolayers reduces the chain tilt angles to zero (Dahmen-Levison *et al.*, 1998). In this case the protein may dehydrate and cooperatively reorient the head groups.

As another variant of DPPC, molecules with flexible (oligoethylenoxide) hydrophilic spacers of systematically varied length between glycerol and phosphocholine have been synthesized and their monolayers have been studied. The freedom to order head groups is increased, which allows for smaller tilt angles. A centered rectangular chain lattice with the NN tilt is always maintained (Struth *et al.*, 1994).

Replacing the phosphoethanolamine by a phosphatidic acid group, one obtains a small head group enabling pressure-induced transitions from a centered rectangular lattice with nearest neighbor tilt to a hexagonal lattice without tilt (de Meijere *et al.*, 1997). Varying the Coulomb interactions between the head groups via *p*H or counter ions, one changes the transition pressures, as is qualitatively expected (Helm *et al.*, 1986). However, x-ray-diffraction measurements with systematic variation of these parameters have not been performed.

Coulomb interactions are also screened upon binding polyelectrolytes to the membrane. However, this also tends to increase disorder. The latter mechanism has been found to dominate for the binding of flexible polymers (de Meijere *et al.*, 1997). In this case a lattice with nearest-neighbor tilt is established with pressure. Probably this situation will change qualitatively if rigid polymers or proteins are electrostatically bound to the membrane surface.

2. Varying the tail interactions

Natural phospholipids have one or two double bonds in the aliphatic region. These generally create disorder and reduce the transition temperatures for bilayers, equivalently the transition pressures for Langmuir monolayers. Such systems have not been studied by x-ray diffraction, which is probably also difficult due to the radiation sensitivity of the unsaturated bond. An alternative way to create disorder, also used by nature, is to attach methyl or ethyl groups to the aliphatic tails. The effect of these branches is weak if they are close to the head groups because they may orient towards water and thus not disturb the chain lattice (Bringezu *et al.*, 1995). A long branch serves as an additional tail, giving rise to three or four aliphatic tails per head [Fig. 1(e)]. The configuration and phases of the triple-chain lipids are then not qualitatively different from double chain ones with a small head (Brezesinski, Dietrich, Dobner *et al.*, 1995). The four-chain lipid does not favor any chain tilt and prefers a hexagonal lattice. Probably the constraint from the planar water surface on the backbone inhibits chain tilt and enforces direct transitions from a disordered to an ordered state without an intermittent tilted phase. One interesting feature of lipids with more than two chains is that the head groups have sufficient space to arrange. However, the heads are decoupled only for the four-chain compounds. For triple-chain lipids one finds chiral structures with chirality corresponding to the head-group chirality (Bringezu *et al.*, 1996). This means that the heads are orientationally ordered, probably due to lateral dipolar forces.

Structures similar to those of triple-chain lipids can be observed for a monolayer of a double-chain lipid like

DPPC in contact with a long-chain alkane. The alkane then assumes the space of a chain in the ordered lattice and an equivalent lattice is established (Brezesinski *et al.*, 1996). This points to an interesting way of structure manipulation via contact with hydrophobic molecules mimicking the action of anaesthetics.

IX. CONCLUDING REMARKS

Our present knowledge of structures and phase transitions in Langmuir monolayers is primarily based on x-ray diffraction and optical microscopy studies of the simplest amphiphiles. The main features of the phase diagrams are fairly well understood. However, even the simplest amphiphiles are not completely characterized. New phases are still being discovered, and some discrepancies between different observations remain unresolved. The information about positional correlations contained in the x-ray-diffraction peak profiles has not been explored.

Molecular-dynamics simulations with realistic interaction potentials between atoms have mainly been performed with fixed simulation cell size and shape. These prevent changes in the lattice, and thus restrict backbone packing, an essential element of the ordering in real monolayers. We expect that constant-pressure simulations with variable shape simulation cells will provide better agreement with the behavior of real systems, but this remains to be demonstrated. The currently used models of polar heads and their interactions with water are extremely simplified; more realistic models, as well as simulations including water molecules, may help explain the observed head-group effects on monolayer structure. Simplified models of lipid molecules allow larger systems to be simulated. The molecules are usually treated as cylinders or beads on a string; less attention is paid to the ordering of the molecular backbones.

Molecular models of the tilting phase transitions are rather well developed; they also represent the molecule as a cylinder or as beads on a string. The molecular heads are either grafted to a lattice or disordered as in a 2D liquid. Hexatic order, inherent to the condensed phases of Langmuir monolayers, is not treated by these models. Studies of backbone ordering are also restricted by the lattice models. In contrast, experiments and the Landau theory of phase transitions show simultaneous translational ordering of molecular positions and orientational ordering of their backbones in the herringbone structure.

The basic features of the phase diagrams of simple amphiphiles have been explained in terms of the Landau theory, with a quite limited number of order parameters describing translational and orientational degrees of freedom of the molecule as a whole. The theory includes phases with periodicity in one direction in the monolayer plane, described by an order parameter which involves both translational and orientational ordering. Fluctuation effects at the phase transitions have not yet been explored theoretically nor experimentally.

Many features of the biologically important class of amphiphiles, phospholipids, can be described on the basis of our knowledge of the structures of single-chain compounds. Potentially there can be additional order due to the linkage between chains, but such order has not been observed by x-ray or microscopy techniques, and in general the experimental situation is not gratifying. To enhance our understanding, experimental techniques are needed that measure directly the arrangements of the chains and the head groups. Infrared techniques are now emerging as most promising tools.

In sum, therefore, much progress has been made and much remains to be done. We expect that investigations of Langmuir monolayers will be both technically challenging and scientifically rewarding for many years to come.

Note added in proof: Several studies performed after submission of the manuscript have focused on problems discussed in the present review. Kaganer *et al.* (1998, 1999) studied positional order in the phases LS and S of octadecanol monolayers by accurately measuring profiles of the diffraction peaks and determining the pair correlation function of the positional order. The found an algebraic decay of positional correlations, which suggests solid-like order in both phases on the length scales accessible to this experiment (<800). The transition from LS to S introduces strong positional disorder, which is evident from the drastic increase of the exponent η in the correlation function. The resolution of this experiment does not allow one to judge the order (crystalline or hexatic) at longer distances; this will require a high-resolution diffraction study of positional order.

Kaganer and Osipov (1998) developed a molecular model describing simultaneous translational and orientational ordering into a herringbone phase in a two-dimensional liquid. A microscopic definition of the herringbone order parameter, combining translational and orientational degrees of freedom, has been given.

Stadler, Lange, and Schmid (1999) performed constant-pressure Monte Carlo simulations of a bead-spring model with the head beads somewhat larger than the chain beads. In this simple model, they found a fairly rich phase diagram which contains the liquid expanded and three distinct condensed (untilted, NN- and NNN-tilted) phases. Upon increasing the head size, Stadler and Schmid (1999) found a modulated phase with an intermediate tilt direction, stemming from competition between the head size and the chain diameter.

Luty, Swanson, and Eckhardt (1999) analyzed the L_2-L_2' transition in terms of a coupling between the tilt and the strain order parameters in a deformable 2D solid. This free energy expansion is sufficient to describe the L_2-L_2' transition (Kaganer and Indenbom, 1993; Durbin *et al.*, 1997) but fails to simultaneously explain the strain and the tilt azimuths at two of the tilting transitions, LS-L_2 and S-L_2' (Kaganer and Indenbom, 1993).

ACKNOWLEDGMENTS

We have benefited from long-term collaborations, discussions, exchange of ideas, and results with a large

number of people. We particularly mention (in alphabetical order) J. Als-Nielsen, G. Brezesinski, M. K. Durbin, V. L. Indenbom, K. Kjaer, C. Knobler, E. Loginov, M. Osipov, I. Peterson, E. Scalas, M. C. Shih, and E. B. Sirota. V.M.K. thanks the Alexander von Humboldt-Stiftung for a fellowship. P.D. was supported by the U.S. Department of Energy under Grant No. DE-FG02-84ER45125.

REFERENCES

Acero, A. A., M. Li, B. Lin, S. A. Rice, M. Goldmann, I. B. Azouz, A. Goudot, and F. Rondelez, 1993, J. Chem. Phys. **99**, 7214.

Adam, N. K., 1922, Proc. R. Soc. London, Ser. A **101**, 516.

Albrecht, O., H. Gruler, and E. Sackmann, 1978, J. Phys. (France) **39**, 301.

Alexander, S., and J. McTague, 1978, Phys. Rev. Lett. **41**, 702.

Als-Nielsen, J., D. Jacquemain, K. Kjaer, F. Leveiller, M. Lahav, and L. Leiserowitz, 1994, Phys. Rep. **246**, 251.

Als-Nielsen, J., and H. Möhwald, 1991, in *Handbook of Synchrotron Radiation*, edited by S. Ebashi, M. Koch, and E. Rubenstein (Elsevier Science, Amsterdam), Vol. 4, Chap. 1, p. 1.

Andelman, D., 1989, J. Am. Chem. Soc. **111**, 6536.

Andelman, D., 1990, Physica A **168**, 172.

Andelman, D., F. Brochard, and J.-F. Joanny, 1987, J. Chem. Phys. **86**, 3673.

Andelman, D., F. Brochard, C. M. Knobler, and F. Rondelez, 1994, in *Micelles, Membranes, Microemulsions, and Monolayers*, edited by M. Gelbart, A. Ben Shaul, and D. Roux (Springer, New York), p. 599.

Andelman, D., and H. Orland, 1993, J. Am. Chem. Soc. **115**, 12322.

Balashov, S. M., and V. A. Krylov, 1994, Thin Solid Films **239**, 127.

Bareman, J. P., G. Cardini, and M. L. Klein, 1988, Phys. Rev. Lett. **60**, 2152.

Bareman, J. P., and M. L. Klein, 1990, J. Phys. Chem. **94**, 5202.

Barton, S. W., A. Goudot, O. Bouloussa, F. Rondelez, B. H. Lin, F. Novak, A. Acero, and S. A. Rice, 1992, J. Chem. Phys. **96**, 1343.

Benattar, J. J., F. Moussa, and M. Lambert, 1983, J. Chim. Phys. **80**, 99.

Berge, B., O. Konovalov, J. Lajzerowicz, A. Renault, J. P. Rieu, M. Vallade, J. Als-Nielsen, G. Grübel, and J. F. Legrand, 1994, Phys. Rev. Lett. **73**, 1652.

Berlinsky, A. J., and A. B. Harris, 1978, Phys. Rev. Lett. **40**, 1579.

Bibo, A. M., C. M. Knobler, and I. R. Peterson, 1991, J. Phys. Chem. **95**, 5591.

Bibo, A. M., and I. R. Peterson, 1990, Adv. Mater. **2**, 309.

Bohanon, T. M., B. Lin, M. C. Shih, G. E. Ice, and P. Dutta, 1990, Phys. Rev. B **41**, 4846.

Böhm, C., F. Leveiller, D. Jacquemain, H. Möhwald, K. Kjaer, J. Als-Nielsen, I. Weissbuch, and L. Leiserowitz, 1994, Langmuir **10**, 830.

Böhm, C., H. Möhwald, L. Leiserowitz, J. Als-Nielsen, and K. Kjaer, 1993, Biophys. J. **64**, 553.

Bommarito, G. M., W. J. Foster, P. S. Pershan, and M. L. Schlossman, 1996, J. Chem. Phys. **105**, 5265.

Bourdieu, L., P. Silberzan, and D. Chatenay, 1991, Phys. Rev. Lett. **67**, 2029.

Brazovskii, S. A., 1975, Zh. Eksp. Teor. Fiz. **68**, 175 [Sov. Phys. JETP **41**, 85 (1975)].

Brezesinski, G., R. Rietz, K. Kjaer, W. G. Bouwman, and H. Möhwald, 1994, Nuovo Cimento D **16**, 1487.

Brezesinski, G., A. Dietrich, B. Dobner, and H. Möhwald, 1995, Prog. Colloid Polym. Sci. **98**, 255.

Brezesinski, G., A. Dietrich, B. Struth, C. Böhm, W. G. Bouwman, K. Kjaer, and H. Möhwald, 1995, Chem. Phys. Lipids **76**, 145.

Brezesinski, G., E. Scalas, B. Struth, H. Möhwald, F. Bringezu, U. Gehlert, G. Weidemann, and D. Vollhardt, 1995, J. Phys. Chem. **99**, 8758.

Brezesinski, G., M. Thoma, B. Struth, and H. Möhwald, 1996, J. Phys. Chem. **100**, 3126.

Bringezu, F., G. Brezesinski, P. Nuhn, and H. Möhwald, 1995, in *Short and Long Chains at Interfaces*, edited by J. Daillant (Editions Frontières, Gif-sur-Yvette), p. 171.

Bringezu, F., G. Brezesinski, P. Nuhn, and H. Möhwald, 1996, Biophys. J. **70**, 1789.

Brock, J. D., A. Aharony, R. J. Birgeneau, K. W. Evans-Lutterodt, J. D. Litster, P. M. Horn, G. B. Stephenson, and A. R. Tajbakhsh, 1986, Phys. Rev. Lett. **57**, 98.

Brzezinski, V., and I. R. Peterson, 1995, J. Phys. Chem. **99**, 12545.

Cai, Z.-X., 1991, Phys. Rev. B **43**, 6163.

Cai, Z., and S. A. Rice, 1990, Faraday Discuss. Chem. Soc. **89**, 211.

Cai, Z., and S. A. Rice, 1992, J. Chem. Phys. **96**, 6229.

Cantor, R. S., and P. M. McIlroy, 1989a, J. Chem. Phys. **90**, 4423.

Cantor, R. S., and P. M. McIlroy, 1989b, J. Chem. Phys. **90**, 4431.

Cardini, G., J. P. Bareman, and M. L. Klein, 1988, Chem. Phys. Lett. **145**, 493.

Chacón, E., and P. Tarazona, 1989, Phys. Rev. B **39**, 7111.

Chen, Z.-Y., J. Talbot, W. M. Gelbart, and A. Ben-Shaul, 1988, Phys. Rev. Lett. **61**, 1376.

Collazo, N., S. Shin, and S. A. Rice, 1992, J. Chem. Phys. **96**, 4735.

Costas, M. E., Z.-G. Wang, and M. Gelbart, 1992, J. Chem. Phys. **96**, 2228.

Dahmen-Levison, U., G. Brezesinski, and H. Möhwald, 1998, Thin Solid Films **327–329**, 616.

de Gennes, P. G., and J. Prost, 1993, *The Physics of Liquid Crystals* (Oxford University Press, London).

de Meijere, K., G. Brezesinski, and H. Möhwald, 1997, Macromolecules **30**, 2337.

Dervichian, D. G., 1939, J. Chem. Phys. **7**, 931.

Desai, R. C., 1997, Phys. Canada **53**, 210.

Durbin, M., A. Malik, R. Ghaskadvi, P. Zschack, and P. Dutta, 1994, J. Phys. Chem. **98**, 1753.

Durbin, M. K., M. C. Shih, A. Malik, P. Zschack, and P. Dutta, 1995, Colloids Surf., A **102**, 173.

Durbin, M. K., A. Malik, A. G. Richter, R. Ghaskadvi, T. Gog, and P. Dutta, 1997, J. Chem. Phys. **106**, 8216.

Durbin, M. K., A. Richter, C.-J. Yu, J. Kmetko, J. M. Bai, and P. Dutta, 1998, Phys. Rev. E **58**, 7686.

Dutta, P., J. B. Peng, B. Lin, J. B. Ketterson, M. Prakash, P. Georgopoulos, and S. Ehrlich, 1987, Phys. Rev. Lett. **58**, 2228.

Eckhardt, C. J., N. M. Peachey, D. R. Swanson, J. M. Takacs, M. A. Khan, X. Gong, J.-H. Kim, J. Wang, and R. A. Uphaus, 1993, Nature (London) **362**, 614.
Elder, M., P. Hitchcock, R. Mason, G. G. Shipley, 1977, Proc. R. Soc. London, Ser. A **354**, 157.
Embs, F., D. Furhoff, A. Laschewsky, U. Licht, H. Ohst, W. Pross, H. Ringsdorf, G. Wegner, and R. Wehrmann, 1991, Adv. Mater. **3**, 25.
Engel, M., H. J. Merle, I. R. Peterson, H. Riegler, and R. Steitz, 1991, Ber. Bunsenges. Phys. Chem. **95**, 1514.
Fainerman, V. B., D. Vollhardt, and V. Melzer, 1996, J. Phys. Chem. **100**, 15478.
Felsteiner, J., D. Cabib, and Z. Friedman, 1978, Phys. Rev. A **18**, 1261.
Fischer, B., E. Teer, and C. M. Knobler, 1995, J. Chem. Phys. **103**, 2365.
Foster, W. J., M. C. Shih, and P. S. Pershan, 1996, J. Chem. Phys. **105**, 3307.
Fradin, C., J. Daillant, A. Braslau, D. Luzet, M. Alba, and M. Goldmann, 1998, Eur. Phys. J. B **1**, 57.
Germer, L. H., and K. H. Storks, 1938, J. Chem. Phys. **6**, 280.
Gibson, M. D., D. R. Swanson, C. J. Eckhardt, and X. C. Zeng, 1997, J. Chem. Phys. **106**, 1961.
Goldmann, M., P. Nassoy, F. Rondelez, A. Renault, S. Shin, and S. Rice, 1994, J. Phys. II **4**, 773.
Gourier, C., J. Daillant, A. Braslau, M. Alba, K. Quinn, D. Luzet, C. Blot, D. Chatenay, C. Grübel, J.-F. Legrand, and G. Vignaud, 1997, Phys. Rev. Lett. **78**, 3157.
Gray, G. W., and J. W. Goodby, 1984, *Smectic Liquid Crystals: Textures and Structures* (Leonard Hill, Glasgow).
Guinier, A., 1968, *X-Ray Diffraction* (Freeman, San Francisco).
Haas, F. M., and R. Hilfer, 1996, J. Chem. Phys. **105**, 3859.
Haas, F. M., R. Hilfer, and K. Binder, 1995, J. Phys. Chem. **102**, 2960.
Haas, F. M., R. Hilfer, and K. Binder, 1996, J. Phys. Chem. **100**, 15290.
Halperin, A., S. Alexander, and I. Schechter, 1987, J. Phys. Chem. **86**, 6550.
Harkins, W. D., and L. E. Copeland, 1942, J. Chem. Phys. **10**, 272.
Harkins, W. D., T. F. Young, and G. E. Boyd, 1940, J. Chem. Phys. **8**, 954.
Harris, A. B., and A. J. Berlinsky, 1979, Can. J. Phys. **57**, 1852.
Harris, A. B., R. D. Kamien, and T. C. Lubensky, 1997, Phys. Rev. Lett. **78**, 1476.
Harris, J., and S. A. Rice, 1988, J. Chem. Phys. **39**, 5898.
Hautman, J. and M. L. Klein, 1989, J. Chem. Phys. **91**, 4994.
Hautman, J., and M. L. Klein, 1990, J. Chem. Phys. **93**, 7483.
Helm, C. A., L. Laxhuber, M. Lösche, and H. Möhwald, 1986, Colloid Polym. Sci. **264**, 46.
Helm, C. A., H. Möhwald, K. Kjaer, and J. Als-Nielsen, 1987a, Biophys. J. **52**, 381.
Helm, C. A., H. Möhwald, K. Kjaer, and J. Als-Nielsen, 1987b, Europhys. Lett. **4**, 697.
Helm, C. A., P. Tippmann-Krayer, H. Möhwald, J. Als-Nielsen, and K. Kjaer, 1991, Biophys. J. **60**, 1457.
Hénon, S., and J. Meunier, 1991, Rev. Sci. Instrum. **62**, 936.
Hönig, D., and D. Möbius, 1991, J. Phys. Chem. **95**, 4590.
Huang, Z., A. Acero, N. Lei, S. A. Rice, and Z. Zhang, 1996, J. Chem. Soc., Faraday Trans. **92**, 545.
Israelachvili, J., 1994, Langmuir **10**, 3774.
Jacquemain, D., F. Leveiller, S. P. Weinbach, M. Lahav, L. Leiserowitz, K. Kjaer, and J. Als-Nielsen, 1991, J. Am. Chem. Soc. **113**, 7684.
Jacquemain, D., S. G. Wolf, F. Leveiller, F. Frolow, M. Eisenstein, M. Lahav, and L. Leiserowitz, 1992, J. Am. Chem. Soc. **114**, 9983.
Kaganer, V. M., G. Brezesinski, H. Möhwald, P. B. Howes, and K. Kjaer, 1998, Phys. Rev. Lett. **81**, 5864.
Kaganer, V. M., G. Brezesinski, H. Möhwald, P. B. Howes, and K. Kjaer, 1999, Phys. Rev. E **59**, 2141.
Kaganer, V. M., and V. L. Indenbom, 1993, J. Phys. II **3**, 813.
Kaganer, V. M., and E. B. Loginov, 1993, Phys. Rev. Lett. **71**, 2599.
Kaganer, V. M., and E. B. Loginov, 1995, Phys. Rev. E **51**, 2237.
Kaganer, V. M., and M. A. Osipov, 1998, J. Chem. Phys. **109**, 2600.
Kaganer, V. M., M. A. Osipov, and I. R. Peterson, 1993, J. Chem. Phys. **98**, 3513.
Kaganer, V. M., I. R. Peterson R. M. Kenn, M. C. Shih, M. Durbin, and P. Dutta, 1995, J. Chem. Phys. **102**, 9412.
Karaborni, S., 1993a, Langmuir **9**, 1334.
Karaborni, S., 1993b, Tenside, Surfactants, Deterg. **4**, 256.
Karaborni, S., and J. I. Siepmann, 1994, Mol. Phys. **83**, 345.
Karaborni, S., and S. Toxvaerd, 1992a, J. Chem. Phys. **96**, 5505.
Karaborni, S., and S. Toxvaerd, 1992b, J. Chem. Phys. **97**, 5876.
Karaborni, S., S. Toxvaerd, and O. H. Olsen, 1992, J. Phys. Chem. **96**, 4965.
Karaborni, S., and G. Verbist, 1994, Europhys. Lett. **27**, 467.
Kats, E. I., V. V. Lebedev, and A. R. Muratov, 1993, Phys. Rep. **228**, 91.
Kenn, R. M., C. Böhm, A. M. Bibo, I. R. Peterson, H. Möhwald, J. Als-Nielsen, and K. Kjaer, 1991, J. Phys. Chem. **95**, 2092.
Kenn, R. M., K. Kjaer, and H. Möhwald, 1996, Colloids Surf., A **117**, 171.
Kitaigorodskii, A. I., 1961, *Organic Chemical Crystallography* (Consultants Bureau, New York).
Kjaer, K., J. Als-Nielsen, C. A. Helm, L. A. Laxhuber, and H. Möhwald, 1987, Phys. Rev. Lett. **58**, 2224.
Kjaer, K., J. Als-Nielsen, C. A. Helm, P. Tippmann-Krayer, and H. Möhwald, 1989, J. Phys. Chem. **93**, 3200.
Knobler, C. M., 1990, Science **249**, 870.
Knobler, C. M., and R. C. Desai, 1992, Annu. Rev. Phys. Chem. **43**, 207.
Kramer, D., A. Ben-Shaul, Z.-Y. Chen, and W. M. Gelbart, 1992, J. Chem. Phys. **96**, 2236.
Kreer, M., K. Kremer, and K. Binder, 1990, J. Chem. Phys. **92**, 6195.
Kuzmenko, I., V. M. Kaganer, and L. Leiserowitz, 1998, Langmuir **14**, 3882.
Landau, L. D., 1937, Phys. Z. Sowjetunion **11**, 545 [*The Collected Papers of L. D. Landau*, edited by D. ter Haar (Gordon and Breach-Pergamon, New York, 1965), p. 193].
Landau, L. D., and E. M. Lifshitz, 1980, *Statistical Physics* Pt. 1 (Pergamon Press, Oxford, UK).
Langmuir, J., 1917, J. Am. Chem. Soc. **39**, 1848.
Lautz, C., and Th. M. Fischer, 1997, J. Phys. Chem. B **101**, 8790.
Lautz, C., and T. M. Fischer, 1999, Eur. Phys. J. B **7**, 263.
Lautz, C., Th. M. Fischer, and J. Kildea, 1997, J. Chem. Phys. **106**, 7448.

Lawrie, G. A., and G. T. Barnes, 1994, J. Colloid Interface Sci. **162**, 36.
Leveiller, F., C. Böhm, D. Jacquemain, H. Möhwald, L. Leiserowitz, K. Kjaer, and J. Als-Nielsen, 1994, Langmuir **10**, 819.
Leveiller, F., D. Jacquemain, L. Leiserowitz, K. Kjaer, and J. Als-Nielsen, 1992, J. Phys. Chem. **96**, 10380.
Li, M. Y., and S. A. Rice, 1996, J. Chem. Phys. **104**, 6860.
Lin, B., J. B. Peng, J. B. Ketterson, P. Dutta, B. N. Thomas, J. Buontempo, and S. A. Rice, 1989, J. Chem. Phys. **90**, 2393.
Lin, B., M. C. Shih, T. M. Bohanon, G. E. Ice, and P. Dutta, 1990, Phys. Rev. Lett. **65**, 191.
Lord Rayleigh, 1899, Philos. Mag. **48**, 321.
Lösche, M., and H. Möhwald, 1984, Rev. Sci. Instrum. **55**, 1968.
Lösche, M., E. Sackmann, and H. Möhwald, 1983, Ber. Bunsenges. Phys. Chem. **87**, 848.
Lundquist, M., 1971a, Chem. Scr. **1**, 5.
Lundquist, M., 1971b, Chem. Scr. **1**, 197.
Luty, T., and C. J. Eckhardt, 1995, J. Phys. Chem. **99**, 8872.
Luty, T., and C. J. Eckhardt, 1996, J. Phys. Chem. **100**, 6793.
Luty, T., D. R. Swanson, and C. J. Eckhardt, 1999, J. Chem. Phys. **110**, 2606.
Majewski, J., R. Popovitz-Biro, W. G. Bouwman, K. Kjaer, J. Als-Nielsen, M. Lahav, and L. Leiserowitz, 1995, Chem.-Eur. J. **35**, 304.
Marchenko, V. I., 1991, Zh. Eksp. Teor. Fiz. **100**, 1370 [Sov. Phys. JETP **73**, 759].
McConnell, M., 1991, Annu. Rev. Phys. Chem. **42**, 171.
Mendelsohn, R., J. W. Brauner, and A. Gericke, 1995, Annu. Rev. Phys. Chem. **46**, 305.
Meyer, R. J., 1975, Phys. Rev. A **12**, 1066.
Meyer, R. J., 1976, Phys. Rev. A **13**, 1613.
Möhwald, H., 1993a, Rep. Prog. Phys. **56**, 653.
Möhwald, H., 1993b, in *Phospholipids Handbook*, edited by G. Cevc (Marcel Dekker, New York), Chap. 16, p. 579.
Moller, M. A., D. J. Tildesley, K. S. Kim, and N. Quirke, 1991, J. Chem. Phys. **94**, 8390.
Moore, B. G., C. M. Knobler, S. Akamatsu, and F. Rondelez, 1990, J. Phys. Chem. **94**, 4588.
Moy, V. T., D. J. Keller, H. E. Gaub, and H. M. McConnell, 1986, J. Phys. Chem. **90**, 3198.
Nassoy, P., M. Goldmann, O. Bouloussa, and F. Rondelez, 1995, Phys. Rev. Lett. **75**, 457.
Neundorf, M., S. Diele, S. Ernst, S. Saito, D. Demus, T. Inikai, and K. Murashiro, 1993, Ferroelectrics **147**, 95.
Ostlund, S., and B. I. Halperin, 1981, Phys. Rev. B **23**, 335.
Overbeck, G. A., D. Hönig, and D. Möbius, 1993, Langmuir **9**, 7999.
Overbeck, G. A., and D. Möbius, 1993, J. Phys. Chem. **97**, 7999.
Pershan, P. S., 1988, *Structure of Liquid Crystal Phases* (World Scientific, Singapore).
Peters, G. H., N. B. Larsen, T. Bjornholm, S. Toxvaerd, K. Schaumburg, and K. Kjaer, 1998, Phys. Rev. E **57**, 3153.
Peters, G. H., S. Toxvaerd, O. H. Olsen, and A. Svendsen, 1995, Langmuir **11**, 4072.
Peters, G. H., S. Toxvaerd, A. Svendsen, and O. H. Olsen, 1994, J. Chem. Phys. **100**, 5996.
Peterson, I. R., V. Brzezinski, R. M. Kenn, and R. Steitz, 1992, Langmuir **8**, 2995.
Peterson, I. R., and R. M. Kenn, 1994, Langmuir **10**, 4645.
Peterson, I. R., R. M. Kenn, A. Goudot, P. Fontaine, F. Rondelez, W. G. Bouwman, and K. Kjaer, 1996, Phys. Rev. E **53**, 667.
Peterson, I. R., R. Steitz, H. Krug, and I. Voigt-Martin, 1990, J. Phys. (France) **51**, 1003.
Pockels, A., 1891, Nature (London) **43**, 437.
Popielawski, J., and S. A. Rice, 1988, J. Chem. Phys. **88**, 1279.
Qiu, X., J. Ruiz-Garcia K. J. Stine, C. M. Knobler, and J. V. Selinger, 1991, Phys. Rev. Lett. **67**, 703.
Renault, A., J. F. Legrand, M. Goldmann, and B. Berge, 1993, J. Phys. II **3**, 761.
Rettig, W., H.-D. Dörfler, and C. Koth, 1985, Colloid Polym. Sci. **263**, 647.
Rettig, W., C. Koth, and H.-D. Dörfler, 1984, Colloid Polym. Sci. **262**, 745.
Rietz, R., G. Brezesinski, and H. Möhwald, 1993, Ber. Bunsenges. Phys. Chem. **97**, 1394.
Rietz, R., W. Rettig, G. Brezesinski, W. G. Bouwman, K. Kjaer, and H. Möhwald, 1996, Thin Solid Films **284**, 211.
Rivière, S., S. Hénon, J. Meunier, D. K. Schwartz, M.-W. Tsao, and C. M. Knobler, 1994, J. Chem. Phys. **101**, 10045.
Rivière-Cantin, S., S. Hénon, and J. Meunier, 1996, Phys. Rev. E **54**, 1683.
Sackmann, H., and D. Demus, 1966, Mol. Cryst. **2**, 81.
Sackmann, H., and D. Demus, 1973, Mol. Cryst. Liq. Cryst. **21**, 239.
Safran, S. A., M. O. Robbins, and S. Garoff, 1986, Phys. Rev. A **33**, 2186.
Scalas, E., G. Brezesinski, H. Möhwald, V. M. Kaganer, W. G. Bouwman, and K. Kjaer, 1996, Thin Solid Films **284**, 56.
Scalas, E., G. Brezesinski, V. M. Kaganer, and H. Möhwald, 1998, Phys. Rev. E **58**, 2172.
Scheringer, M., R. Hilfer, and K. Binder, 1992, J. Chem. Phys. **96**, 2269.
Schlossman, M. L., D. K. Schwartz, P. S. Pershan, E. H. Kawamoto, G. J. Kellogg, and S. Lee, 1991, Phys. Rev. Lett. **66**, 1599.
Schmid, F., 1997, Phys. Rev. E **55**, 5774.
Schmid, F., D. Johannsmann, and A. Halperin, 1996, J. Phys. II **6**, 1331.
Schmid, F., and H. Lange, 1997, J. Chem. Phys. **106**, 3757.
Schmid, F., and M. Schick, 1995, J. Chem. Phys. **102**, 2080.
Schmid, F., C. Stadler, and H. Lange, 1997, in *Computer Simulations in Condensed Matter*, edited by D. P. Landau, K. K. Mon, and B. Schüttler (Springer, Heidelberg), Vol. 10, p. 37.
Schmidt, M. E., S. Shin, and S. A. Rice, 1996a, J. Chem. Phys. **104**, 2101.
Schmidt, M. E., S. Shin, and S. A. Rice, 1996b, J. Chem. Phys. **104**, 2114.
Schofield, J., and S. A. Rice, 1995, J. Chem. Phys. **103**, 5792.
Schwartz, D. K., J. Garnaes, R. Viswanathan, S. Chiruvolu, and J. A. N. Zasadzinski, 1993, Phys. Rev. E **47**, 452.
Schwartz, D. K., and C. M. Knobler, 1993, J. Phys. Chem. **97**, 8849.
Schwartz, D. K., M. L. Schlossman, and P. S. Pershan, 1992, J. Chem. Phys. **96**, 2356.
Seddon, J. M., G. Cevc, R. D. Kaye, and D. Marsh, 1984, Biochemistry **23**, 2634.
Selinger, J. V., and D. R. Nelson, 1988, Phys. Rev. Lett. **61**, 416.
Selinger, J. V., and D. R. Nelson, 1989, Phys. Rev. A **39**, 3135.
Selinger, J. V., Z.-G. Wang, R. F. Bruinsma, and C. M. Knobler, 1993, Phys. Rev. Lett. **70**, 1139.
Seul, M., and D. Andelman, 1995, Science **267**, 476.

Shih, M. C., T. M. Bohanon, J. M. Mikrut, P. Zschack, and P. Dutta, 1992a, J. Chem. Phys. **96**, 1556.
Shih, M. C., T. M. Bohanon, J. M. Mikrut, P. Zschack, and P. Dutta, 1992b, J. Chem. Phys. **97**, 4485.
Shih, M. C., T. M. Bohanon, J. M. Mikrut, P. Zschack, and P. Dutta, 1992c, Phys. Rev. A **45**, 5734.
Shih, M. C., M. K. Durbin, A. Malik, P. Zschack, and P. Dutta, 1994, J. Chem. Phys. **101**, 9132.
Shih, M. C., J. B. Peng, K. G. Huang, and P. Dutta, 1993, Langmuir **9**, 776.
Shin, S., N. Collazo, and S. A. Rice, 1992, J. Chem. Phys. **96**, 1352.
Shin, S., N. Collazo, and S. A. Rice, 1993, J. Chem. Phys. **98**, 3469.
Shin, S., and S. A. Rice, 1994, J. Chem. Phys. **101**, 2508.
Shin, S., Z. G. Wang, and S. A. Rice, 1990, J. Chem. Phys. **92**, 1427.
Siepmann, J. I., S. Karaborni, and M. L. Klein, 1994, J. Chem. Phys. **98**, 6675.
Siepmann, J. I., and I. R. McDonald, 1993, Langmuir **9**, 2351.
Sikes, H. D., and D. K. Schwartz, 1997, Science **278**, 1604.
Simon-Kutscher, J., A. Gericke, and H. Hühnerfuss, 1995, Langmuir **12**, 1027.
Sirota, E. B., 1997, Langmuir **13**, 3849.
Sirota, E. B., H. E. King, H. H. Shao, and D. M. Singer, 1995, J. Phys. Chem. **99**, 798.
Sirota, E. B., H. E. King, D. M. Singer, and H. Shao, 1993, J. Chem. Phys. **98**, 5809.
Sirota, E. B., P. S. Pershan, L. B. Sorensen, and J. Collett, 1987, Phys. Rev. A **36**, 2890.
Smith, R. D., and J. C. Berg, 1980, J. Colloid Interface Sci. **74**, 273.
Smith, G. S., E. B. Sirota, C. R. Safinya, R. J. Plano, and N. A. Clark, 1990, J. Chem. Phys. **92**, 4519.
Somoza, A. M., and R. C. Desai, 1992, J. Phys. Chem. **96**, 1401.
Stadler, C., H. Lange, and F. Schmid, 1999, Phys. Rev. E, in press.
Stadler, C., and F. Schmid, 1999, J. Chem. Phys., in press.
Ställberg-Stenhagen, S., and E. Stenhagen, 1945, Nature (London) **156**, 239.
Standish, M. M., and B. A. Pethica, 1968, Trans. Faraday Soc. **64**, 1113.
Steitz, R., E. E. Mitchell, and I. R. Peterson, 1991, Thin Solid Films **205**, 124.
Steitz, R., J. B. Peng, I. R. Peterson, I. Gentle, R. M. Kenn, M. Goldmann, and G. T. Barnes, 1995 (unpublished).
Stenhagen, E., 1955, in *Determination of Organic Structures by Physical Methods*, edited by E. A. Braude and F. C. Nachod (Academic, New York), Chap. 8, p. 325.
Strandburg, K. J., 1988, Rev. Mod. Phys. **60**, 161.
Struth, B., E. Scalas, G. Brezesinski, H. Möhwald, F. Bringezu, W. G. Bouwman, and K. Kjaer, 1994, Nuovo Cimento D **16**, 1545.
Swanson, D. R., R. J. Hardy, and C. J. Eckhardt, 1993, J. Chem. Phys. **99**, 8194.
Swanson, D. R., R. J. Hardy, and C. J. Eckhardt, 1996, J. Chem. Phys. **105**, 673.
Swanson, D. R., T. Luty, and C. J. Eckhardt, 1997, J. Chem. Phys. **107**, 4744.
Szleifer, I., A. Ben-Shaul, and W. M. Gelbart, 1990, J. Phys. Chem. **94**, 5081.
Tarazona, P., and E. Chacón, 1989, Phys. Rev. B **39**, 7157.
Teer, E., C. M. Knobler, C. Lautz, S. Wurlitzer, J. Kidae, and T. M. Fischer, 1997, J. Chem. Phys. **106**, 1913.
Thomas, R. K., and J. Penfold, 1996, Curr. Opin. Colloid Interface Sci. **1**, 1.
Tippmann-Krayer, P., R. M. Kenn, and H. Möhwald, 1992, Thin Solid Films **210/211**, 577.
Tippmann-Krayer, P., and H. Möhwald, 1991, Langmuir **7**, 2303.
Toxvaerd, S., 1990, J. Chem. Phys. **93**, 4290.
Urbakh, M., and J. Klafter, 1993, J. Phys. Chem. **97**, 3344.
Vainshtein, B. K., 1994, *Modern Crystallography* (Springer, Berlin), Vol. 1.
Viswanathan, R., J. A. Zasadzinski, and D. K. Schwartz, 1994, Nature (London) **368**, 440.
Wang, Z., and C. Gong, 1996, Phys. Rev. B **54**, 17067.
Wang, J.-L., F. Leveiller, D. Jacquemain, K. Kjaer, J. Als-Nielsen, M. Lahav, and L. Leiserowitz, 1994, J. Am. Chem. Soc. **116**, 1192.
Weinbach, S. P., D. Jacquemain, F. Leveiller, K. Kjaer, J. Als-Nielsen, and L. Leiserowitz, 1993, J. Am. Chem. Soc. **115**, 11110.
Weinbach, S. P., K. Kjaer, J. Als-Nielsen, M. Lahav, and L. Leiserowitz, 1993, J. Phys. Chem. **97**, 5200.
Weidemann, G., and D. Vollhardt, 1995, Thin Solid Films **264**, 94.
Weissbuch, I., M. Berfeld, W. Bouwman, K. Kjaer, J. Als-Nielsen, M. Lahav, and L. Leiserowitz, 1997, J. Am. Chem. Soc. **119**, 933.
Weissbuch, I., G. Berkovic, R. Yam, J. Als-Nielsen, K. Kjaer, M. Lahav, and L. Leiserowitz, 1995, J. Phys. Chem. **99**, 6036.
Weissbuch, I., J. Majewski, K. Kjaer, J. Als-Nielsen, M. Lahav, and L. Leiserowitz, 1993, J. Phys. Chem. **97**, 12858.
Wu, X. Z., E. B. Sirota, S. K. Sinha, B. M. Ocko, and M. Deutsch, 1993, Phys. Rev. Lett. **70**, 958.
Zakri, C., A. Renault, J.-P. Rieu, M. Vallde, and B. Berge, 1997, Phys. Rev. B **55**, 14163.